INFLUENCE OF VANADIUM(V) COMPLEXES ON THE CATALYTIC

ACTIVITY OF PROTEIN TYROSINE PHOSPHATES

by

Fikile Nxumalo

B.Sc. Hon., Trent University, 1994

THESIS SUBMITTED IN PARTIAL FULFILLMENT OF

THE REQUIREMENTS FOR THE DEGREE OF

MASTER OF SCIENCE

in the Department

of

Chemistry

© Fikile Nxumalo 1997

SIMON FRASER UNIVERSITY

August 1997

Your file Votre référence

Our file Notre référence

0-612-24218-8

Canada

Approval

Name: Fikile Nxumalo

Degree: Master of Science

Title of Thesis: Influence of Vanadium(V) Complexes on the Catalytic
Activity of Protein Tyrosine Phosphatases

Examining Committee:

                     Chair: Dr. F.W.B. Einstein

_____

Dr. A.S. Tracey,
Senior Supervisor

_____

Dr. R.B. Cornell
Committee Member

_____

Dr. D. Sen
Committee Member

_____

Dr. W. Richards,
Institute of Molecular Biology and Biochemistry,
Internal Examiner

Date approved: _____

Abstract

The influence of vanadium(V) complexes on the activity of two protein tyrosine phosphatases (PTPase) was investigated with enzyme kinetic studies and vanadium nuclear magnetic resonance spectroscopy (^{51}V NMR) experiments. (Glycylde-N-hydroglycinato-$\kappa^3 N^2, N^N, O^1$)oxoperoxovanadate (glyglypV) and N,N-dimethylhydroxylamine/vanadate complexes were the vanadium(V) complexes used in these studies. Domain 1 of leukocyte common antigen-related PTPase (LAR-D1) and protein tyrosine phosphatase 1B (PTP1B) were the enzymes that were investigated. Using ultraviolet (UV) absorption spectroscopy, kinetics experiments with the glyglypV complex revealed that the inhibition of LAR-D1 by this complex is irreversible in the presence of 1 mM EDTA. These results indicated that the glycylglycine monoperoxovanadate complex influences PTPase activity via an oxidative inactivation mechanism. Kinetics experiments were also used to determine the inhibition constants for dimethylhydroxylamine/vanadate complexes. The results were consistent with inhibition via a reversible and competitive mechanism. Furthermore, the results obtained, together with the results from N,N,-dimethylhydroxylamine and dithiothreitol concentration variation experiments, indicated that the inhibitors were the bisligand dimethylhydroxylamine/vanadate complex (Vl_2) and, a complex formed by the reaction of dithiothreitol and dimethylhydroxylamine/vanadate (V/T). From solution equilibrium studies, the concentrations of each of the vanadium species present in the kinetic studies were determined and the individual inhibition constant (K_i) values for Vl_2 and V/T were calculated. K_i values of 1.0 µM and 2.3 µM were obtained for Vl_2 and V/T respectively. In order to investigate the mode of coordination in the V/T complex, ^{51}V NMR studies were carried out with several thiolate-containing compounds. These studies revealed that although coordination of vanadium is not monodentate with respect to the thiolate group, this group is critical for complex formation.

Furthermore, it was established that cysteine, which is an integral component of the catalytic site of protein tyrosine phosphatases, is also able to form complexes with dimethylhydroxylamine/vanadate. These results are considered in terms of the mechanism by which the inhibition of PTPases by Vl_2 and VlT complexes occurs.

To my mother and my grandmother: Sibongile and Lillian Mavuso,

for the inspiration to pursue my goals.

Acknowledgements

I would like to thank Dr. Alan Tracey for the invaluable guidance and insight which he has given me throughout this program, and for the opportunity to work on this project - I could not have had a better teacher.

I would also like to thank Dr. Pradip Paul for synthesising the vanadium compounds and for his friendship. To Barbara Campbell; thank you for sharing your SDS equipment and for your encouragement. Thank you also to Nick Glover for sharing the results from your molecular dynamics work and, to Marcy Tracey for acquiring the NMR spectra and for your warmth.

I am also grateful to Dr. Michael Gresser and the rest of the phosphatase group at Merck Frosst for providing the purified PTP1B enzyme and FDP substrate, particularly to Greg Huyer for sharing his unpublished data and for helpful advice. I would also like to thank Dr. Frank Jirik for providing the GST-LAR-D1 plasmid and for the opportunity to work in his laboratory. I also thank Nicole Jensen in Dr. Jirik's laboratory for her guidance during the protein purification phases of my project.

Finally, I would like to extend my thanks to all of my family in Swaziland for their support and encouragement and, to Marlon Mate for always managing to lift my spirits through the tough times.

Table of Contents

Chapter 6.

6. Complexation of Vanadate, N,N-Dimethylhydroxylamine
    and Dithiothreitol

Chapter 7.

7. Complexation of Vanadate, N,N-Dimethylhydroxylamine
    and L-Cysteine.

Chapter 8.

8. Inhibition Studies:
 Influence of N,N-dimethylhydroxylamine/vanadate and
N,N-dimethylhydroxylamine/vanadate-DTT Complexes
on GST-LAR-D1 PTPase and FLAG-PTP1B.

List of Tables

List of Figures

List of Abbreviations

Amp	ampicillin
boc	t-Butyloxycarbonyl group
BSA	bovine serum albumin
CAH	carbonic anhydrase
CBZ	carbobenzoxy group
c_L	total concentration of N,N,-dimethylhydroxylamine ligand
cV_t	sum of the concentrations of the dimethylhydroxylamineDTT/vanadate and monoligand dimethylhydroxylamine/vanadate complexes
Cys	cysteine
ddH_2O	distilled, deionised water
DMHA	N,N-dimethylhydroxylamine hydrochloride
DNase	deoxyribonuclease
DTT	dithiothreitol
EDTA	ethylenediaminetetraacetic acid
EGF	epidermal growth factor
ER	endoplasmic reticulum
f.c	final concentration
FDP	3,6-fluorescein diphosphate
FLAG	phenyalanine-leucine-alanine-glycine
FMP	fluorescein monophosphate
GEF	guanine nucleotide exchange factor
glyglypV	(glycylde-N-hydroglycinato-$\kappa^3 N^2, N^N, O^1$)oxoperoxovanadate
GST	glutathione-S-transferase
H_3PO_4	phosphoric acid

H_3VO_4	vanadic acid
HCP	hematopoietic cell protein tyrosine phosphatase
HEPES	N-(2-hydroxyethyl)-piperazine-N'-(2-ethane sulfonic acid)
[I]	inhibitor concentration
IC_{50}	concentration of inhibitor at 50% enzyme inhibition
IPTG	isopropylthio-β-galactoside
IRS-1	insulin receptor substrate 1
k_{cat}	catalytic rate constant / turnover number
kDa	kilo daltons
K_i	Inhibition Constant
K_m	Michaelis constant
$K_{m(app)}$	apparent value of the Michaelis constant
l	N,N,-dimethylhydroxylamine ligand
LAR	leukocyte common antigen-related
Lb	Luria broth
LCA	leukocyte common antigen
LIP.1	LAR interacting protein
NaCl	sodium chloride
NaOH	sodium hydroxide
NMR	nuclear magnetic resonance
PAGE	polyacrylamide gel electrophoresis
PDGF	platelet-derived growth factor
PTP1B	protein tyrosine phosphatase 1B
PTPase	protein tyrosine phosphatases
RPTPβ	receptor-like protein tyrosine phosphatase β
[S]	concentration of substrate
SDS	Sodium dodecyl sulfate
SH2	*src* homology 2

T cell	thymus cell
TCR	T cell antigen receptor
TEMED	N,N,N',N'-tetramethylenediamine
Tris	tris(hydroxymethyl)methylamine
UV	ultraviolet
v	enzyme reaction rate
V-DMHA-CYS	dimethylhydroxylamineCysteine/vanadate complexes
V-DMHA-DTT	dimethylhydroxylamineDTT/vanadate complex
v/v	volume per volume
V_1	monomeric vanadate
V_2O_5	vanadium pentoxide
Vl_1	monoligand dimethylhydroxylamine/vanadate complex
Vl_2	bisligand dimethylhydroxylamine/vanadate complex
VlC	dimethylhydroxylamineCysteine/vanadate complexes
VlT	dimethylhydroxylamineDTT/vanadate complex
V_{max}	maximal velocity
$[V_t]$	total vanadium concentration

CHAPTER 1

1. Introduction:

1.1. The Structural Features of Protein Tyrosine Phosphatases.

Protein tyrosine phosphatases (PTPases) are a family of enzymes, of which more than 50 have been identified, that are responsible for the dephosphorylation of phosphotyrosine residues in proteins. In conjunction with protein tyrosine kinases, PTPases regulate the balance of the tyrosyl-phosphorylation state of proteins (1,2). This is a critical function in signal transduction events, triggering or inhibiting several cellular processes such as cell cycle control, cell growth and differentiation, lymphocyte activation, and insulin receptor signalling (3-6).

Figure 1 illustrates the structural features of protein tyrosine phosphatases. These enzymes are commonly characterised as either intracellular or receptor-like PTPases (7,8). The intracellular PTPases are distinguished by a single catalytic domain of approximately 250 amino acid residues. Intracellular PTPases also contain non-catalytic regions which may perform regulatory functions and may be responsible for targeting the enzymes to certain types of substrates and to specific cellular sites (9). For example, src homology 2 (SH2) domains (as found in hematopoietic cell protein tyrosine phosphatase; also known as HCP or SH-PTP1), contain binding sites for phosphotyrosine on tyrosine kinases of various receptors such as the fibroblast growth receptor, platelet-derived growth factor (PDGF) receptor and the epidermal growth factor (EGF) receptor (4,10,11). Recent studies have suggested that the SH2 domains in PTPases may also serve to auto-inhibit the enzymes via an intramolecular association with the catalytic domain. This interaction can be reversed by the presence of competing phosphotyrosine (12). The intramolecular regulation and cellular targeting of protein tyrosine phosphatases is therefore expected to exert a tight control over the signal transduction pathways mediated by these enzymes.
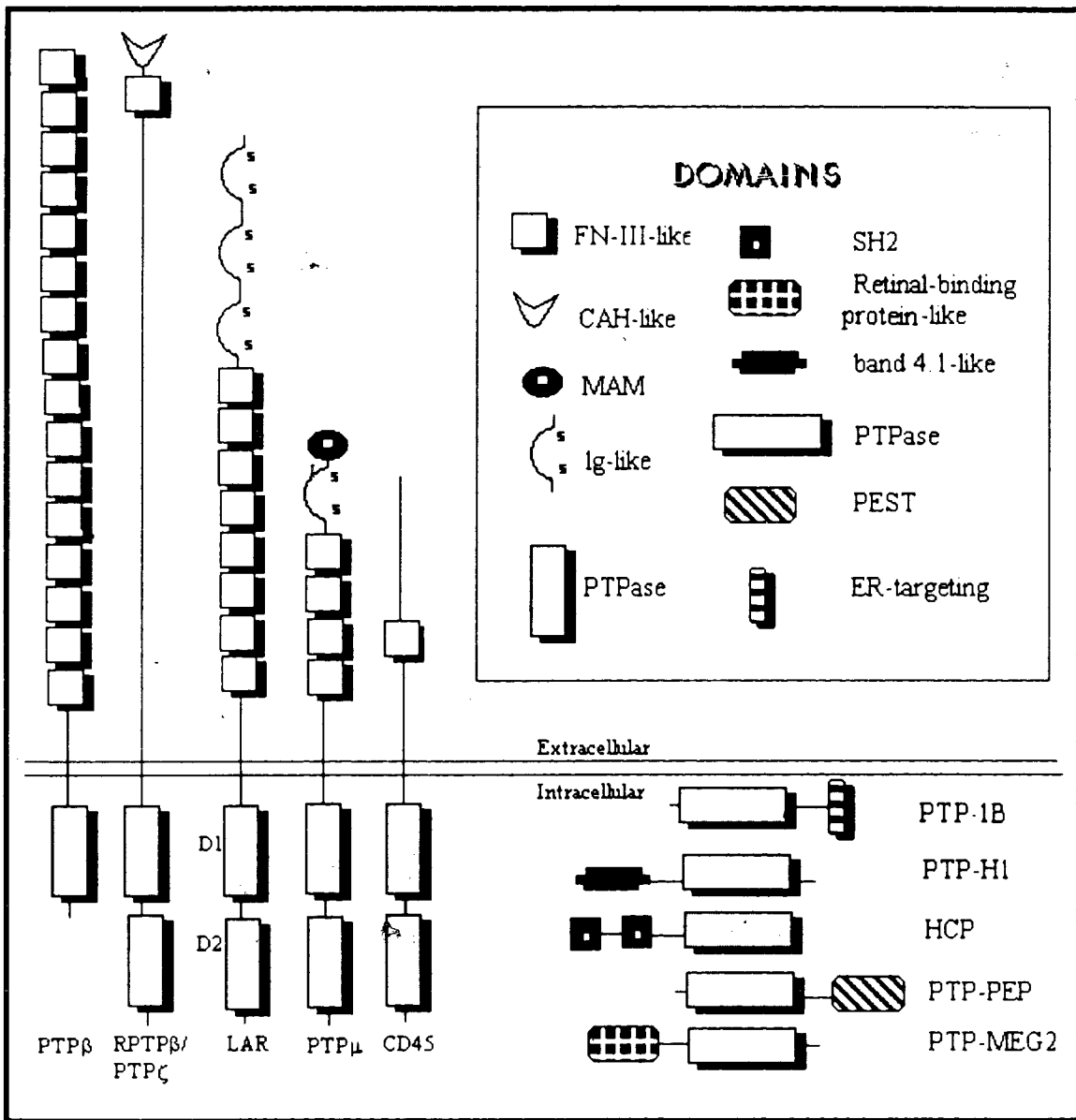
FIGURE 1.

Schematic diagram of the structural features of mammalian PTPases:

The figure illustrates the structural diversity and common features in a selection of the mammalian PTPases (adapted from reference 4). PEST: proline, aspartic acid, serine, threonine; ER: endoplasmic reticulum; MAM: meprin, A5, μ; Ig: immunoglobulin; FN-III: fibronectin type-III; CAH: carbonic anhydrase; SH2: *src* homology 2 (4).

2

Receptor-like PTPases are characterised by an extracellular domain, a single transmembrane segment, and a singular or repeated intracellular catalytic region of approximately 250 amino acids (13, 20). The biological role of the second catalytic domain is not clear at present. This domain may have a regulatory role and may also influence substrate specificity *in vivo*. In the CD45 PTPase (also referred to as leukocyte common antigen or LCA), mutagenesis studies have indicated that both catalytic domains are required for phosphatase activity (14). Conversely, studies on leukocyte common antigen-related (LAR) PTPase have demonstrated that the activity of the membrane proximal domain I is almost identical to the activity of the full length protein containing domain I and II. These investigations also revealed that domain II by itself has no catalytic activity (15,16).

The external regions of the receptor-like PTPases function as ligand-binding sites. For example, the extracellular carbonic-anhydrase-like domain in RPTPβ has been shown to bind contactin, a neural adhesion protein, thereby initiating neuronal adhesion and neurite growth (17). Furthermore, one of the ligands for CD45 has been identified as T cell antigen receptor (TCR). Binding of TCR to the extracellular domain of CD45 in T-lymphocytes results in the activation of a cascade of protein tyrosine kinases which are intrinsic to T-cell activation and the resultant onset of the immune response (18,19). Despite rapid progress in the investigation of these enzymes, the majority of the physiological ligands and substrates for protein tyrosine phosphatases have not been identified. Consequently, the sequence of events following protein-ligand association has yet to be determined for several of the PTPases and their respective ligands.

Protein tyrosine phosphatases are also characterised by the presence of one or two highly conserved catalytic domains consisting of about 250 amino acids (20). The active site signature sequence common to all PTPases is $(H/V)C(X)_5R(S/T)$ (21). These residues form a phosphate binding loop as evidenced from the crystal structure of protein tyrosine phosphatase 1B (PTP1B) (22). The invariant cysteine and arginine

3

residues are critical for PTPase activity as they are involved in the formation and stabilisation of a phosphoenzyme intermediate respectively (23,24).

1.2. The Catalytic Mechanism of PTPases.

The mechanism of the reaction catalysed by PTPases has been studied in great detail. The proposed catalytic sequence is summarised in Figure 2 (25). The reaction catalysed by tyrosyl phosphatases is initiated by nucleophilic attack by the thiolate of the PTPase active site cysteine on the phosphorus atom of the substrate. Phosphorylation of the enzyme is accompanied by protonation (by an aspartate residue) and expulsion of the tyrosyl group. The phosphorus atom of the thio-phosphate enzyme intermediate is then attacked by an activated water molecule, yielding free inorganic phosphate (25,26).

The transition states for phosphoenzyme intermediate formation and dissociation are stabilised by an extensive hydrogen bonding network between the active site residues and the substrate. Included in this network are the invariant serine/threonine hydroxyl groups which facilitate hydrolysis of the thio-phosphate enzyme intermediate (the rate limiting step) via hydrogen bonding with the thiolate group of the active site cysteine. This association stabilises the negative charge on the thiolate group (27,28). Furthermore, the side chain of the active site histidine is involved in hydrogen bonding to the carbonyl of the active site cysteine. This interaction is believed to stabilise the optimal orientation of the cysteine for nucleophilic attack on the phosphotyrosyl substrate (22). Additional stabilisation is provided by the side chain of the critical arginine residue found in the PTPase signature sequence. The guanidinium side chain of this residue forms a bidentate salt bridge with the terminal oxygens of the phosphate bound to the enzyme. This association is believed to stabilise the trigonal bipyramidal structure of the transition state (8, 22).

4

FIGURE 2.

Schematic figure of the reaction catalysed by protein tyrosine phosphatases:

1. Nucleophilic attack of the phosphotyrosyl residue by the thiolate ion of the catalytic cysteine is accompanied by protonation of the tyrosyl oxygen by the side chain of a catalytic aspartate. The first transition state is produced in this step.

2. Dephosphorylated product and a phosphoenzyme intermediate are released by cleavage of the phosphotyrosine bond.

3 and 4. Nucleophilic attack by an activated water molecule (likely deprotonated by side chain of a nearby aspartate) on the phosphorus atom of the thio-phosphate enzyme intermediate results in the regeneration of free enzyme and release of the phosphate group. The second transition state structure is produced in step 3 (25).

(Figure 2 is adapted from reference 25).
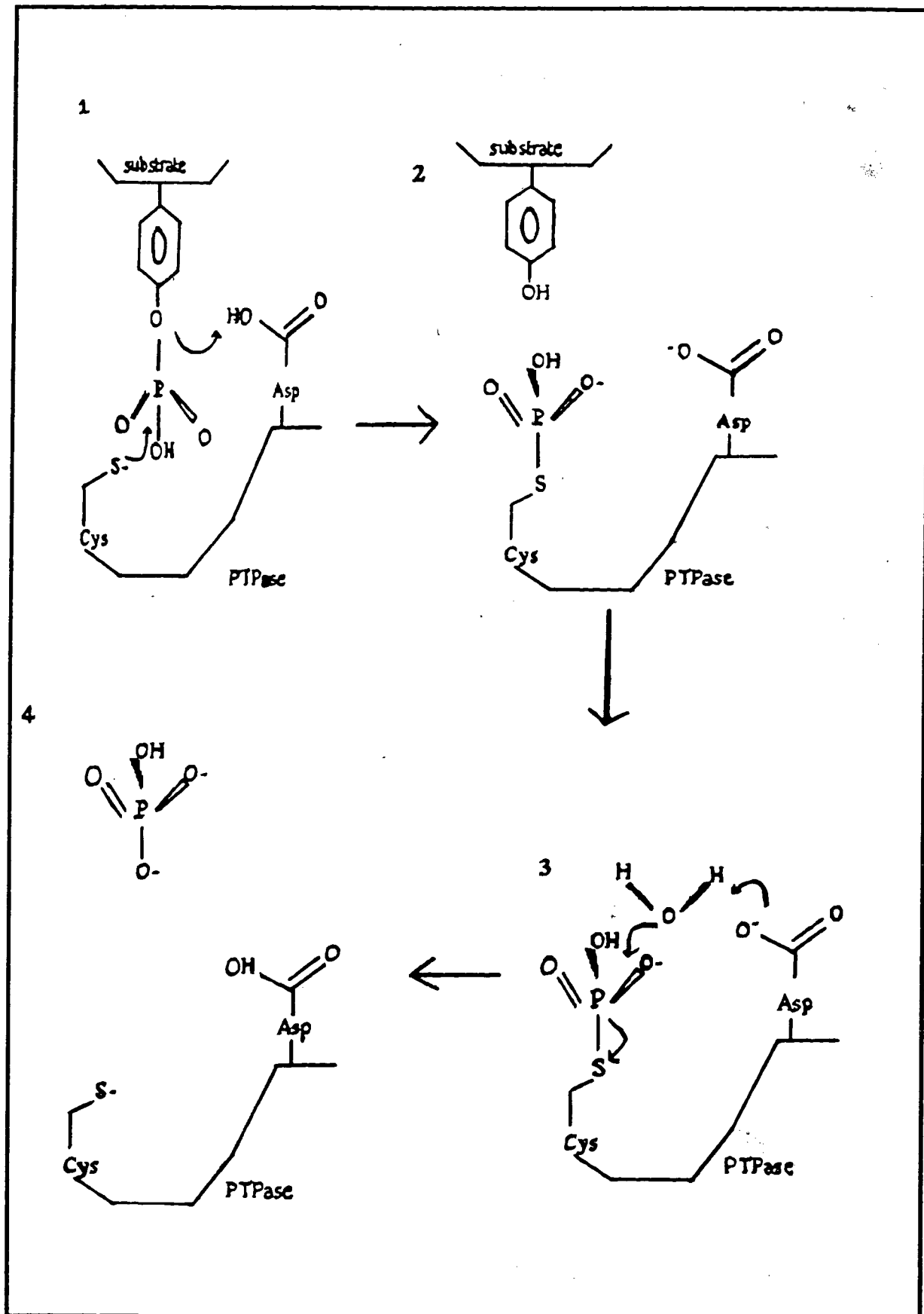
1.3. The Functional Significance of LAR PTPase and PTP1B.

There is little known about the cellular substrate specificity and functional roles of the tyrosine phosphatase enzymes used in this study; LAR PTPase and PTP1B. Both enzymes, however, have been implicated in the regulation of insulin receptor signal transduction. In 1992, Ramachandran and co-workers (29) demonstrated that PTP1B dephosphorylates the insulin receptor *in vitro*, at a phosphotyrosine region critical for activation of the receptor. Direct binding between insulin-stimulated insulin receptor and PTP1B has also been demonstrated, both in whole-cell lysates and in purified receptor assays (30, 31).

A recent study investigated the role of PTP1B in insulin receptor signalling. Kenner et al.(32) were able to show that overexpression of active PTP1B in fibroblast cell lines inhibits insulin-activated insulin receptor autophosphorylation. Insulin-stimulated phosphorylation of insulin receptor substrate proteins and incorporation of glucose into glycogen were also inhibited. These findings suggest that PTP1B is involved in down-regulation of insulin receptor signalling. The precise function of PTP1B in the insulin response has yet to be determined but this enzyme appears to play a key role in the modulation of insulin-stimulated signalling.

LAR PTPase has also been implicated in the regulation of insulin-mediated signalling pathways. This enzyme is expressed in insulin-sensitive tissues such as liver, skeletal muscle and adipose tissue and, has been shown to dephosphorylate the insulin receptor at critical tyrosyl residues (33,34). Furthermore, in 1995, Kulas and co-workers found that insulin-dependent autophosphorylation of the insulin receptor was increased by the suppression of LAR PTPase levels in rat hepatoma cell lines. The suppression of the enzyme also resulted in increases in the tyrosine kinase activity of insulin receptor substrate 1 (IRS-1) and phosphatidylinositol-3-kinase (a substrate for IRS-1) (35,36). Consistent with these observations, over-expression of LAR PTPase has been shown to have inhibitory effects on insulin receptor activity (37). Taken together, these results are consistent with a negative regulatory effect of LAR

on the insulin receptor. However, as with PTP1B, the physiological mechanisms involved in the mediation of insulin signalling by this enzyme are yet to be determined.

LAR PTPase has also been implicated in the regulation of other cellular signal transduction pathways. It has been proposed that LAR regulates the dissociation of focal adhesions, a process which involves tyrosine-dephosphorylation of several proteins. Focal adhesions are regions where the cell membrane and extracellular matrix associate to facilitate signal transduction events involved in processes such as cell migration, division and differentiation. This association also anchors actin stress fibres to the cell membrane. A LAR interacting protein (LIP.1) which binds domain 2 of the LAR PTPase (LAR-D2) has been isolated. This protein appears to localise LAR to focal adhesions, where there are several potential substrates for LAR PTPase during transmembrane signalling (38). LAR-D2 PTPase has also been shown to bind Trio, a tyrosine kinase protein containing *rac* and *rho*-specific guanine nucleotide exchange factor (GEF) domains. Since these domains are involved in regulating cytoskeletal reconstruction and focal adhesion formation, the LAR-Trio complex may mediate several related events which are critical to cell migration (39).

1.4. The Influence of Vanadates on Phosphoryl Transfer Enzymes.

It is apparent from the preceding discussion that PTPases not only act as inhibitors of protein tyrosine kinases, but, can also catalyse dephosphorylation events which activate tyrosine kinase activity and thereby amplify the corresponding signal transduction events. This observation has stimulated research into inhibitors of protein tyrosine phosphatases. These inhibitors can potentially serve as models for the development of therapeutic agents for conditions associated with aberrant PTPase activity such as diabetes, immune dysfunction and certain carcinomas. In addition, PTPase-specific inhibitors may be used to further probe the cellular function of particular tyrosine phosphatases (40).

8

Vanadium compounds are examples of PTPase inhibitors that have been utilised both as probes of PTPase function and as potential therapeutic agents. Vanadium is a transition metal found in all cells of both plants and animals. This element is essential for the growth of algae and certain species of *Azobacter* (41,42). However, the biochemical function of vanadium in humans is not known, and deficiency of vanadium in humans has not been correlated with a specific abnormality (43). Vanadium compounds have been recognised as inhibitors of protein tyrosine phosphatases and it is by this inhibition that they are thought to effect their insulin-mimetic actions (44). Vanadium compounds mimic a wide range of insulin-like actions both *in vitro* and *in vivo*. Examples of these effects are activation of insulin receptor kinase, glucose uptake and oxidation, and lipid biosynthesis (45,46,47). However, the mechanisms by which these influences are exerted are not well understood, primarily due to the complex solution chemistry of vanadium.

A key contributing factor to this complexity is the ability of vanadium to readily undergo redox chemistry and thereby exist in multiple oxidation states. In aqueous solution at physiological pH, vanadium is found in the +5 oxidation state, although vanadium (IV) (also known as vanadyl) may predominate under reducing conditions. The vanadium (+5) species found at neutral pH in aqueous solution are referred to as oxovanadates. The predominant species of oxovanadate found under these conditions is monomeric (V_1) vanadate, although other oligomers are also present in various protonated states (48,49).

In addition to redox chemistry, the ability of vanadium compounds to inhibit phosphoryl-transfer enzymes also derives from the flexibility of the coordination geometry of vanadium, and the similarity of the vanadate ion to the phosphate ion. For example, phosphate P-O bond lengths (0.17 nm) are very similar to vanadate V-O bond lengths (0.15 nm) and, the pKa values for vanadic acid (H_3VO_4) are similar to those for phosphoric acid (H_3PO_4) (50). In addition, five-coordinate trigonal bipyramidal geometry is a well known structure for vanadate, and is easily acquired

9

by complexation with various ligands. On the contrary, this coordination represents a high energy transition state for phosphate. Vanadate can thereby function as a transition state analog in certain phosphoryl transfer reactions by complexing with the dephosphorylated substrate. The vanadate-substrate complex then binds tightly to the enzyme, forming a stable structure which resembles the transition state for the formation of the phospho-enzyme intermediate. This mode of inhibition has been observed when additional binding interactions between the phosphate donor and the enzyme are critical for transition-state stabilisation, or, when the enzyme does not catalyse hydrolysis of a phosphoenzyme intermediate, with the exception of reactions of nucleoside phosphates. Vanadate (V_i) itself can also inhibit phosphoryl transfer. In this case, vanadate becomes bound to the functional group on the enzyme that becomes phosphorylated in the catalytic reaction. The vanadate-protein complex then functions as a transition state analog for the dephosphorylation step in catalysis (51).

The biochemistry of peroxovanadates has been the focus of several recent studies, which have noted the ability of these compounds to influence the activity of phosphoryl-transfer enzymes and induce several of the major metabolic effects of insulin (52,53,54). Peroxovanadate complexes are formed by the coordination of vanadate with one or more peroxo (O_2^{2-}) ligands from hydrogen peroxide. Peroxovanadates are able to coordinate other ligands such as peptides and amino acids to form compounds which are generally more stable than those of the parent peroxovanadate (55,56). Several studies have suggested that peroxovanadate compounds are more potent insulin-mimetics than vanadate (57,58). These influences of peroxovanadates are likely to be a consequence of the oxidising ability of these compounds and, for monoperoxovanadate and/or diperoxovanadate, have recently been correlated with the oxidation of the critical cysteine residue in protein tyrosyl phosphatases (59).

1.5. Objective of this Study:

The Influence of N,N-Dimethylhydroxylamine/vanadate and Glycylglycine/peroxovanadate Complexes on LAR PTPase and PTP1B.

Several studies have reported on the ability of vanadate and peroxovanadate complexes to mimic insulin function, and this has been linked to the ability of these compounds to inhibit PTPases (45-54). Despite the multitude of studies on the insulin mimetic actions of vanadate and peroxovanadate complexes (where various ligands are coordinated to the vanadate or peroxovanadate moiety) there is very little detailed information on the mechanisms by which these compounds influence the activity of PTPases. This is largely due to the lack of studies which have utilised purified enzymes and have attempted to identify the inhibitory species. Several of the investigations on the influence of vanadium compounds on PTPase activity have been performed from a biological perspective, using either whole cells or animal models of diabetes, and, largely ignoring the solution chemistry of vanadium. In these systems, there are often several enzymes present, in addition to the other compounds such as redox buffers and chelating agents which are commonly added to the assay solutions.

These additional components not only have the potential to complex with the vanadium compound under investigation, they may also promote hydrolysis, oxidation or reduction of the complex to form vanadate and/or other derivatives. Accurate determination of the inhibitory species of vanadium present is therefore difficult in these conditions. Consequently, no clear picture has emerged regarding the mechanisms by which vanadate and peroxovanadate complexes act to directly influence PTPase activity. A detailed investigation of the mechanisms of inhibition by examples of vanadate and peroxovanadate complexes therefore appeared to be of value in addressing these concerns.

In this study, kinetics experiments were carried out using ultraviolet (UV) absorption spectroscopy in order to observe and evaluate the inhibition of purified GST-LAR-D1 PTPase and FLAG-PTP1B enzymes by (glycylde-N-hydroglycinato-

κ^3N^2,N^N,O^1) oxoperoxovanadate (glyglypV) and dimethylhydroxylamine/vanadate complexes (shown in Figure 3). The N,N,-dimethylhydroxylamine and glycylglycine ligands were chosen as ligands to examine the effects of the inclusion of a metal-coordinating ligand on the mode of inhibition and on the inhibitory potency.

^{51}V nuclear magnetic resonance (NMR) spectroscopy was used in control experiments to determine the stability of the vanadium complexes under investigation, and, to determine the stoichiometry and formation constants of the complexes formed by the reaction of dimethylhydroxylamine/vanadate with cysteine and dithiothreitol. ^{51}V NMR was also utilised to determine the formation constants of the dimethylhydroxylamine/vanadate species present under the conditions of the inhibition assays. These NMR studies facilitated the calculation of the concentrations of each species present in the inhibition studies, and correction of the inhibition constants for the concentration of inhibitory species present in each assay solution.

This study investigates the influence of structurally different vanadium complexes on PTPase activity and provides evidence that a vanadate complex that inhibits PTPases is able to associate with thiolate groups of cysteine, a critical residue in these enzymes.

A:
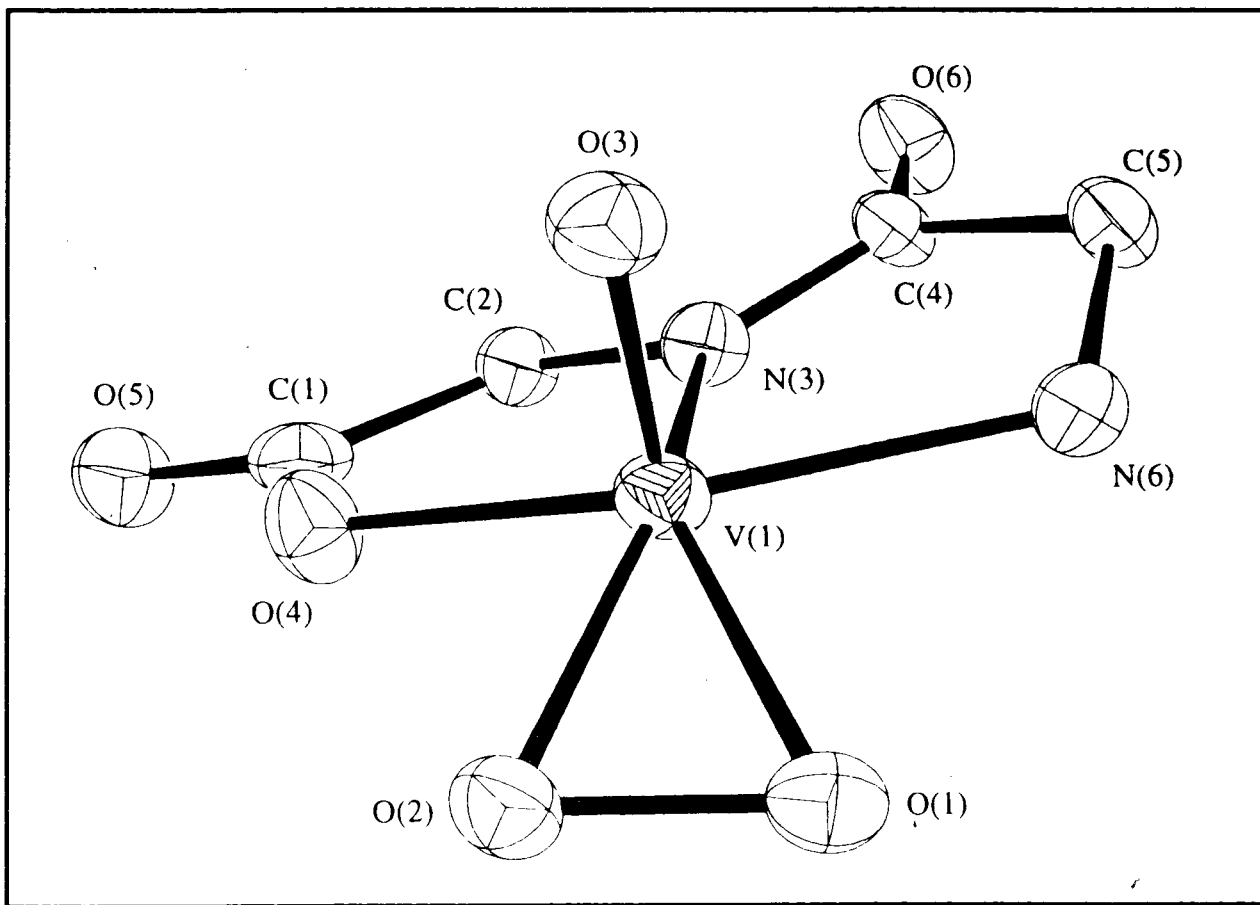
FIGURE 3.

A: Molecular structure of the (glycylde-N-hydroglycinato-κ^3N^2,N^N,O^1)

oxoperoxovanadate(V) anion:

The crystalline complex occurs as a weakly bound dimer which dissociates to two monomers in aqueous solution. One of the anions of the dimer is represented above. The hydrogen atoms are not shown (60).

B:
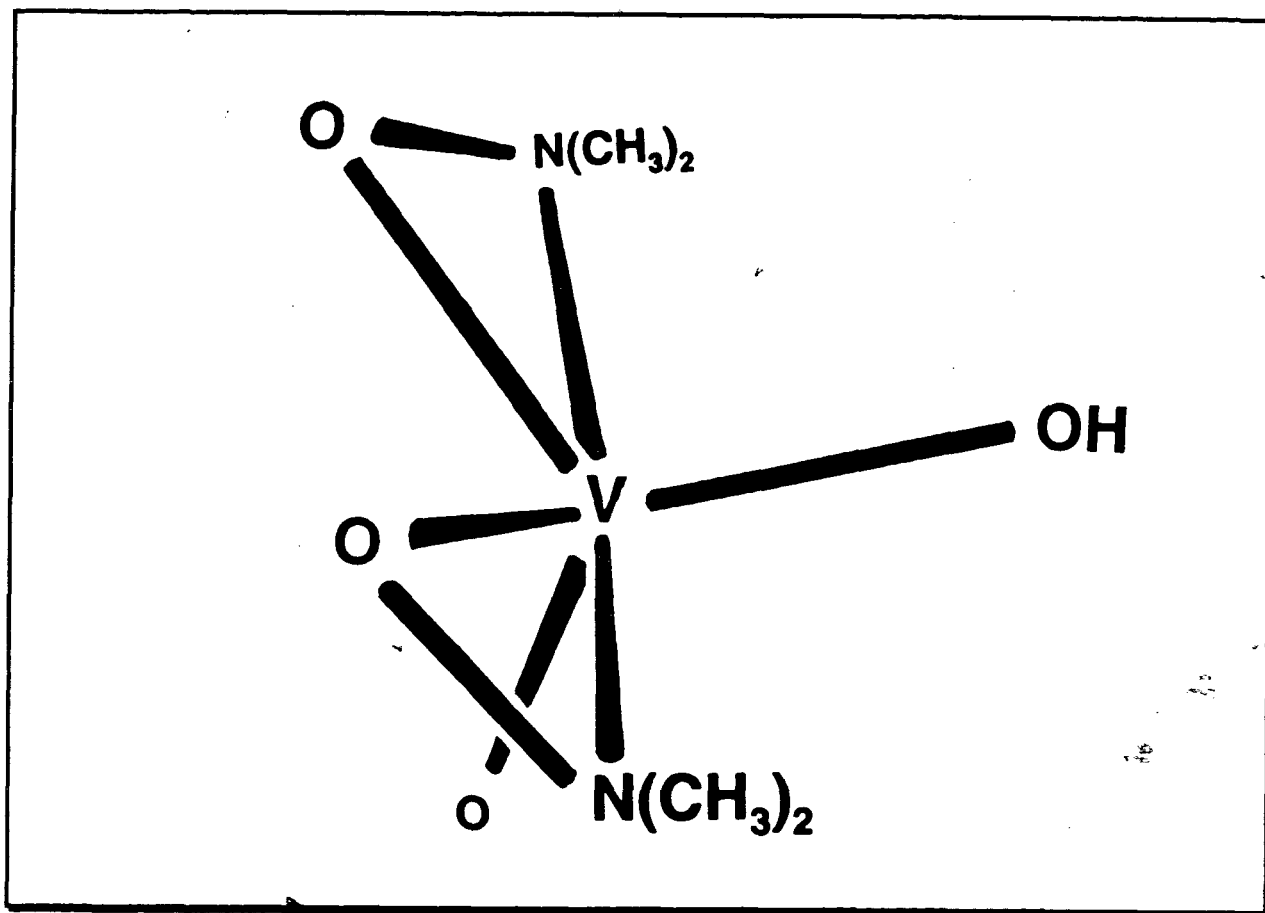
FIGURE 3B.

B: Molecular structure of bis(N,N-dimethylhydroxamido)hydroxooxovanadate:

The structure shown corresponds to the major bisligand product formed by the reaction of vanadate with N,N-dimethylhydroxylamine. The complex exists as a dimer in the crystalline form and hydrolyses in aqueous solution to the monomers, one of which is represented above (61).

CHAPTER 2

2. Materials:

All chemicals used were either of ultrapure or reagent grade. Ampicillin, isopropylthio-β-galactoside (IPTG), β-mercaptoethanol, ammonium persulfate, N,N,N',N'-tetramethylenediamine (TEMED), Triton X-100, reduced glutathione, deoxyribonuclease (DNase), magnesium chloride, lysozyme, Luria broth (Lb) medium ingredients, tris(hydroxymethyl)methylamine (Tris) base, Coomasie brilliant blue R-250 and bromophenol blue were purchased from Sigma Chemicals.

Sodium dodecyl sulfate (SDS), acrylamide and N,N',-methylene-bisacrylamide were obtained from Bio-Rad. Glycine, glycerol and sodium chloride (NaCl) were obtained from BDH. All of the protease inhibitors, Tris-HCl and bovine serum albumin (BSA) were obtained from Boehringer Mannheim. Glutathione-Sepharose 4B was purchased from Pharmacia. The centricon concentrators (molecular weight cut-off 50,000 daltons) were purchased from Amicon. The pGEX-LAR-D1 plasmid and *Escherichia coli* strain UT5600 were obtained courtesy of Dr. F. Jirik (University of British Columbia; Biomedical Research Centre).

Ethylenediaminetetraacetic acid (EDTA) and sodium hydroxide (NaOH) were purchased from Fisher Scientific. The protein tyrosine phosphatase (PTPase) substrate 3,6-fluorescein diphosphate (FDP) and the PTP1B enzyme (FLAG-PTP1B fusion protein) were provided courtesy of Dr. M. Gresser at Merck Frosst (Canada). N-(2-hydroxyethyl)-piperazine-N'-(2-ethane sulfonic acid) (HEPES) buffer, L-cysteine, D,L-cysteine, L-serine, L-cysteine-ethyl ester, mercaptoacetic acid, N,S-diCBZ-L-cysteine and dithiothreitol (DTT) were purchased from Sigma Chemicals. The glycylde-N-hydroglycinato-$\kappa^3 N^2, N^N, O^1$)oxoperoxovanadate (glyglypV) and bis(N,N-dimethylhydroxamido)hydrooxovanadate compounds were obtained crystallised in the laboratory (60,61). Vanadium(V) oxide (99.9%), N,N-dimethylhydroxylamine hydrochloride (DMHA) and *tert*butylmercaptan (3-methyl-2-propanethiol) were purchased from Aldrich Chemical Co. N-boc-L-cysteine was purchased from Fluka.

CHAPTER 3

3. Bacterial Expression and Purification of GST-LAR-D1:

3.1. Experimental Procedures.

3.1.1. Preparation of stock solutions and reagents:

Buffer A was composed of 25 mM Tris-HCl at pH 7.5, 150 mM NaCl, 10 mM β-mercaptoethanol. Elution buffer B contained 50 mM NaCl, 90 mM Tris-HCl pH 8.0 and 1 mM β-mercaptoethanol. Elution buffer C consisted of 50 mM reduced glutathione, 500 mM NaCl, 250 mM Tris-HCl pH 8.0 and 1 mM β-mercaptoethanol. Storage buffer D consisted of 30 mM Tris-HCl pH 8.0 and 10 mM β-mercaptoethanol.

Protease inhibitors were added to Buffer A to the following final concentrations (f.c): 100 μg/mL phenylmethylsulfonyl fluoride, 1 μg/mL aprotinin, 0.5 μg/mL leupeptin, 0.7 μg/mL pepstatin, 10 μg/mL soybean trypsin inhibitor, 40 μg/mL bestatin.

To remove the preservative from glutathione-Sepharose 4B, the beads were washed several times with Buffer A and 1% (v/v) Triton X-100. After the last wash the beads were resuspended in 1/3 bead volume Buffer A and 1% (v/v) Triton X-100 and stored at 4°C.

3.1.2. Preparation of GST-LAR-D1:

The preparation of the protein was accomplished as described by Dechert et al. (62), with modifications. The LAR-D1 cDNA, encoding the active catalytic domain of human LAR was provided (courtesy of Dr. Frank Jirik) sub-cloned in the Glutathione-S-transferase (GST) bacterial expression vector pGEX-2T.

The *Escherichia coli* strain UT5600 was transformed with the plasmid pGEX-LAR-D1. Selected colonies were grown overnight at 37°C in 50 mL of LB media at 100 μg/mL ampicillin (Amp). The overnight cultures were each diluted into 1 litre of

LB-Amp medium and incubated at 37°C until the OD_{600} was 0.7-0.8; typically about 4 hours. The cultures were then induced by the addition of isopropyl-β-thiogalactoside (f.c. 0.1 mM) and incubated overnight at 30°C with shaking.

The bacterial cells were sedimented by centrifugation at 4,000 rpm at 4°C for 20 minutes and resuspended in 2 mL of Buffer A containing protease inhibitors as described above. Lysis of the cells was accomplished by the addition of lysozyme (f.c 0.5 mg/mL) followed by incubation at 25°C for 15 minutes. The samples were subsequently frozen in liquid nitrogen and thawed in a 25°C water bath. The freeze-thaw procedure was repeated twice before the addition of $MgCl_2$ (f.c 10 mM), and DNase (f.c 0.1 μg/mL) followed by incubation for 20 minutes at 25°C.

EDTA (f.c 20 mM) and Triton X-100 (f.c 2.5% v/v) were then added and the lysates were incubated for 15 minutes at 25°C. The lysates were subsequently centrifuged at 30,000 rpm for 30 minutes at 4°C. The supernatant was then immediately aliquoted into 1 mL samples.

400 μL of washed glutathione-Sepharose 4B beads were added to each 1 mL aliquot of crude lysate. The mixture was then incubated for one hour at 4°C with periodic gentle rotation of the samples. After centrifugation at 2,000 rpm for 1 minute to sediment the beads, the supernatant was discarded.

In order to remove non-specifically bound contaminants, the protein-bead mixture was washed three times in Buffer A containing 1% Triton X-100 (v/v). The procedure involved the addition of 5 bed volumes of buffer to each sample, gentle mixing, sedimentation of the mixture by centrifugation at 2,000 rpm and, subsequent removal of the supernatant.

In order to elute the protein from the glutathione-Sepharose beads, the bead matrix was washed in elution buffer B and incubated in 3 bed volumes of glutathione elution buffer C, at 4°C for two hours with periodic mixing. After sedimenting the bead matrix, the supernatants were dispensed into centricon tubes (50,000 molecular

16

weight cut-off) in 2 mL volumes, and centrifuged at 5,000 x g at 4°C for 90 minutes in order to remove the low molecular weight contaminants. The retentate solutions obtained from this procedure were combined and exchanged to storage buffer D and glycerol at 20% (v/v).

The proteins were analysed using 10% or 12.5% SDS-polyacrylamide gel electrophoresis (SDS-PAGE; Bio-Rad minigel) and stained with Coomasie Brilliant Blue R-250. Protein concentrations were determined according to the Bradford (63) method with 1 to 10 µg BSA standards.

3.2. Experimental Results.

The yield of GST-LAR-D1 was approximately 5.8 mg from 3 litres of bacterial culture. Figures 4 and 5 illustrate the stages of the purification process. Corresponding to the GST-LAR-D1 fusion, a tyrosyl phosphatase protein of molecular weight 66 (kilo daltons) kDa, was obtained as the major band after purification using glutathione-Sepharose 4B and centricon filtration.
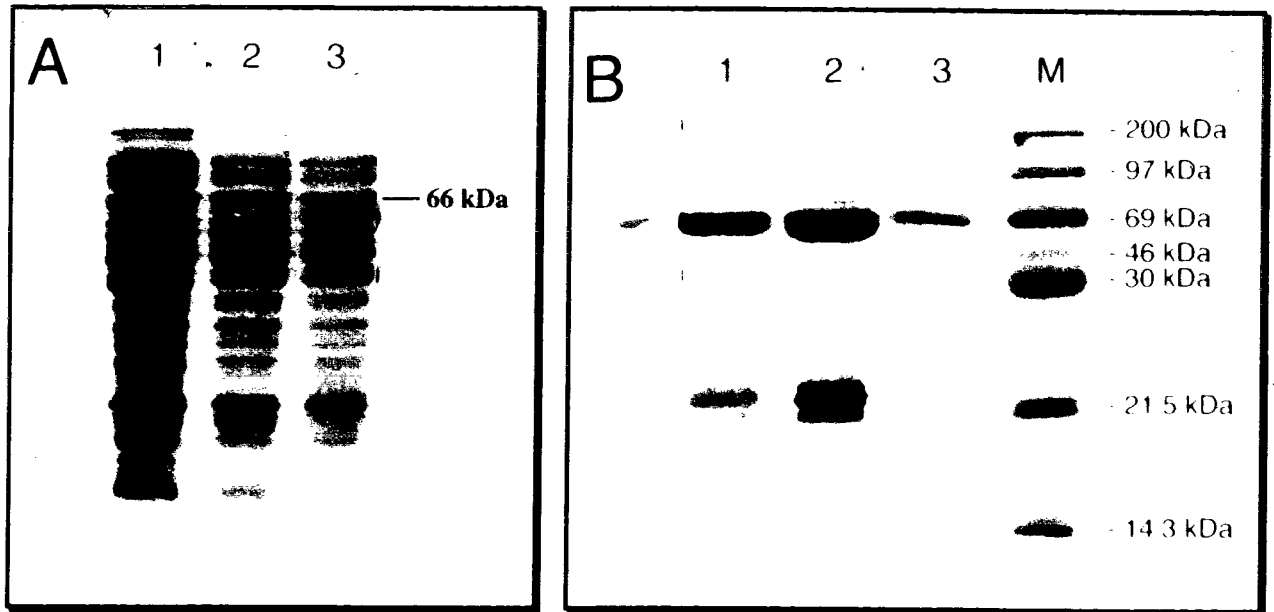
FIGURES 4A and 4B.

SDS-PAGE analysis of GST-LARD1:

Proteins were separated on 12.5% acrylamide gels and stained with Coomasie blue.

A:Crude lysates from bacterial cells before incubation with glutathione-Sepharose 4B beads.

Lanes 1-3 show crude extracts obtained from preparations of bacterial cells.

B: Crude lysates from bacterial cells after incubation with glutathione-Sepharose 4B beads.

Lanes 1-3 show the crude extracts from bacterial cells after incubation in the glutathione-Sepharose 4B bead matrix.

Lane M is the molecular weight marker.
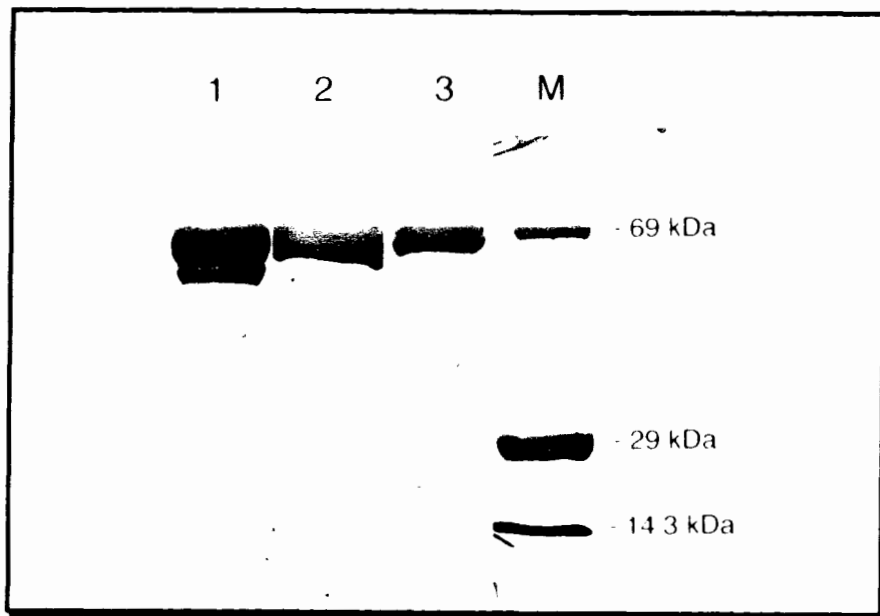
FIGURE 5.

SDS-PAGE analysis of purified GST-LAR-D1:

Lane 1 shows the GST-LAR-D1 fusion protein after combining the retentate solutions from the centricon filtration procedure.

Lanes 2 and 3 show the GST-LAR-D1 fusion protein obtained as the retentate after the centricon filtration procedure.

Lane M is the reference molecular weight marker.

19

CHAPTER 4

4. Inhibition Studies with a Glycylglycine Complex of Monoperoxovanadate:

4.1. Experimental Procedures.

4.1.1. FDP as a protein tyrosine phosphatase substrate:

3,6-fluoresçein diphosphate (FDP) was used as the substrate for the enzyme kinetic assays. The conditions for the assay of PTPase activity using FDP as a substrate were provided by Merck Frosst (Huang Z, personal communication). The primary product during the time course of the kinetic studies is fluorescein monophosphate (FMP), which is detectable in the 450-475 nm absorbance range. The reaction monitored is illustrated in Figure 6.

4.1.2. Preparation of stock solutions and reagents:

Stock solutions of the glycylglycine monoperoxovanadate complex (glyglypV) were prepared from the crystalline compound as follows. A stock solution of glyglypV of 1 mM was prepared in distilled, deionised water (ddH$_2$O), from which appropriate dilutions were made to prepare solutions of 1, 5, 10, 100, 500 and 800 μM final concentrations. The stock solutions were then left to equilibrate overnight.

The enzyme was diluted in the assay buffer which was freshly prepared and was composed of 20 mM HEPES; pH 7.3, 10 mM DTT and 50 μg/ml BSA as a stabiliser. FDP stock solution was prepared to a final concentration (f.c) of 188 μM. The inhibition assay solutions contained 50 μL buffer, 10 μL glyglypV stock solution, 1μL EDTA (f.c 1 mM), 10 μL diluted GST-LAR-D1 enzyme (f.c. 0.23 ng/μL), and 15 μL FDP (f.c. 28 μM). The solutions were made up to 100 μL with ddH$_2$O. The reaction rates were compared to a control prepared in the same manner, with the exclusion of glyglypV.

FDP (3,6-fluorescein diphosphate)

FMP
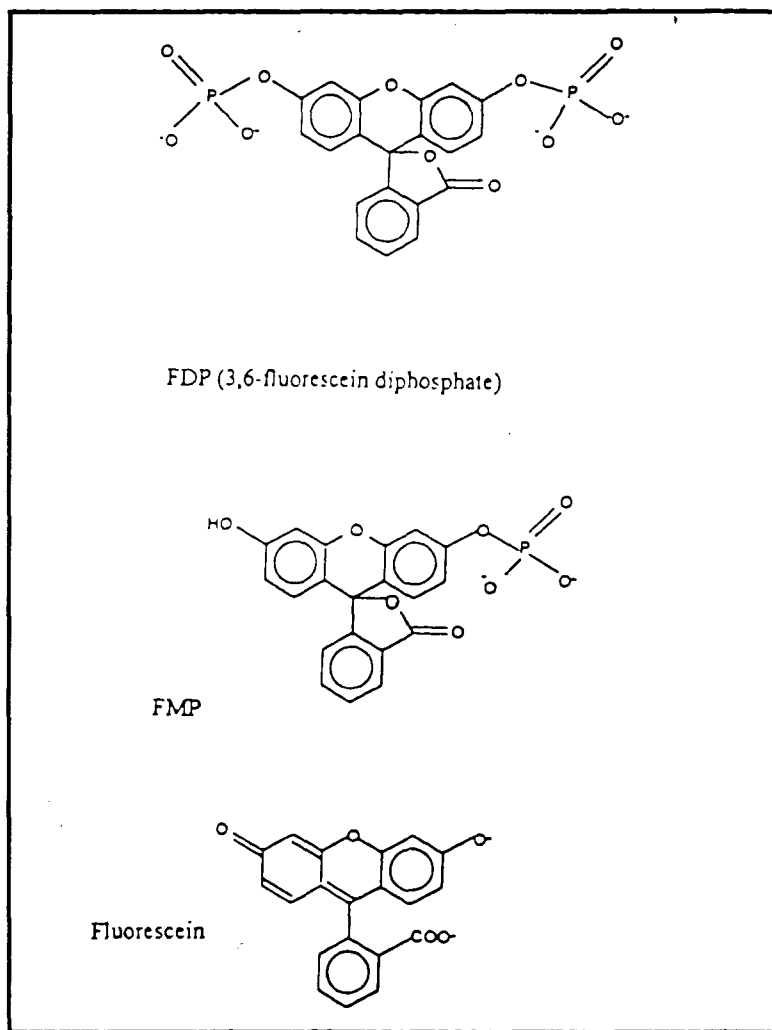
Fluorescein

FIGURE 6.

Dephosphorylation of FDP by protein tyrosine phosphatases:

The product monitored in the time period of the kinetic assays (10-20 minutes) is fluorescein monophosphate (FMP) which absorbs at 450-475 nm in the UV spectrum. Fluorescein absorbs at 488 nm and this second dephosphorylation occurs after several hours with PTPases. FDP is stable, with a half life of 2 years at pH 7, 25°C (Sylvie Desmarias, Merck Frosst, unpublished report).

4.1.3. Kinetic studies:

The kinetic measurements were made using a Hewlett Packard 8452A diode array spectrophotometer. The rates were calculated from a linear, least squares fit to the absorbance data. The analytical wavelength was 450 nm and the values were subtracted from those at 550 nm for internal referencing. The assay buffer was used as a blank for the kinetic studies. The reaction rates were recorded for 10 minutes at 30 second time intervals. The signal averaging time was 1 second such that each rate computed was the average of 10 scans.

The assay buffer, glyglypV, EDTA and water were mixed and pre-equilibrated at room temperature for 15 minutes prior to the addition of enzyme followed by a further incubation for 3 minutes. The reaction was then initiated by the addition of FDP to the solution with stirring. The kinetic measurements were started 3 minutes after the addition of substrate.

The dilution experiments were carried out by diluting the enzyme and glyglypV solution five-fold in assay buffer, FDP substrate and EDTA. The dilutions were made such that the final concentrations of FDP substrate, buffer and EDTA remained unchanged and, such that the glyglypV and enzyme were both diluted five-fold. Prior to the dilution, the rate was measured for 10 minutes. The contents of the cuvette were then diluted as described, stirred, and the rate re-measured for a further ten minutes, beginning five minutes after the dilution procedure. The reaction rates before and after dilution were compared to a control, prepared in the absence of glyglypV and diluted accordingly. The inhibition data before and after dilution is therefore given as the percentage of the control rate obtained prior to and following dilution, respectively.

4.1.4. ^{51}V NMR spectroscopy:

^{51}V NMR spectroscopy was used to monitor the purity of the compound in the absence and presence of EDTA. The spectra were obtained at 105 MHz using a Bruker AMX-400 NMR spectrophotometer. The parameters used were 60° pulse

widths, 60 KHz spectral widths and 0.05 second acquisition times. The vanadium chemical shifts were reported relative to the external reference $VOCl_3$ which was assigned as 0 ppm. These conditions apply to all the experiments to be described that were carried out with ^{51}V NMR.

4.2. Results and Discussion.

4.2.1. Kinetic studies in the absence of glyglypV:

Preliminary kinetic experiments were carried out in the absence of glyglypV in order to accurately determine the K_m concentration for FDP to be used in the inhibition assays. A rectangular hyperbola typical of enzyme saturation kinetics was observed in a plot of the reaction rate (v) versus the concentration of substrate $([S])$ as shown in Figure 7. Both sides of the Michaelis Menten equation were inverted as follows to give a linear transformation of the equation where K_m refers to the Michaelis constant and V_{max} to the maximal velocity at enzyme saturation:

$$v = \frac{V_{max}\,[\,S\,]}{K_m + [\,S\,]} \qquad [1]$$

$$\frac{1}{v} = \frac{K_m}{V_{max}}\frac{1}{[S]} + \frac{1}{V_{max}} \qquad [2]$$

A plot of $1/v$ versus $1/[S]$ gave a linear relationship as illustrated in Figure 8. A rate of 0.029 ± 0.002 sec^{-1} was obtained for V_{max}, and the K_m was calculated to be 28 $\pm$ 6 μM. Inhibition studies with the GST-LAR-D1 fusion protein were therefore performed at 28 μM. When the computed maximal rate was expressed in enzyme rate units of mols L^{-1} sec^{-1} (the extinction co-efficient for FMP at 450 nm is 27,500 M^{-1} cm^{-1} (59)), k_{cat} was calculated to be 5.2 ± 0.2 sec^{-1} for the GST-LAR-D1 enzyme.
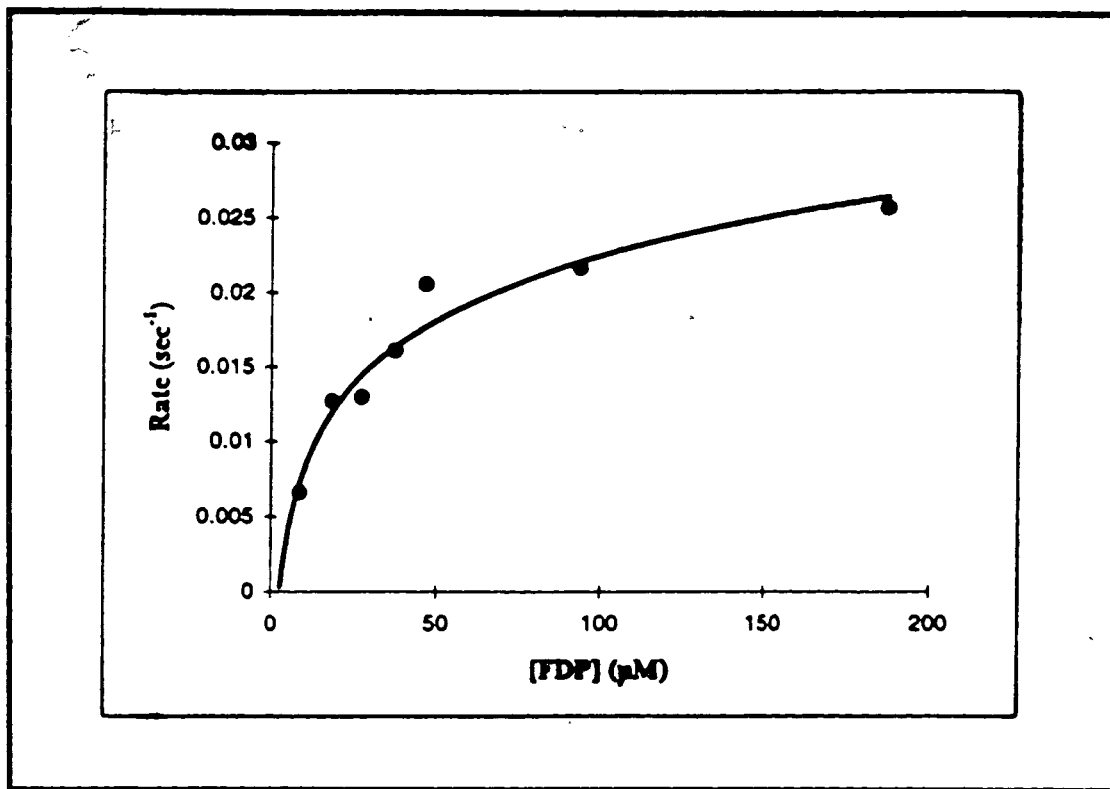
FIGURE 7.

Plot of reaction rate as a function of substrate concentration for GST-LAR-D1:

The rates are given by a linear fit to the absorbance data obtained at 450 nm over the time course (10 minutes; 3 minutes after the addition of FDP) of an experiment performed for each concentration of FDP substrate shown.
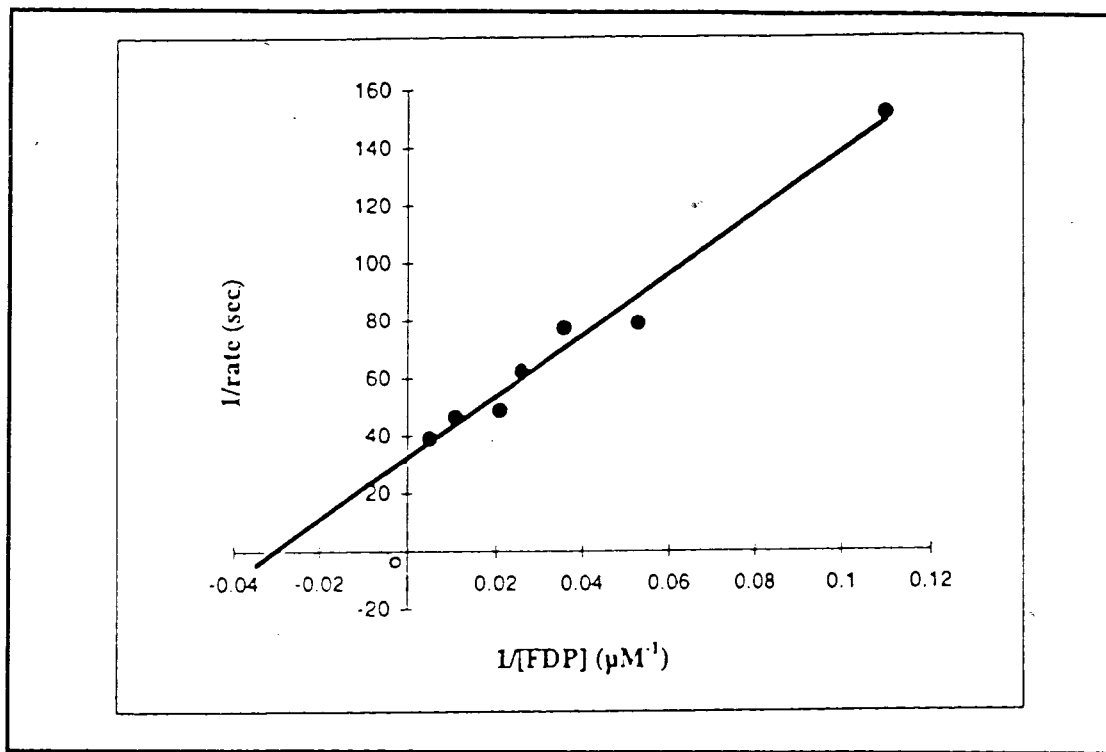
FIGURE 8.

Lineweaver Burke plot of the dephosphorylation of FDP to FMP by GST-LAR-D1 in the absence of inhibitor:

From the y-intercept of the graph the calculated V_{max} is 0.029 sec^{-1} and from the slope, the K_m for FDP is 28 μM.

4.2.2. Inhibition of GST-LAR-D1 PTPase by glyglypV:

EDTA is a known chelator of vanadate and the addition of EDTA has recently been shown to completely reverse PTPase inhibition by vanadate (59). The inclusion of EDTA in the assays thereby served to ensure that the inhibition observed was not due to vanadate. ^{51}V NMR analysis showed that a trace of vanadate was present in the glyglypV preparation (Figure 9), and that a minimum of 50 μM EDTA was sufficient to remove all of the vanadate from a 300 μM solution of glyglypV (Figure 10). NMR spectra taken at increasing EDTA concentrations of up to 1 mM, gave identical spectra to the one seen at 50 μM EDTA. There was no evidence from these NMR spectra to suggest that EDTA complexed the glyglypV compound or that any other reaction occurred between glyglypV and the buffer components. In the presence of sufficient EDTA, the species of vanadium present in the inhibition assays was thereby inferred to be the glyglypV compound. Consistent with the NMR observations, the inclusion of excess (1 mM) EDTA in the assay resulted in an upward shift (from 10 μM to about 100 μM) in the concentration of glyglypV required for 50% inhibition (IC_{50}) (Figure 11). This was expected since the inhibition constant for vanadate inhibition of PTP1B is 0.4 μM, and is expected to be of similar magnitude for LAR-D1 (59). The EDTA, which was pre-incubated with the glyglypV and buffer solution prior to the kinetic analysis, represents a greater than ten-fold excess to that required to chelate vanadate from a 300 μM glyglypV solution. Therefore, in the enzyme inhibition studies, EDTA was present at greater than thirty-fold excess since the maximum glyglypV concentration that was used in the inhibition studies was 100 μM. At these concentrations of EDTA, it was therefore concluded that there was effectively no free vanadate present. The presence of 1 mM EDTA did not influence the activity of the enzyme in the control assay solution, which was prepared in the absence of glyglypV. From these studies, the true IC_{50} of the glyglypV compound was therefore estimated to be 100 μM.
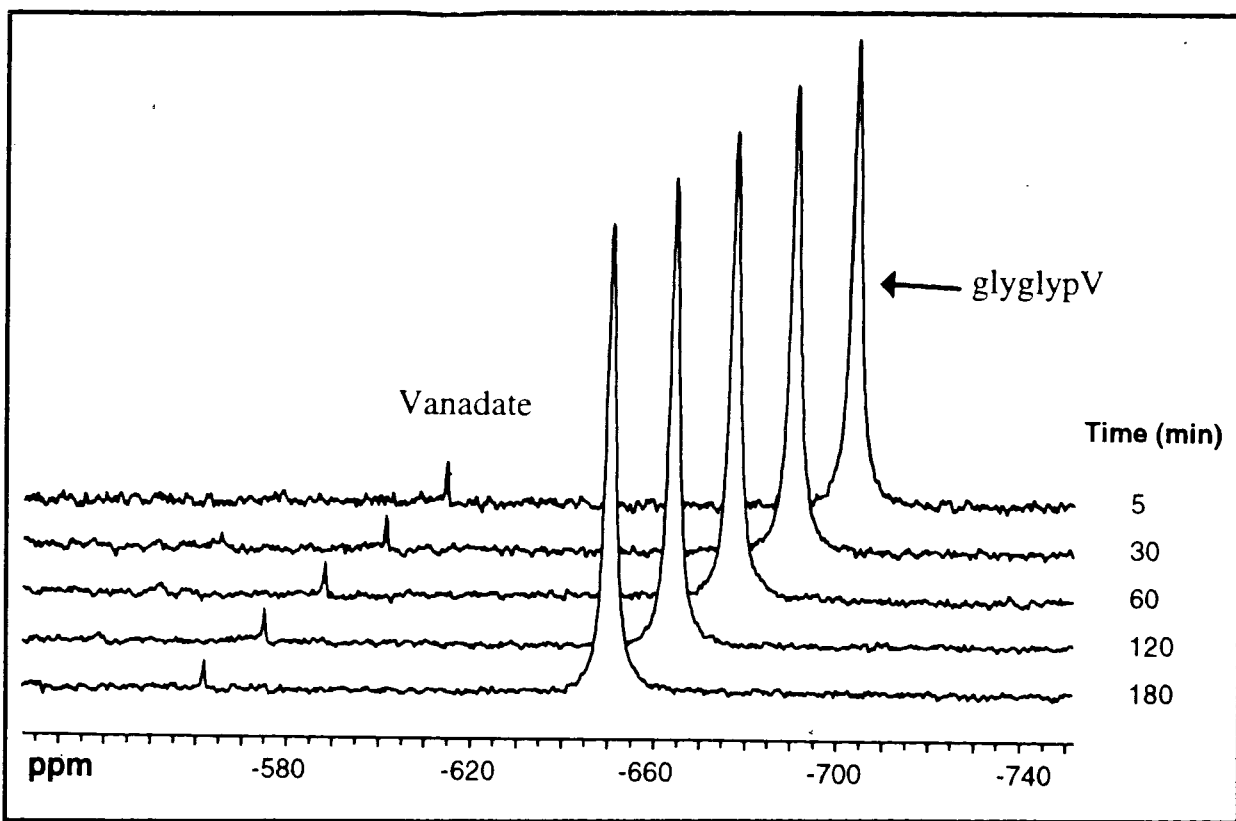
FIGURE 9.

^{51}V NMR spectra of 300 μM glyglypV in kinetic assay buffer:

The signal at -649 ppm corresponds to glyglypV and the signal at -550 ppm corresponds to vanadate. The solution was monitored periodically for up to 3 hours after initial mixing; no change was observed in the spectra.
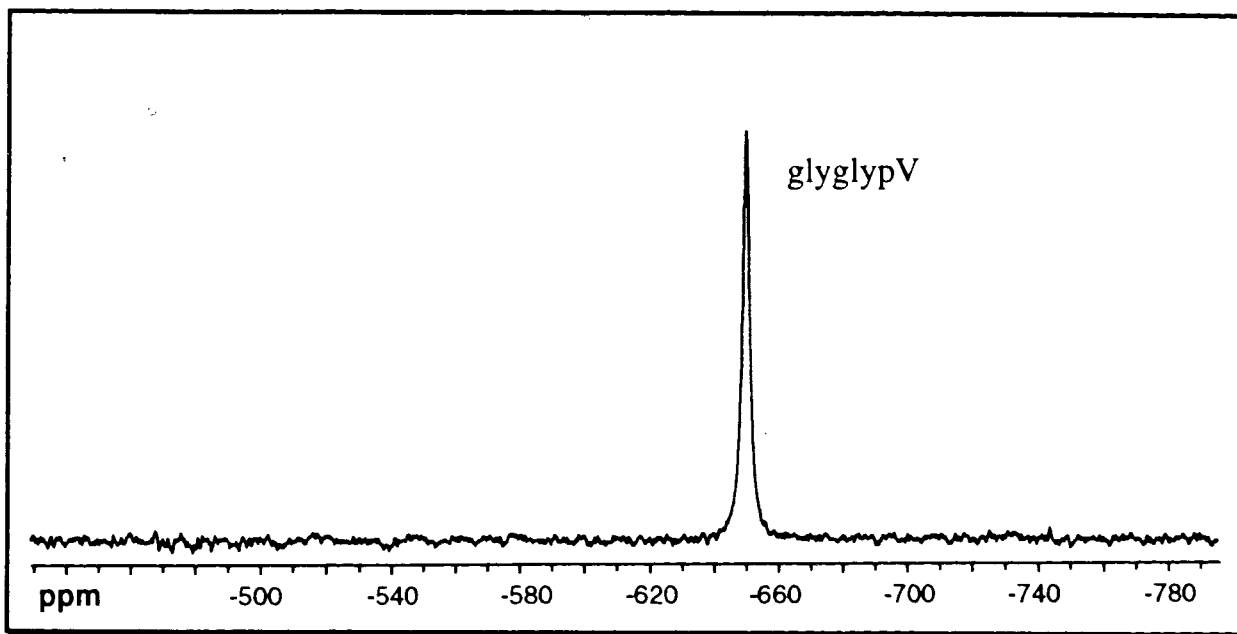
FIGURE 10.

EDTA completely chelates vanadate from the glyglypV solution:

50 μM EDTA was sufficient to remove the trace of vanadate present in a 300 μM

glyglypV sample. Subsequent spectra taken at EDTA concentrations up to 1 mM gave

the same result as shown above for 50 μM EDTA.
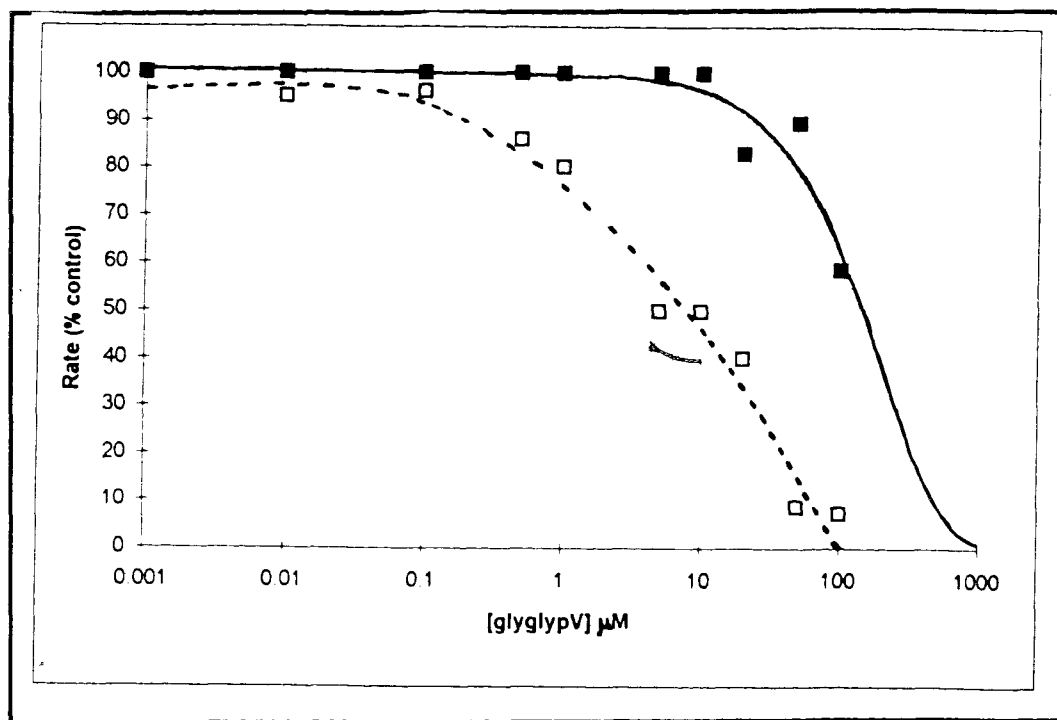
FIGURE 11.

Inhibition of GST-LAR-D1 by glyglypV in the presence and absence of EDTA:

The rates in the absence and presence of EDTA are given as the percentage of the rate of control assays which were prepared in the absence of glyglypV under the respective EDTA conditions. The open squares represent the data obtained in the absence of EDTA. The closed squares represent the data obtained in the presence of 1 mM EDTA.

4.2.3. Inhibition of LAR-D1 by glyglypV is irreversible by dilution:

In order to further establish that the inhibition observed in the presence of excess EDTA was not due to any residual vanadate, the reversibility of the inhibition was examined by a series of dilution experiments which were carried out in the presence of sufficient EDTA to chelate vanadate. Vanadate inhibition of PTPases is completely reversible by dilution. On the contrary, oxidation of the active site cysteine, which is believed to be the primary mechanism by which peroxovanadates inactivate these enzymes, is irreversible by dilution (59). It was therefore expected that irreversibility of the inhibition in the presence of EDTA, would indicate oxidative inactivation of the enzyme and thereby exclude vanadate as the inhibitory species.

The results obtained are shown in Figure 12. There was no recovery of activity at each of the concentrations assayed when five-fold dilutions of the glyglypV inhibitor were made into solutions containing buffer, EDTA and FDP. The IC_{50} was at approximately 90 µM before and after dilution of the inhibitor. This result is consistent with the inference that the inhibition observed in the presence of EDTA was not due to vanadate but rather indicates that irreversible inactivation of enzyme occurred. This agrees with other studies which have demonstrated, using mass spectrometry, that the catalytic cysteine in PTP1B is oxidised by glyglypV to the cysteic acid (Huyer G, unpublished data).

It is therefore proposed that the glycylglycine monoperoxovanadate complex is able to influence PTPase activity by an irreversible inactivation mechanism. At the molecular level, this may be achieved if there is sufficient flexibility in the active site to allow this complex to gain sufficient proximity to donate oxygen to the critical cysteine residue. Examining the IC_{50} values alone would suggest that the glyglypV is not a very potent inhibitor of LAR-D1 PTPase. However, the ability of this compound to oxidise the enzyme at micromolar (90-100 µM IC_{50}) concentrations is surprising given the presence of 10 mM dithiothreitol in these assays. Dithiothreitol is required to keep the enzyme catalytic cysteine in its active reduced state. Since the DTT is

present at much higher concentrations compared to the enzyme, this result indicates that the interaction of glyglypV with the PTPase is highly favoured. This conclusion correlates well with a recent finding for peroxovanadate and DTT, which suggests that peroxovanadate was able to oxidise the catalytic cysteine in PTP1B to the cysteic acid ($-SO_3H$) at DTT concentrations of up to 15 mM (59).

This study provides preliminary evidence suggesting that peroxovanadate complexes themselves have the ability to directly influence enzyme activity in that the NMR spectroscopy and dilution studies both indicated that glyglypV is the inhibitory species in this case. Although the requirements for potent inhibition by peroxovanadate complexes have not been determined by this preliminary work, this result, by showing a direct effect of the complex itself on the PTPase enzyme, opens up the possibility of altering the potency of peroxovanadium compounds by varying the ligands and their mode of coordination to the vanadium atom.
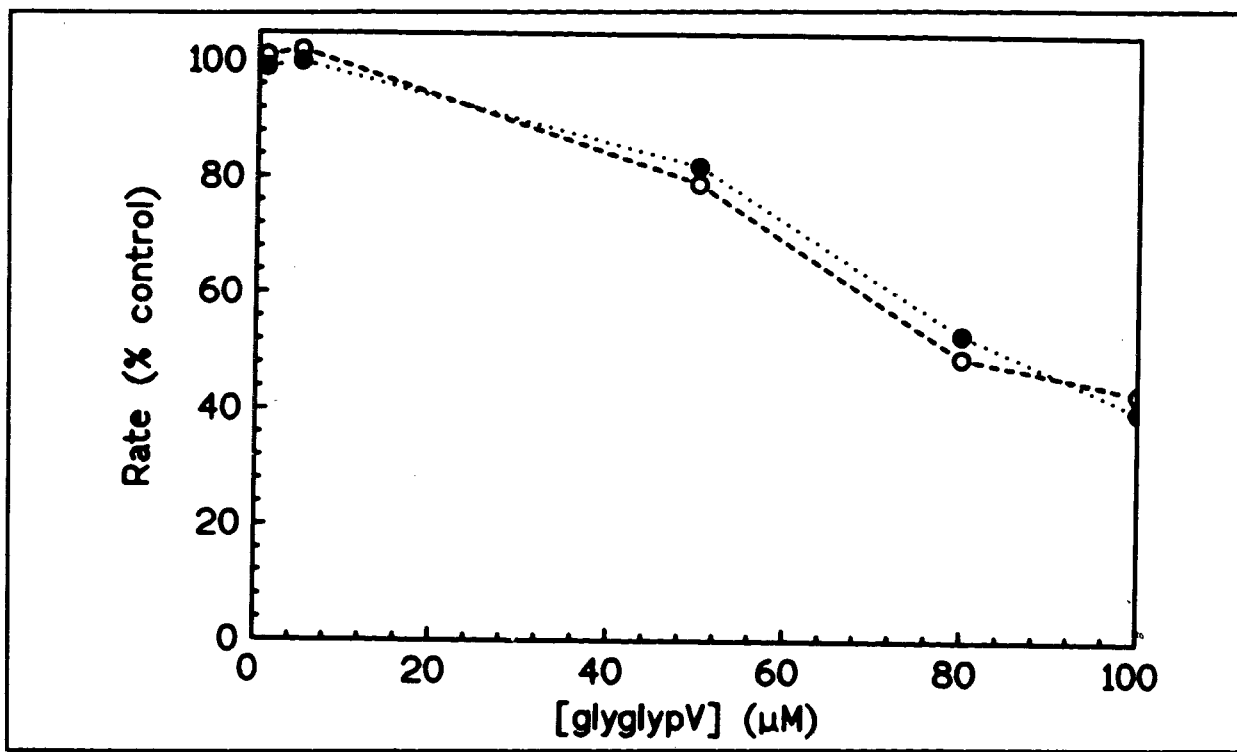
FIGURE 12.

Inhibition of GST-LAR-D1 in the presence of EDTA is irreversible by dilution:

Closed circles represent the inhibition data obtained before dilution and open circles show the data obtained after dilution into buffer and FDP substrate. The results are expressed as the percentage of the control rate. The control was prepared in the absence of inhibitor and diluted in the same manner as the solutions containing glyglypV. This result was reproduced in a replicate experiment.

CHAPTER 5

5. Equilibrium Formation Constants for the Reactions of Vanadate with N,N-Dimethylhydroxylamine:

5.1. ^{51}V NMR.

^{51}V nuclear magnetic resonance spectroscopy càn be used to determine the stoichiometry of vanadium coordination with various ligands. When the corresponding NMR signals are assigned, the equilibrium concentrations of each vanadium species can be calculated by integration of the relative signal intensities. The corresponding formation constants can then be determined from the derivation of an equilibrium equation for the reaction (56).

The formation constants for each of the products formed from the reaction of vanadate with N,N-dimethylhydroxylamine (DMHA) were calculated. This was to facilitate determination of the amounts of each species present under the conditions of each of the enzyme inhibition assays performed with the vanadium-DMHA complexes. NMR conditions were as described previously. Baseline corrections were made to the spectra before they were integrated.

5.2. Experimental Procedures.

5.2.1. Preparation of stock solutions:

Sodium vanadate solution at 0.50 M was prepared by dissolving 0.50 molar equivalents of vanadium pentoxide (V_2O_5) in 1.0 M NaOH. The mixture was then stirred overnight until the solution was colourless, indicating that all the vanadium pentoxide was in solution. The sodium vanadate solution was then diluted to 10 mM with distilled water. Stock solutions of 100 mM DMHA hydrochloride and 50 mM HEPES buffer were prepared in distilled water.

5.2.2. Preparation of solutions for ^{51}V NMR analysis:

All the solutions were prepared at 2.5 mM HEPES, 1 or 2 mM vanadate, and pH 7.3. Solutions of different ligand concentrations were prepared as follows: Stock solutions of vanadate, HEPES, and DMHA were added in appropriate quantities and diluted to close to the final volume with distilled water. Small amounts of NaOH and distilled water were then added as required to make the final volume of 2.5 mL and final pH of 7.3.

5.3. Results and Discussion.

The products formed from the reaction of N,N-dimethylhydroxylamine (DMHA) with vanadate have recently been assigned and are illustrated in Figure 13. The signals near -630 ppm correspond to the monoligand dimethylhydroxylamine products and the signals near -740 ppm correspond to the bisligand products. The broad signals in this region correspond to the major bisligand products which are stereoisomers. The formation constants were calculated from the relative concentrations of each species using the following equilibrium expressions, where V_1 is vanadate, l is the DMHA ligand, Vl_1 is the monoligand product and Vl_2 is the bisligand product (61).

$$V_1 + l \; \overset{K_1}{\rightleftharpoons} \; Vl_1 \qquad\qquad [V_1]\,[l]\,K_1 = [Vl_1] \qquad\qquad [3]$$

$$V_1 + 2l \; \overset{K_{12}}{\rightleftharpoons} \; Vl_2 \qquad\qquad [V_1]\,[l]^2\,K_{12} = [Vl_2] \qquad\qquad [4]$$

$$Vl_1 + l \; \overset{K_2}{\rightleftharpoons} \; Vl_2 \qquad\qquad [Vl_1]\,[l]\,K_2 = [Vl_2] \qquad\qquad [5]$$
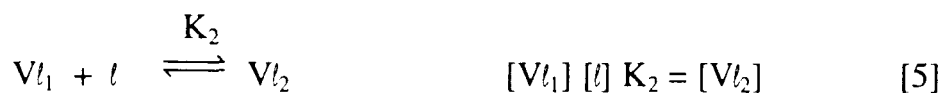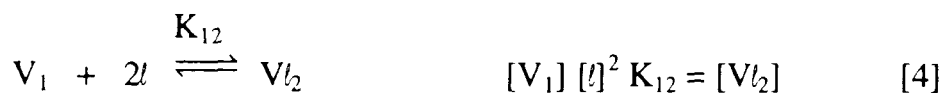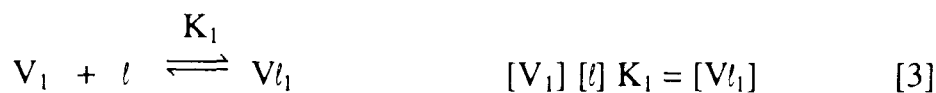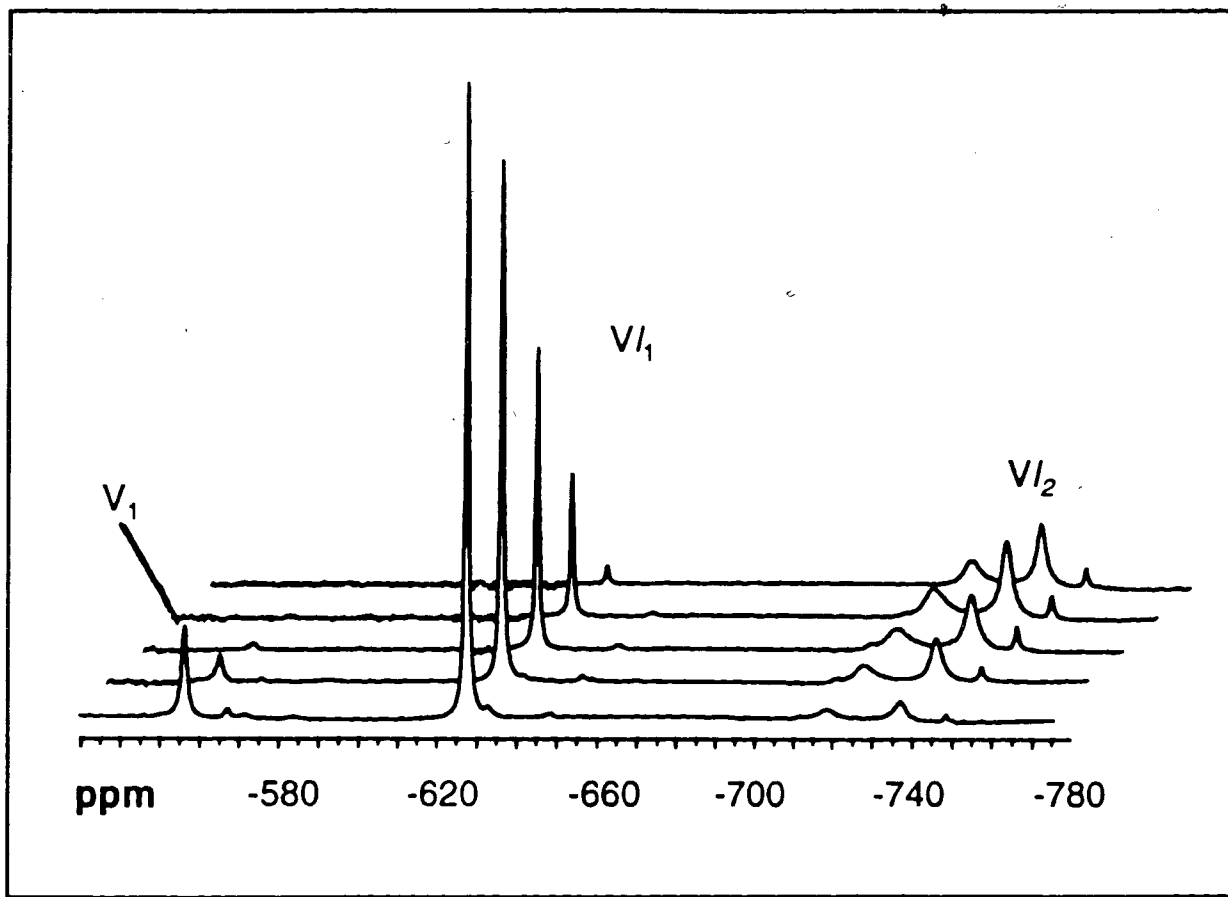
FIGURE 13.

^{51}V NMR spectra of the formation of complexes of vanadate and N,N-dimethylhydroxylamine:

The signals near -550 ppm correspond to vanadate monomer and dimer; V_1 and V_2, from low to high field respectively. The signals near -630 ppm correspond to the monoligand dimethylhydroxylamine/vanadate complexes (Vl_1) and the signals near -740 ppm correspond to the bisligand products (Vl_2). The two major products at -740 ppm correspond to stereoisomers of Vl_2 whereas the minor signal in this region is a Vl_2 complex with different coordination geometry (61). Conditions are pH 7.3, Vanadate 1 mM, DMHA increased from 0.5 to 20 mM and HEPES at 2.5 mM. The spectra shown above correspond to the following concentrations of DMHA, from bottom to top: 2, 3, 5, 7 and 20 mM DMHA.

The conservation equation [6] was used to determine accurately the concentration of free DMHA ligand ($[l]$) in terms of the monoligand and bisligand products' concentration and total ligand concentration (61):

$$c_{l_t} = [l] + [Vl_1] + 2[Vl_2] \qquad [6]$$

Since the formation constants for the products were rather large, very small increases in the amount of ligand resulted in a large decrease in the amount of free vanadate and a large increase in the amounts of bisligand products, as evidenced in Figure 13. In order to minimise the accompanying error in the plots, the DMHA concentration was plotted on the x-axis which gave a larger more convenient spread of the data points than a conventional plot of the product of vanadate and dimethylhydroxylamine concentrations on the x-axis.

The results obtained from a DMHA ligand concentration study are shown in Figures 14, 15, and 16. The values for the formation constants obtained each represent the average of three independent concentration studies. These averaged values were $(2.0 \pm 0.6) \times 10^4 \, M^{-1}$, $(9.7 \pm 0.3) \times 10^2 \, M^{-1}$, and $(2.1 \pm 0.4) \times 10^7 \, M^{-1}$, for K_1, K_2 and K_{12} respectively, where K_{12}, within the experimental error of the studies, is equal to the product of $K_1 K_2$ (From equations [3], [4] and [5], K_{12} should be equal to $K_1 K_2$).
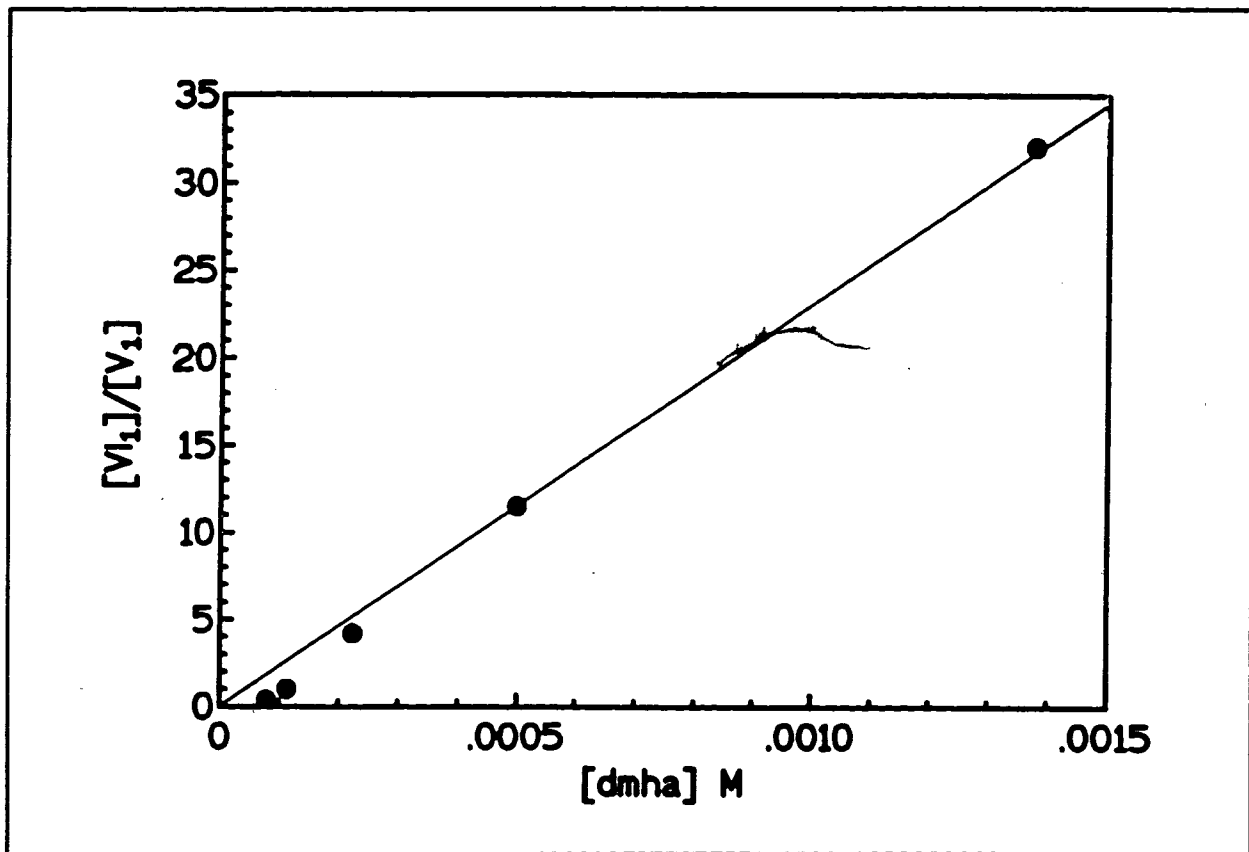
FIGURE 14.

Results from N,N-dimethylhydroxylamine concentration study at pH 7.3

Plot of $[Vl_1]/[V_1]$ versus $[l]$:

The formation constant, K_1, was determined from the slope of the plot as shown in equation [3]. $K_1 = (2.0 \pm 0.6) \times 10^4 \, M^{-1}$. This value for the formation constant K_1 is given by the average of three separate experiments of which one is shown above. The conditions of this experiment were pH 7.3, 2 mM vanadate, and 2.5 mM HEPES. The total concentration of N,N,-dimethylhydroxylamine ligand (cl_t) was varied from 0.5 to 10 mM.
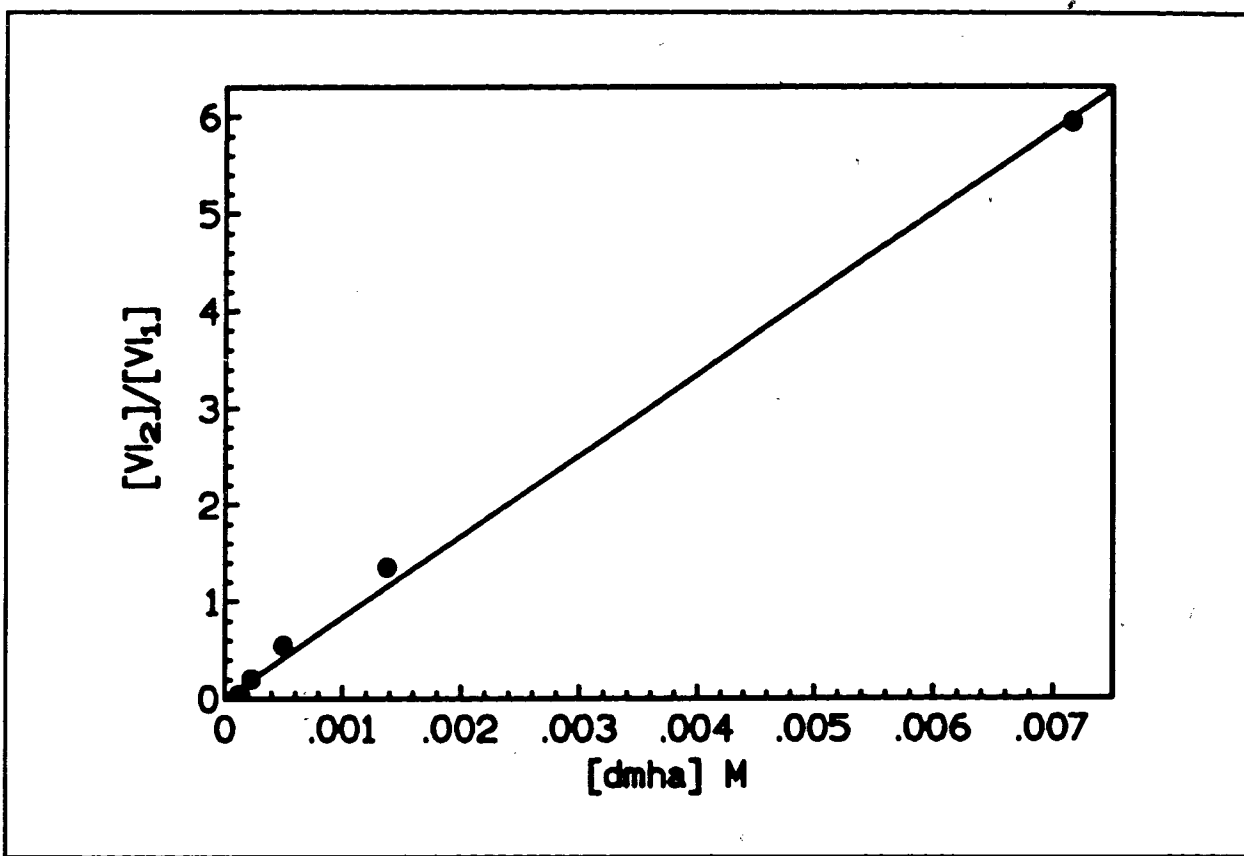
FIGURE 15.

Results from N,N-dimethylhydroxylamine concentration study at pH 7.3

Plot of $[Vl_2]/[Vl_1]$ versus $[l]$: _

The formation constant, K_2, was determined from the slope of the plot as shown in equation [5]. $K_2 = (9.7 \pm 0.3) \times 10^2 \text{ M}^{-1}$. This value for the formation constant K_2 is given by the average of three separate experiments of which one is shown above. The conditions of this experiment were pH 7.3, 2 mM vanadate, and 2.5 mM HEPES. N,N,-dimethylhydroxylamine ligand (cl_t) was varied from 0.5 to 10 mM.
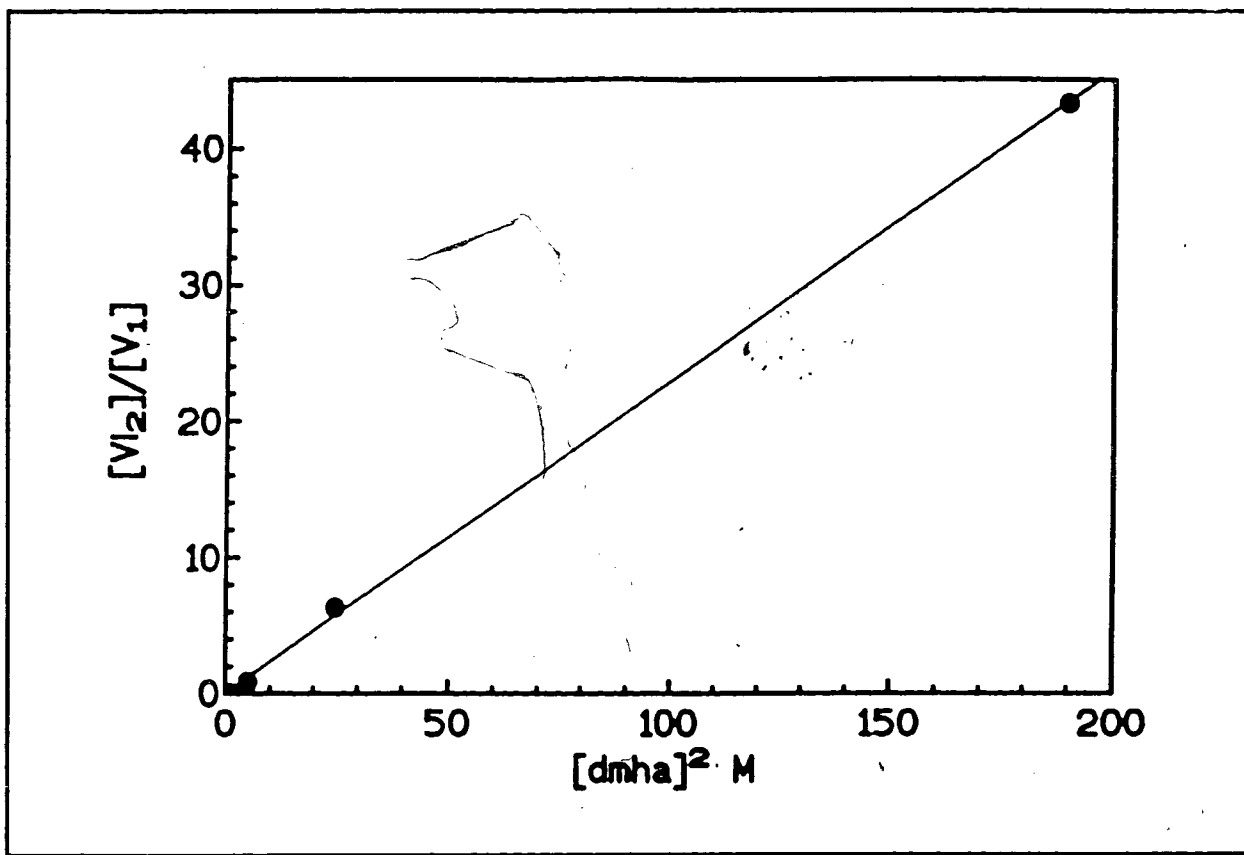
FIGURE 16.

Results from N,N-dimethylhydroxylamine concentration study at pH 7.3

Plot of $[VL_2]/[V_1]$ versus $[l]^2$:

The formation constant, K_{12}, was determined from the slope of the plot as shown in equation [4]. $K_{12} = (2.1 \pm 0.4) \times 10^7 \, M^{-1}$. This value for the formation constant K_{12} is given by the average of three separate experiments, of which one is illustrated above. The conditions of this experiment were pH 7.3, 2 mM vanadate, and 2.5 mM HEPES. N,N-dimethylhydroxylamine ligand was varied from 0.5 to 10 mM.

CHAPTER 6

6. Complexation of Vanadate, N,N-Dimethylhydroxylamine and Dithiothreitol:

6.1. Formation of a DTT-V-DMHA Complex.

During the process of carrying out ^{51}V NMR control experiments to investigate the stability of the bisligand (VL_2) compound in the kinetic assay buffer, it was observed that the compound reacts with a constituent of the buffer, resulting in the formation of a new complex. ^{51}V NMR control experiments established that HEPES and BSA, which were present in the buffer, did not react with the compound at the concentrations used in these studies. Dithiothreitol was determined to be the reagent responsible for the complexation. No evidence was found for the reduction of vanadate by DTT in these control studies. Consequently, DTT and DMHA concentration studies were performed and analysed with ^{51}V NMR spectroscopy in order to determine the stoichiometry of DTT and DMHA complexation, and to calculate the corresponding formation constants. ^{51}V NMR was also used to investigate the mode of coordination in the dimethylhydroxylamineDTT/vanadate (VT) complex.

6.2. Experimental Procedures.

6.2.1. DTT concentration study:

In the dithiothreitol concentration studies, vanadate, HEPES and N,N-dimethylhydroxylamine concentrations were kept constant at 300 µM, 2.5 mM, and 30 mM respectively. The concentration of DTT was varied from 5 to 200 mM. DTT stock solution at 500 mM was prepared just prior to the analysis and adjusted to pH 7.0. The ^{51}V NMR samples were prepared by adding, in sequence, vanadate, DMHA, HEPES, ddH$_2$O and DTT. The pH was then adjusted to 7.3 with NaOH.

6.2.2. DMHA concentration study:

DMHA concentration studies were carried out at 300 μM vanadate, 30 mM DTT and 2.5 mM HEPES. The concentration of DMHA ligand was varied from 5 to 25 mM. The solutions were prepared in a similar manner to those for the DTT concentration study, in this case, reversing the order of DMHA and DTT ligand addition.

6.2.3. Preliminary investigation of the mode of coordination:

The samples for ^{51}V NMR analysis were prepared by the addition of vanadate, HEPES and DMHA at 2 mM, 2.5 mM and 30 mM respectively. The ligand under investigation was subsequently added, and the solutions adjusted to the final volume of 2.5 mL and pH 7 with NaOH and distilled H_2O as required. For the study with mercaptoacetic acid, HEPES was kept at 20 mM and the mercaptoacetic acid was prepared at final concentrations of 58 mM and 115 mM. The ligand tertbutylmercaptan was prepared at 36 mM and 71 mM. The rest of the ligands were studied at 30 mM and 60 mM.

6.3. Results and Discussion.

6.3.1. DTT concentration study:

A product was observed at -630 ppm which increased in intensity as the DTT concentration was increased, with a corresponding decrease in the signal intensities for the bisligand products, as shown in Figure 18. This occurred both when the starting material was vanadate and when it was the crystalline bisligand compound (Vl_2) dissolved in distilled water. This was an unexpected observation since the two monomers which are formed on dissolution of the dimeric crystalline compound, are otherwise stable over several days in distilled water (Figure 17). This result served as an indication that formation of the DTT-DMHA-vanadate complex (VfT) product is driven by an associative mechanism.

The expression for the formation of a vanadate complex with DTT and DMHA from the bisligand product (Vl_2), was derived from the following equilibrium equations where T represents dithiothreitol, V represents vanadate, and l represents N,N-dimethylhydroxylamine. The DTT-DMHA-vanadate complex is represented as VlT, and the monoligand and bisligand products are represented as Vl_1 and Vl_2, respectively.

$$Vl_2 + T \underset{}{\overset{K_3}{\rightleftharpoons}} VlT + l \qquad\qquad [Vl_2][T]K_3 = [VlT]\,[l] \qquad [7]$$

$$Vl_1 + l \underset{}{\overset{K_2}{\rightleftharpoons}} Vl_2 \qquad\qquad [Vl_1][l]K_2 = [Vl_2] \qquad [8]$$
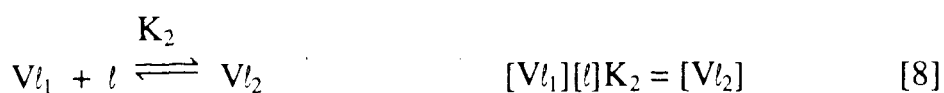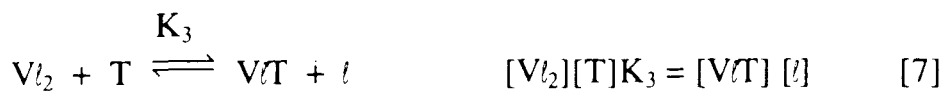
Since the concentrations of Vl_1 and VlT could not be individually determined because of signal overlap in the NMR spectra, the concentration of the DTT-DMHA-vanadate complex ($[VlT]$), was expressed in terms of the sum of these two concentrations such that :

$$cVl = [VlT] + [Vl_1] \qquad\qquad [9]$$

Substituting equation [8] into equation [9] gives the following expression:

$$cVl = [VlT] + \frac{[Vl_2]}{[l]K_2} \qquad\qquad [10]$$

Equation [10] is then substituted into equation [7], to yield equation [11]:

$$[Vl_2][T]K_3 = \left(cVl - \frac{[Vl_2]}{[l]K_2}\right)[l] \qquad\qquad [11]$$

This equation is subsequently re-arranged to give the final expression for the formation of VlT product:

$$[Vl_2][T]K_3 + \frac{[Vl_2]}{K_2} = cVl\,[l] \qquad\qquad [12]$$

$$\frac{cVl\,[l]}{[Vl_2]} = [T]K_3 + \frac{1}{K_2} \qquad\qquad [13]$$

42

In order to correct for the large formation constants for $V\ell T$, $V\ell_1$ and $V\ell_2$, the concentration of free ligand ($[\ell]$), was defined by conservation equation [14], where $c\ell_t$ refers to the total ligand concentration:

$$[\ell] = c\ell_t - (cV\ell + 2[V\ell_2])$$ [14]

Figure 19 shows the plot obtained from the experimental data. A linear relationship was obtained from a plot of the data. The value of K_3, for the formation of $V\ell T$, was given by the slope of the graph to be 1.01 ± 0.08. The Y-intercept is the inverse of K_2. Since the value of K_2 was calculated from previous studies to be rather large, $(9.7 \times 10^2 \text{ M}^{-1})$, the inverse value is comparatively small, which accounts for the absence of a defined Y intercept in the plot. In order to confirm the stoichiometry of the $V\ell T$ product, the equations were re-derived assuming that the product contained two vanadium atoms ($V_2\ell T$). This plot did not give a linear relationship, consistent with this being an incorrect assumption regarding the vanadium stoichiometry. The equations were also re-derived assuming two DTT ligands per $V\ell T$ complex; again these plots showed curvature. The presence of curvature in these plots demonstrates that the experiments adequately probe the stoichiometric relationships and confirm the $V\ell T$ stoichiometry of the product.

The formation constant for $V\ell T$ from the monoligand product $V\ell_1$ was then calculated by re-arranging and substituting the following equilibrium expressions:

$$V\ell_2 + T \overset{K_3}{\rightleftharpoons} V\ell T + \ell \qquad\qquad [V\ell_2][T]K_3 = [V\ell T][\ell] \qquad [7]$$

$$V\ell_1 + \ell \overset{K_2}{\rightleftharpoons} V\ell_2 \qquad\qquad [V\ell_1][\ell]K_2 = [V\ell_2] \qquad [8]$$

$$V\ell_1 + T \overset{K_4}{\rightleftharpoons} V\ell T \qquad\qquad [V\ell_1][T]K_4 = [V\ell T] \qquad [15]$$

Substituting equation [8] into [7] yields

$$[V\ell_1]K_2[T]K_3=[V\ell T] \qquad [16]$$

Equation [15] is then combined with equation [16] to give the final expression

$$K_2K_3 = K_4 \qquad [17]$$

Since K_2 and K_3 were previously determined, K_4 was readily calculated from this equation. A value of $(9.8 \pm 0.4) \times 10^2 \ M^{-1}$ was obtained for K_4. This value is very close to that obtained for the formation of $V\ell_2$ from $V\ell_1$, suggesting that the DMHA and DTT ligands compete equally well for $V\ell_1$, with the resultant formation of $V\ell_2$ and $V\ell T$ respectively.
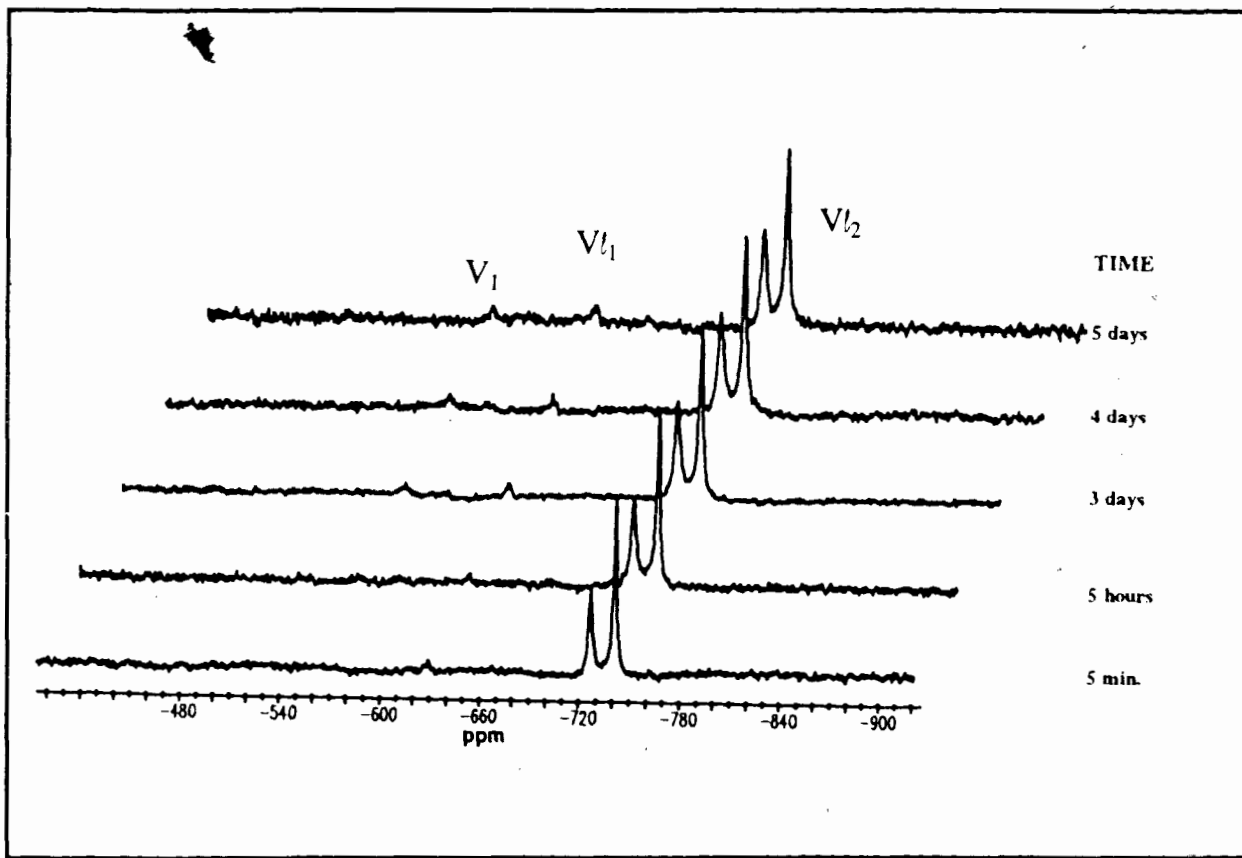
FIGURE 17.

^{51}V NMR spectra of a time course study of the stability of bisligand

dimethylhydroxylamine/vanadate complexes in distilled water:

The spectra show the stability of the bisligand products formed when the crystalline bisligand dimethylhydroxylamine/vanadate complex is dissolved in water (f.c 5 mM). The numbers correspond to the time after dissolution in water that the spectra were acquired. The signals at -740 ppm are the bisligand isomeric products formed in aqueous solution (Vl_2). The monoligand product (Vl_1) is at -630 ppm, as described in Chapter 5. The complex is slow to convert to vanadate (-550 ppm); after 5 days, the bisligand products persist at greater than 90% of the initial concentration. This is in contrast to the rapid reaction of these bisligand products in the presence of DTT, which occurs within 5 minutes of mixing.

45
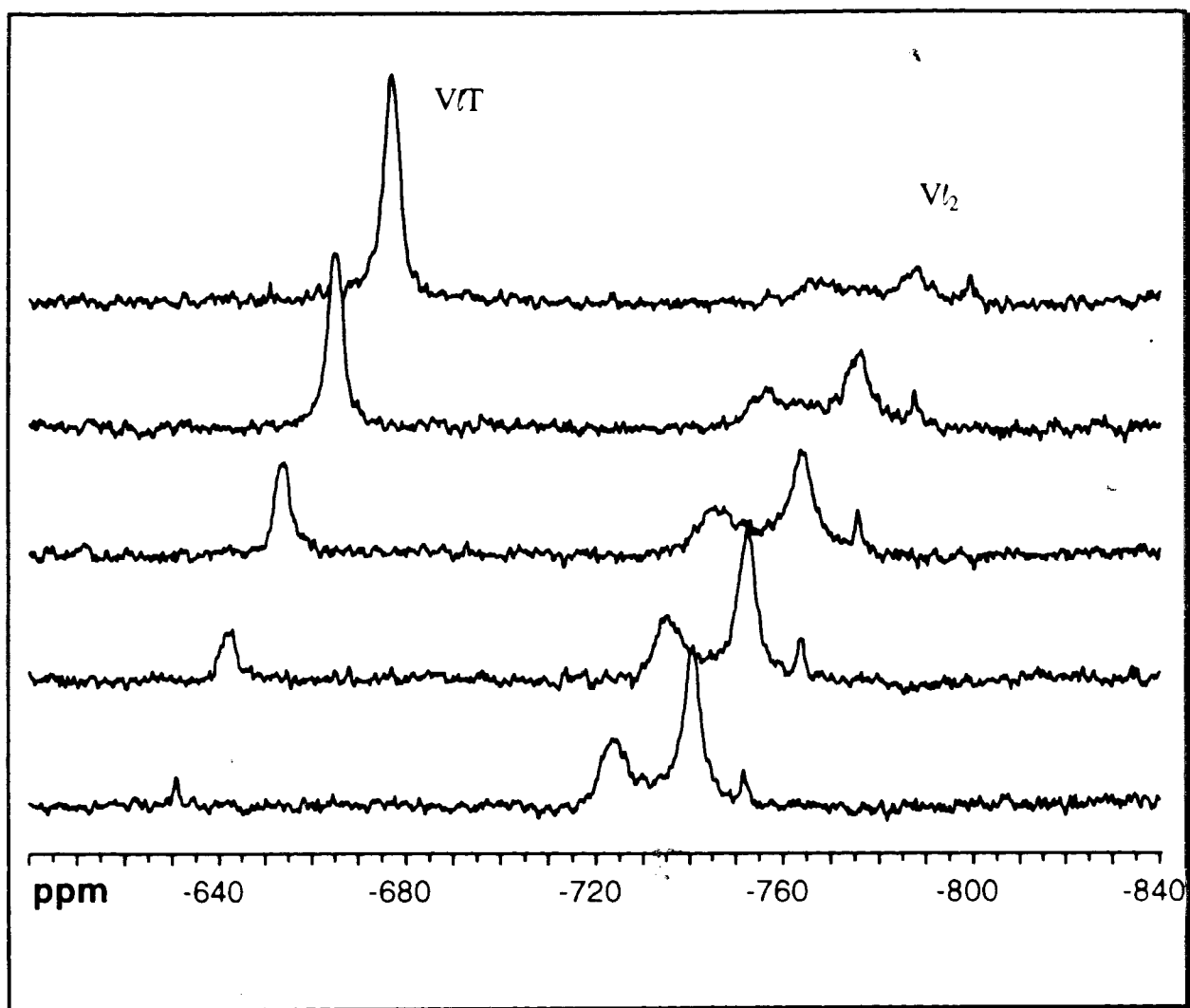
FIGURE 18.

^{51}V NMR spectra of DTT concentration study at 30 mM DMHA:

The spectra show the formation of a dimethylhydroxylamine/vanadate-DTT product (V/T) at -630 ppm which increases as the concentration of DTT is increased, with a corresponding decrease in the signal intensities for the dimethylhydroxylamine /vanadate bisligand products (Vl_2) in the -740 ppm region. The conditions are 30 mM DMHA, 300 μM vanadate, 2.5 mM HEPES, and pH 7.3. The concentration of DTT was varied from 5 to 200 mM. The spectra shown above correspond to the following concentrations of DTT, from bottom to top: 0, 5, 30, 60 and 80 mM DTT.
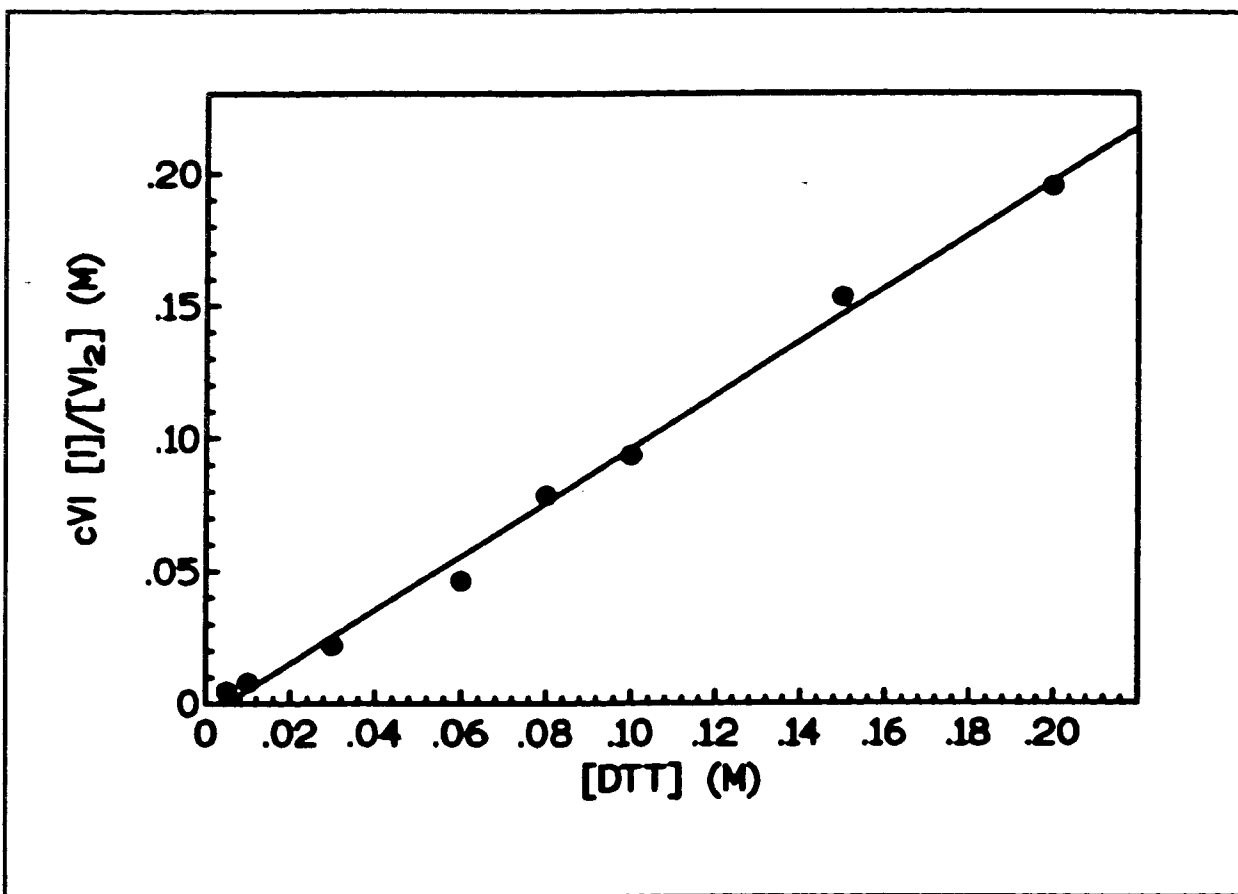
FIGURE 19.

Graph of the formation of V/T as a function of DTT concentration:

The plot shows the linear relationship obtained from a plot of cVl $[l]/[Vl_2]$ against [DTT], as determined from equation [13]. The value for K_3 as given by the slope of the plot is 1.01 ± 0.08. This linear plot is in agreement with the formation of a product containing one vanadium and one DTT ligand.

47

6.3.2. DMHA concentration study:

A dimethylhydroxylamine concentration study was carried out in the presence of 30 mM DTT. As illustrated in Figure 20, two different signals were observed in the -630 ppm region, corresponding to the VtT and Vt_1 products. This provided direct evidence that the VtT complex observed in the presence of the two ligands is different from the Vt_1 product, despite appearing in the same region of the spectrum. As the DMHA concentration was increased, the two signals were no longer resolved, a result which was consistent with an increase in the VtT signal intensity and with the observations from the DTT concentration study (section 6.3.1).

The equilibrium expression for the formation of VtT in this study was derived from a re-arrangement of the equation given by the DTT concentration analysis (equation [13]). This equation was written in terms of the variation of the DMHA ligand concentration as described below.

Multiplication of equation [13] by [Vt_2], yielded equation [18], which was subsequently re-arranged to give the final expression [19].

$$[Vt_2] \left([T]K_1 + \frac{1}{K_2} \right) = cVt\,[\,t\,] \qquad\qquad [18]$$

$$cVt\,/[Vt_2] = 1/[\,t\,] \left([T]K_1 + \frac{1}{K_2} \right) \qquad\qquad [19]$$

Figure 21 shows the linear relationship obtained from a plot of the data. K_3 was calculated from the slope of the graph, giving a value of 0.71 ± 0.13 which is in good agreement with the value of 1.01 ± 0.08 obtained from the DTT variation study.
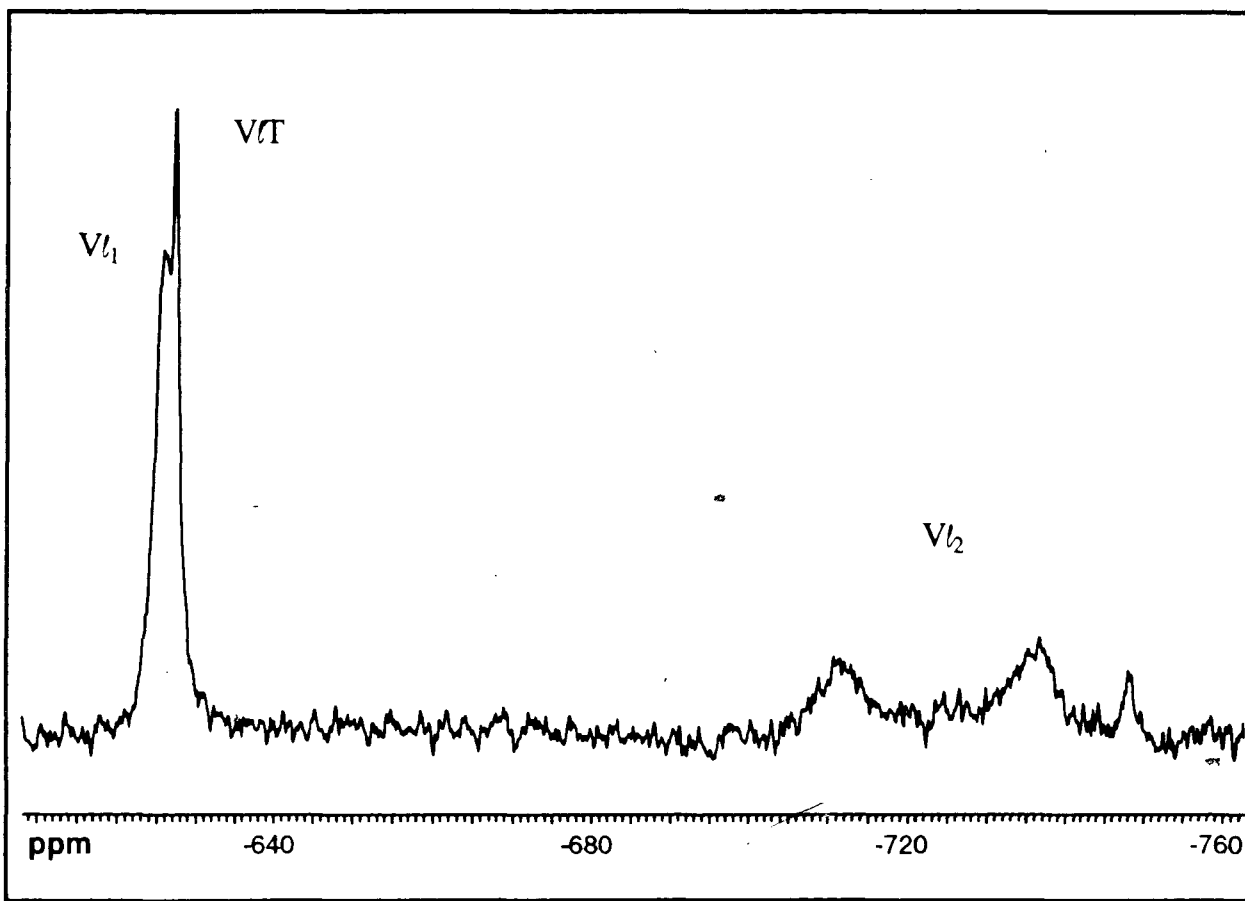
FIGURE 20.

^{51}V NMR spectra showing the formation of VlT and Vl_1 products for the DMHA

concentration study at 30 mM DTT:

One of the two signals observed at -630 ppm corresponds to the DMHA-V-DTT complex (VlT), and the other to the monoligand product (Vl_1). The signals in the -740 ppm region correspond to the bisligand products (Vl_2). The conditions are 30 mM DTT, 300 µM vanadate, 2.5 mM HEPES, and pH 7.3. The concentration of DMHA was varied from 5 to 200 mM; the results shown above are for 15 mM DMHA.
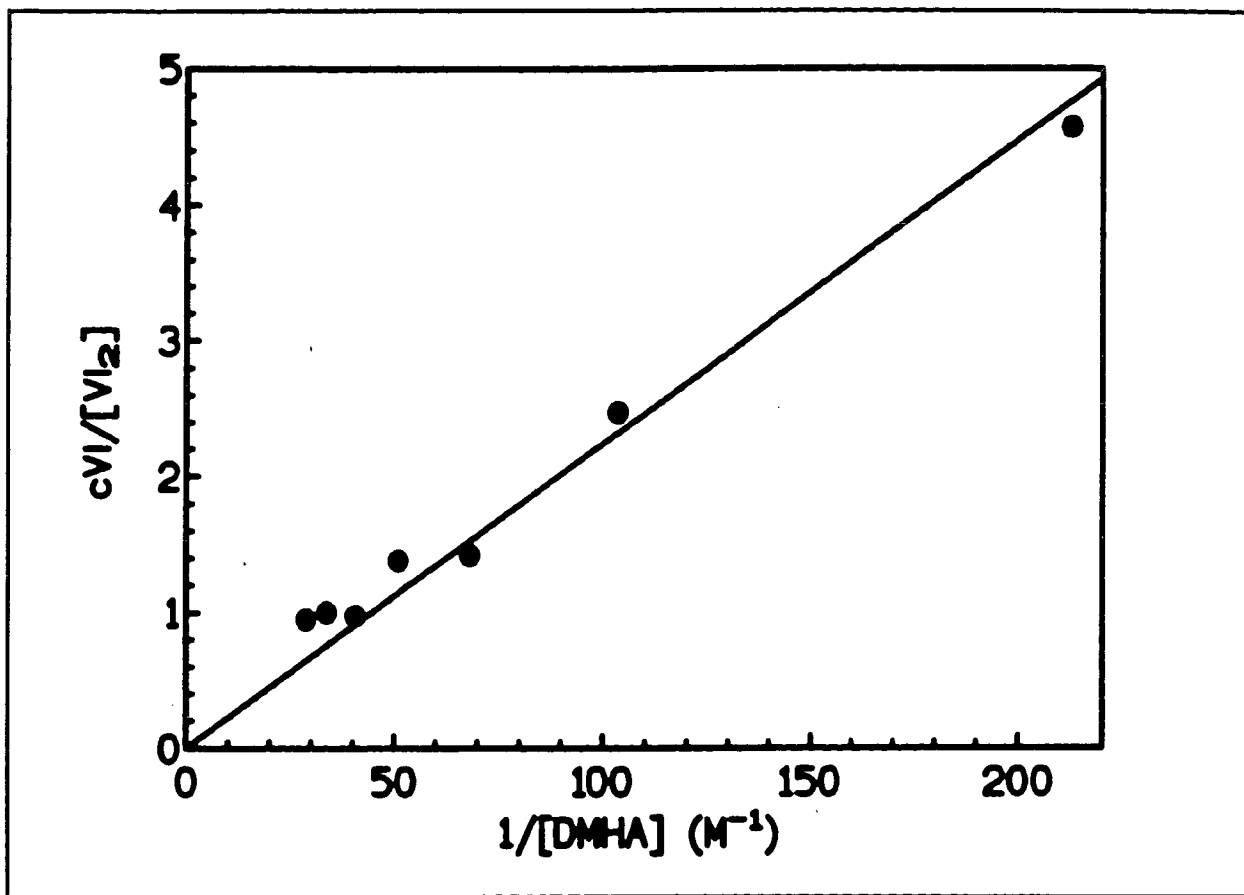
FIGURE 21.

Graph of the formation of V/T as a function of DMHA concentration:

The data obtained from the integration of the spectra obtained in the DMHA concentration study are plotted as given by equation [19]. The value for K_3, which is calculated from the slope of the plot, is 0.71 ± 0.13. This linear graph is in agreement with the coordination of a single N,N-dimethylhydroxylamine ligand in the formation of the product with dithiothreitol and vanadate.

In order to confirm the number of dimethylhydroxylamine ligands coordinated to the V/T product, the equations were re-formulated, assuming the presence of two dimethylhydroxylamine ligands. A plot of the data gave a non-linear graph, indicating that a single dimethylhydroxylamine ligand is involved in the coordination to vanadium.

Taken together with the results from the DTT concentration study, it is therefore proposed that the complex formed from the reaction of vanadate, dithiothreitol and N,N-dimethylhydroxylamine is composed of one vanadium atom, one dithiothreitol moiety, and one dimethylhydroxylamine moiety.

6.3.3. Preliminary investigation of the mode of coordination:

In order gain more insight into the mode of coordination in the V/T product, additional ^{51}V NMR experiments were performed. Since DTT (CH$_2$SHCHOHCHOHCH$_2$SH) contains two thiol groups, it was considered likely that coordination of dithiothreitol in the V-DMHA-DTT product (V/T) involved one or both of the thiol groups. The requirement for the thiol group in forming these types of complexes was studied using various thiol-containing ligands.

Table I summarises the structural features of the ligands studied and the results obtained. As illustrated in Table I, the compounds which did not form complexes of the type observed with DTT and N,N-dimethylhydroxylamine/vanadate either contained no thiol group (ethanol and propylene glycol) or contained a single thiol group with no other functional group present (tertbutylmercaptan). The ligands which were able to form these complexes contained either two thiol groups (Bis(2-mercaptoethylsulfone) or a single thiol group together with a carboxylate (mercaptoacetic acid) or a hydroxyl group (β-mercaptoethanol). These results indicated that although the coordination in these complexes involves the thiol group, the mode of coordination to the vanadium atom is not monodentate with respect to the thiol-containing ligand since another proximal group (hydroxyl, thiolate or carboxylate) is required for complexation to form the types of complexes observed

with the DTT ligand. Although the exact mode of coordination in the V/T complex has yet to be determined, these results are significant in that they demonstrate that the thiolate group of the ligand is critical for complexation to occur with N,N-dimethylhydroxylamine/vanadate. This conclusion is discussed further in the following chapter, after a consideration of the results obtained with L-cysteine and certain derivatives of this amino acid.
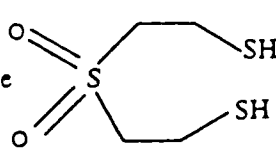
Compound	Structure	Result
DTT	$CH_2SHCHOHCHOHCH_2SH$	complex at -630 ppm
Ethanol	C_2H_5OH	no complex
Propylene glycol	$CH_3\text{-}CHOH\text{-}CH_2OH$	no complex
Terbutylmercaptan	$(CH_3)_3CSH$	no complex
Bis(2-mercaptoethyl)sulfone		complex at -640.6 ppm
Mercaptoacetic acid	$HS\text{-}CH_2\text{-}COOH$	complex at -680.0 ppm
2-Mercaptoethanol	$HS\text{-}CH_2\text{-}CH_2\text{-}OH$	complex at -628.6 ppm

TABLE I.

Investigation of the functional group requirements for coordination with bis (N,N-dimethylhydroxylamino)vanadate:

This table illustrates the structural features of the ligands investigated and, states the result obtained from ^{51}V NMR studies which investigated the ability of the ligand to form a complex in a similar region of the spectrum as the V/T complex.

CHAPTER 7

7. Complexation of Vanadate, N,N-Dimethylhydroxylamine and L-Cysteine:

7.1. Formation of V-DMHA-CYS Complexes.

As discussed in the preceding chapter, ^{51}V NMR experiments with thiol-containing compounds and alcohols indicated that although coordination is not monodentate with respect to the thiol-compound, the thiol group is essential for coordination to form the V/T-type products. Of the compounds mentioned in the preceding section, the complexation of cysteine was investigated in some detail. Cysteine was particularly important to examine since the active sites of PTPases contain a critical cysteine residue. Complexation at the sulfhydryl group of this cysteine is a possible route to the inhibition of these enzymes (59). Consequently, demonstrating that vanadate-dimethylhydroxylamine complexes can bind to cysteine, would provide evidence for a possible mechanism by which these complexes may act in the inhibition of LAR PTPase and FLAG-PTP1B (the enzyme inhibition studies are discussed in the following chapter). This would be achieved by providing evidence showing that a vanadate complex that appears inhibitory, is able to form reversible interactions with cysteine residues. Consequently, a detailed L-cysteine concentration study was performed. Furthermore, functional-group protected cysteines, serine and glutathione were utilised to investigate the mode of coordination in the vanadate-DMHA-cysteine products (V/C) observed in the L-cysteine concentration study.

7.2. Experimental Procedures.

A stock solution of L-cysteine was prepared in distilled water at 100 mM and pH 6.0 just prior to the NMR analysis. In addition to L-cysteine, the NMR samples consisted of DMHA, vanadate, and HEPES at 30, 2 and 2.5 mM respectively. The

concentration of L-cysteine was varied from 10 to 40 mM. Distilled water, HEPES, DMHA, vanadate and L-cysteine were added sequentially. The solution was then adjusted to the final volume of 2.5 mL and pH 7.3 with NaOH and distilled water as required. Preliminary NMR studies indicated that equilibrium was attained within 10 minutes of mixing, with no significant change in the spectra for up to 30 minutes after mixing. All the spectra were therefore obtained between 10 and 20 minutes of sample preparation. Studies with the other amino acids and glutathione were performed similarly with the exception that these ligands were studied at 30 mM and 60 mM. The purity of the blocked cysteine compounds and reduced glutathione was checked by ^{1}H NMR spectroscopy. All of the compounds were used as supplied.

7.3. Results and Discussion.

7.3.1. L-cysteine concentration study:

The results of the L-cysteine ligand concentration study are shown in Figure 22. Two vanadate-DMHA-cysteine products (VlC) were observed at -636 and -640 ppm. The signal intensities for these products increased as the concentration of L-cysteine was increased. The signal for the monoligand dimethylhydroxylamine compound (Vl_1) at -630 ppm did not overlap with the two cysteine (Cys) product signals (-636 and -639 ppm) and could thus be integrated separately. As expected, an increase in the concentration of L-cysteine was accompanied by an increase in the signal intensity for the VlC products and a decrease in the signal intensities from both the Vl_1 and Vl_2 complexes.

Figure 23 shows an example of the entire spectrum obtained in this analysis. Additional products were obtained (as seen at -724 to -751 ppm) which overlapped with the Vl_2 signal, giving rise to the broad signals seen in this region. Similar products have recently been assigned for a complex of bishydroxamidovanadate with glycylglycine, and in this case, the signals correspond to complexes where coordination to the peptide ligand involves the carboxyl group and/or the amine

nitrogen atoms (66). In this analysis, these signals can therefore be assigned as complexes involving coordination to cysteine via one or both of these side chains. No attempt was made to characterise the products at chemical shifts at -763 to -769 ppm.

For the purposes of this study, it was not necessary to attempt to separate the integrals for these additional products as the Vl_1 and VlC signals could be individually integrated. The formation constant for the VlC products was therefore calculated directly from the Vl_1 and VlC signal intensities and the total remaining integral, as defined by equation [20]. In this expression, Vl_1 refers to the monoligand dimethylhydroxylaminovanadate product, l represents the dimethylhydroxylamine ligand (DMHA), C represents cysteine (Cys) and VlC collectively refers to the dimethylhydroxylamineCys/vanadate complexes observed at -636 and -639 ppm.

$$Vl_1 \ + \ C \ \overset{K_5}{\rightleftharpoons} \ VlC \qquad\qquad [Vl_1][C]K_5 = [VlC] \qquad\qquad [20]$$

A graph of $[VlC]$ against $[Vl_1][C]$ was constructed from the experimental results. Figure 24 shows a plot of the data obtained from a cysteine concentration study at constant DMHA and vanadate. A linear plot was obtained with a slope ($=K_5$) of $(3.5 \pm 0.1) \times 10^2$ M^{-1}. The value of the formation constant is approximately 2.7 times less than that obtained for the formation of VlT, from DTT and DMHA ligands $(9.7 \times 10^2$ $M^{-1})$. This is consistent with the conclusion made in these studies that coordination of these complexes is bidentate with respect to the DTT or cysteine ligand; involving one thiol group and one other group (NH_3^+ or COO^- or OH^-). Since DTT contains two thiol groups and two hydroxyl groups it has the possibility to form at least two VlT complexes for each one that L-cysteine can form. There are likely to be other charge and structural differences that will also influence the favourability of complex formation for both DTT and cysteine ligands.
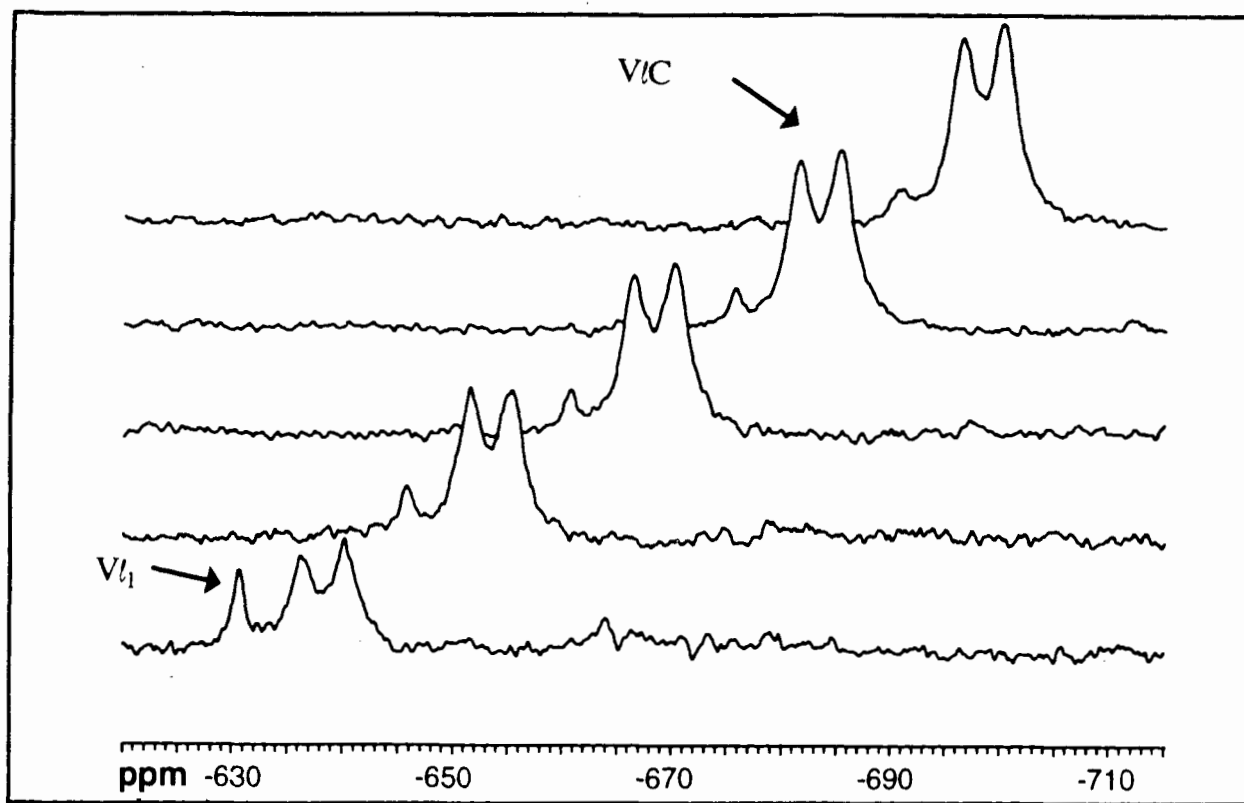
FIGURE 22.

^{51}**V NMR spectra showing the formation of dimethylhydroxylamine/vanadate-Cys (VlC) complexes:**

The two signals observed at -636 and -639 ppm correspond to the VlC products, which increase in intensity as L-cysteine concentration is increased. The signal at -630 ppm is the monoligand dimethylhydroxylamine/vanadate product (Vl_1), which decreases in intensity as the concentration of L-cysteine is increased. The conditions are 30 mM DMHA, 2 mM vanadate, 2.5 mM HEPES, and pH 7.3. The concentration of L-cysteine was varied from 10 to 40 mM. The spectra shown above correspond to the following concentrations of L-cysteine, from bottom to top: 10, 20, 25, 30 and 40 mM L-cysteine.
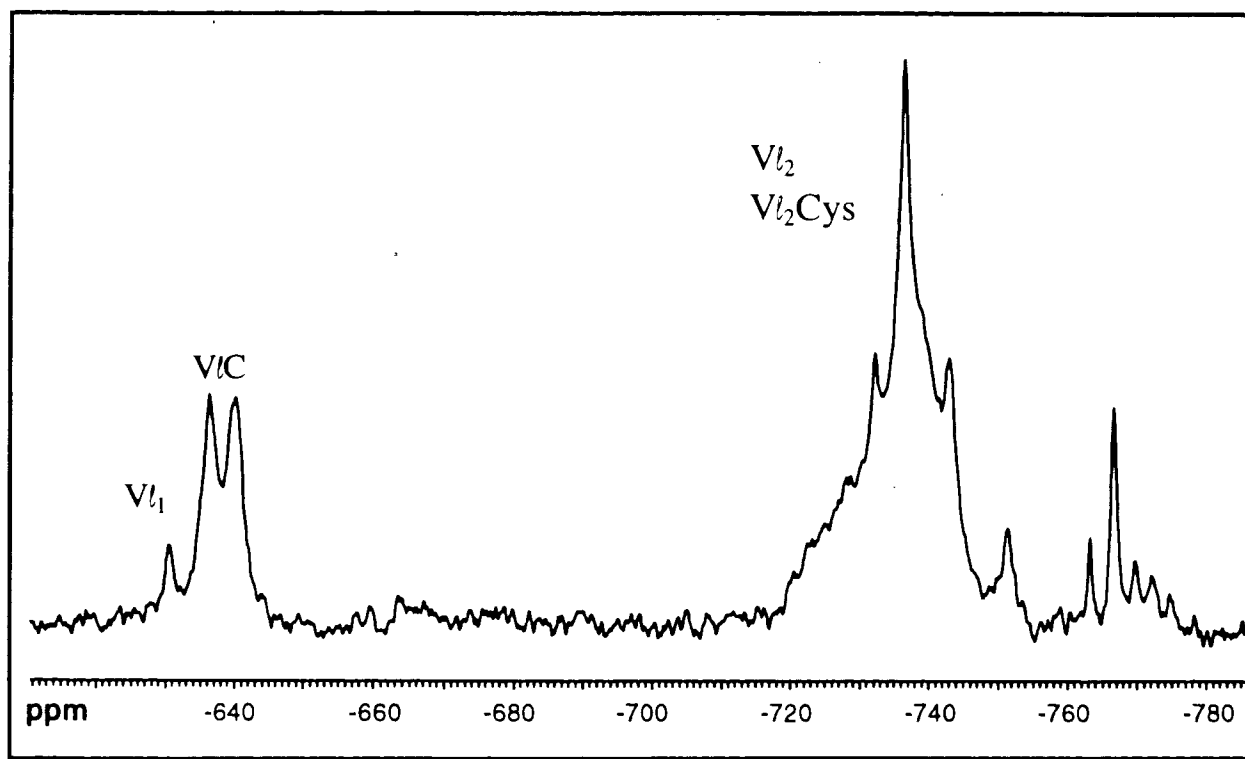
FIGURE 23.

^{51}V NMR spectrum showing the formation of additional dimethylhydroxylamine / vanadate complexes with cysteine:

This spectrum shows the additional complexes observed in the -724 to -750 ppm region. The signals for the complexes of dimethylhydroxylamineCys/vanadate where coordination of vanadate to cysteine occurs via the carboxyl and/or amine groups (not the thiol groups) are superimposed over the signals for the Vl_2 products, resulting in the broad signals observed in this region. In order to calculate the formation constant for VlC, the total integral for these signals was measured since the equation ([20]) did not require separation of the integrals.
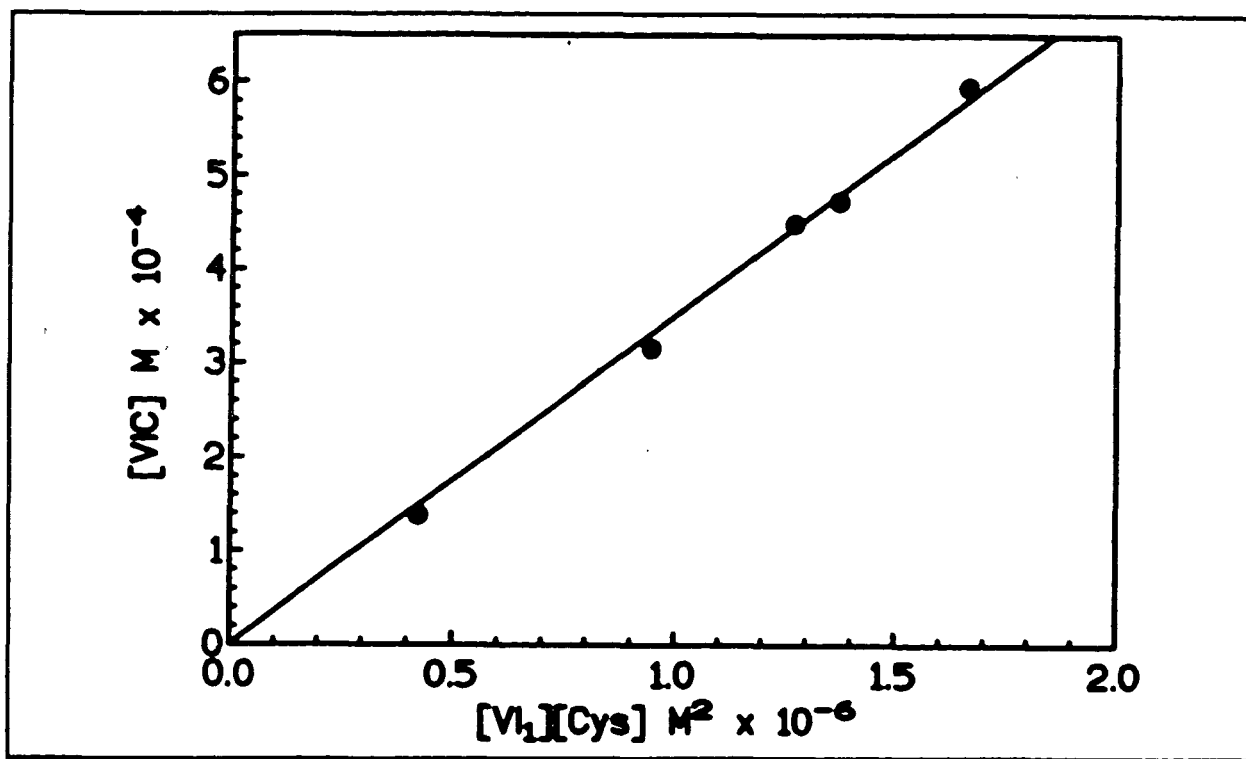
FIGURE 24.

Graph of the formation of dimethylhydroxylamine/vanadate-Cys

(V*l*C) complexes as a function of total L-cysteine concentration at pH 7.3.

The graph shows the linear relationship obtained from a plot of the data from an L-cysteine concentration study as given by equation [20]. The formation constant (K_5), as obtained from the slope is equal to $(3.5 \pm 0.1) \times 10^2 \, M^{-1}$. The conditions are 30 mM DMHA, 2 mM vanadate, 2.5 mM HEPES, and pH 7.3. The concentration of L-cysteine was varied from 10 to 40 mM.

7.3.2. Preliminary investigation of the mode of coordination:
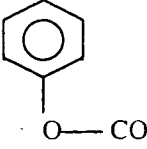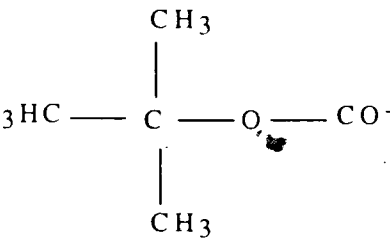
In order to further investigate the mode of coordination in the V*l*C products, a selection of amino acids were investigated, as summarised in Table II. The vanadium NMR spectra showed that both L-cysteine-ethyl-ester and N-boc-L-cysteine gave a single V*l*C product, not two products as observed with either L-cysteine or D,L-cysteine. Taken together with the observations from the thiol compounds discussed in the preceding chapter (primarily that both mercaptoacetic acid and 2-mercaptoethanol appear to form single V*l*T-type products), this suggests that the two complexes observed with L-cysteine may correspond to two different compounds, both with the L-cysteine ligand coordinated in a bidentate manner to the vanadium atom. One of the complexes could correspond to the cysteine coordinated via the amine side chain (NH_3^+) and the thiolate group (SH). The second complex may involve coordination of the ligand through the carboxylate (COO^-) and SH groups. Interestingly, the complexes observed in the -724 to -751 ppm region of the spectrum in the L-cysteine study were not seen with L-cysteine-ethyl-ester, suggesting that with the dimethylhydroxylamine/vanadate system, these amino acid side-chain complexes require the carboxylate group for their formation.

The observation that L-serine, N,S-diCBZ-L-cysteine and S-CBZ-L-cysteine did not form the complexes observed with cysteine and the cysteine derivatives discussed above, further supported the conclusion made in the preceding chapter that the thiolate group is critical for this type of complexation to occur. Reduced glutathione was also examined for the ability to form these complexes. In this case, two complexes appeared in the same region as the V*l*C products. Since the terminal carboxylate and amino groups in this tripeptide would be expected to be involved in the bonding to form the V*l*C-type of complexes, this result suggests that there may be a certain degree of flexibility in the distance between the SH group and the second coordinating functional group in these complexes.

TABLE II.

Investigation of the functional group requirements for the coordination of cysteine with N,N-dimethylhydroxamidovanadate:

This table illustrates the structural features of the ligands investigated. The results obtained from NMR studies are also given. NMR studies were used to investigate the ability of the ligand to form a complex with dimethylhydroxylamine/vanadate in a similar region of the spectrum as the VlC complex.

Compound	Structure	Result
L-serine		no complex
N,S,-diCBZ-L-cysteine	NH_3^+ and SH groups on L-cysteine blocked with carbobenzoxygroup =	no complex
S-CBZ-L-cysteine	SH group on L-cysteine blocked with carbobenzoxy group	no complex
L-cysteine-ethyl ester		single complex at -642 ppm
N-boc-L-cysteine	NH_3^+ group on L-cysteine blocked with t-Butyloxycarbonyl group =	single complex at -625 ppm
D,L-cysteine	mixture of D- and L- isomers	two complexes at -636 and -639 ppm
Reduced glutathione	Glu-Cys-Gly	two complexes at -633 and -635 ppm

CHAPTER 8

8. Inhibition Studies:
Influence of N,N-dimethylhydroxylamine/vanadate and N,N-dimethylhydroxylamine/vanadate-DTT Complexes on GST-LAR-D1 PTPase and FLAG-PTP1B.

8.1. Experimental Procedures:

8.1.1. Determination of Inhibition Constant (K_i) values for GST-LAR-D1 and FLAG-PTP1B:

Stock solutions of the bisligand N,N-dimethylhydroxylamine/vanadate complexes were prepared from crystalline bis(N,N-dimethylhydroxamido) hydrooxovanadate as follows. The crystalline material was freshly prepared in distilled water to a final concentration of 1 mM. Solutions of 5, 25, 50, and 100 μM concentration were then prepared by dilution of appropriate volumes of the 1 mM solution. The stock solutions were then adjusted to 30 mM N,N-dimethylhydroxylamine and pH 7.0.

The assay buffer was also freshly prepared and contained 10 mM HEPES at pH 7.3, 10 mM DTT, and 100 μg/mL BSA. The inhibition assay solutions contained 25 μL assay buffer (f.c 1/4 concentrations in buffer), 10 μL of the appropriate inhibitor stock solution (f.c. 1/10 stock solution concentration of inhibitor and f.c 3 mM N,N-dimethylhydroxylamine), 10 μL diluted enzyme (f.c 0.23 ng/μL for GST-LAR-D1 and 0.21 ng/μL for FLAG-PTP1B). ddH$_2$O was added as required to make the final volume of the assay solution up to 100 μL. Varying amounts of 188 μM FDP substrate (final concentrations were varied from 9 to 94 μM) were added to initiate the reaction. The enzyme and inhibitor were pre-incubated together, as described for glyglypV. A control solution was similarly prepared, in the absence of inhibitor.

The kinetics of the assays were followed essentially as described in section 4.1.3., with the following exceptions. In this case, the analytical wavelength was

chosen at 470 nm as this was the wavelength at which minimal absorbance of inhibitor sample occurred. In these experiments, the reaction rates were followed for 10 minutes at 20 second time intervals.

Dilution experiments were also carried out. The procedure followed with the dimethylhydroxlamine/vanadate complexes is essentially as described previously for glyglypV (section *4.1.3.*), with the inclusion of DMHA rather than EDTA in this case.

8.1.2. Investigation of the individual inhibitory potencies of VI_1, VI_2 and VIT:

Further inhibition studies were carried out at high DMHA and at high DTT concentrations, in order to further confirm the inhibitory potencies of the complexes present in these assays. For the study at high DMHA concentration, the N,N-dimethylhydroxylamine/vanadate compound stock solutions were prepared from vanadate and N,N-dimethylhydroxylamine by adding the appropriate amounts of these compounds. Stock solutions of 10, 20, 30, 40, 50 and 100 μM total vanadium concentration were prepared, all at 100 mM DMHA. Distilled H_2O and NaOH were then added to adjust the solutions to a final volume of 2 mL and a final pH of 7.3. The stock solutions were then left to equilibrate overnight. The inhibition assay solutions were then prepared, as described in section *8.1.1.*, using these inhibitor stock solutions. The final concentrations of DMHA and vanadium were one tenth those of the stock solutions. In these experiments, the buffer was prepared at 5 mM DTT, so that the final concentration of DTT in each of the assays was 1.25 mM. The kinetics experiments were then carried out at each concentration of inhibitor, with GST-LAR-D1 and 28 μM FDP substrate, as described above.

The study at high DTT concentration was also carried out with GST-LAR-D1 enzyme. The procedure was as described above for the experiment at high DMHA concentration, with the following exceptions. Firstly, the inhibitor stock solutions were prepared at 30 mM DMHA, so that the final concentration of N,N-dimethylhydroxylamine in the assay solutions was 3 mM. Additionally, the assay

buffer was prepared at 200 mM DTT, to a final concentration of 50 mM in the inhibition assay solutions. Finally, in order to facilitate adequate buffering in the desired pH range at this DTT concentration, HEPES buffer was added to a final concentration of 27.5 mM in these assays.

Separate control experiments were performed which confirmed that HEPES, DMHA and DTT did not themselves significantly influence the activity of the enzyme at the concentrations used in these studies. Accordingly, the rates in the presence of inhibitors could then be directly compared to the rates obtained for control solutions prepared in the absence of the dimethylhydroxylamine/vanadate preparations, and prepared at the same HEPES buffer, DTT and N,N-dimethylhydroxlamine (DMHA) concentrations.

DMHA titration experiments were carried out in order to investigate the effect of varying the ratio of vanadate to the monoligand (Vl_1) complex. The conditions and procedures were as described in section 8.1.1. with the following exceptions. The total vanadium concentration was kept constant at 2 μM, and the DMHA concentration was varied from 0.1 to 5 mM. The FDP substrate was maintained at 28 μM in these analyses.

8.2. Results and Discussion:

8.2.1 Determination of Inhibition Constant (K_i) values for GST-LAR-D1 and FLAG-PTP1B:

According to the competitive mechanism of inhibition, the rate equation for the enzyme inhibition studies is given by equation [21] (67), where [I] refers to the concentration of inhibitor; in this case the total vanadium concentration (V_t) from the N,N-dimethylhydroxylamine/vanadate preparations:

$$v = \frac{V_{max}[\,S\,]}{K_m(1+[\,I\,]/K_i) + [\,S\,]} \tag{21}$$

$$K_{m(app)} = K_m\left(\frac{1+[I]}{K_i}\right) \qquad [22]$$

By the substitution of equation [22], equation [21] can be re-written as follows, where $K_{m(app)}$ is the apparent value of the Michaelis constant:

$$v = \frac{V_{max}[S]}{K_{m(app)} + [S]} \qquad [23]$$

Consistent with a competitive mechanism of inhibition, when each of the plots of the reaction rate (v) versus the concentration of substrate ([S]) were fitted according to equation [23], a constant maximal velocity (V_{max}) was obtained. The experimental and calculated curves are shown for GST-LAR-D1 and FLAG-PTP1B in Figures 25A and 26B, respectively. The corresponding Lineweaver Burke plots of these curves are shown in Figures 25B and 26B.

In order to determine the inhibition constants (K_i), a re-arrangement of equation [22] to give the linear form (equation [24]) was made. The $K_{m(app)}$ values obtained from fitting the rate curves to equation [23] were then plotted against the total inhibitor concentrations ([I] = total vanadium concentration = $[V_t]$) for GST-LAR-D1 and FLAG-PTP1B as shown in Figures 27 and 28 respectively. The K_i in each case was then calculated from the values of the slope of the graph (K_m/K_i) and the y intercept (K_m). From these analyses, K_i values of 2.2 ± 0.3 μM and 3.4 ± 0.6 μM were obtained for GST-LAR-D1 and FLAG-PTP1B, respectively. These inhibition constants represent the combined inhibition due to all of the inhibitors present in the analyses.

$$K_{m(app)} = \frac{K_m}{K_i}[I] + K_m \qquad [24]$$
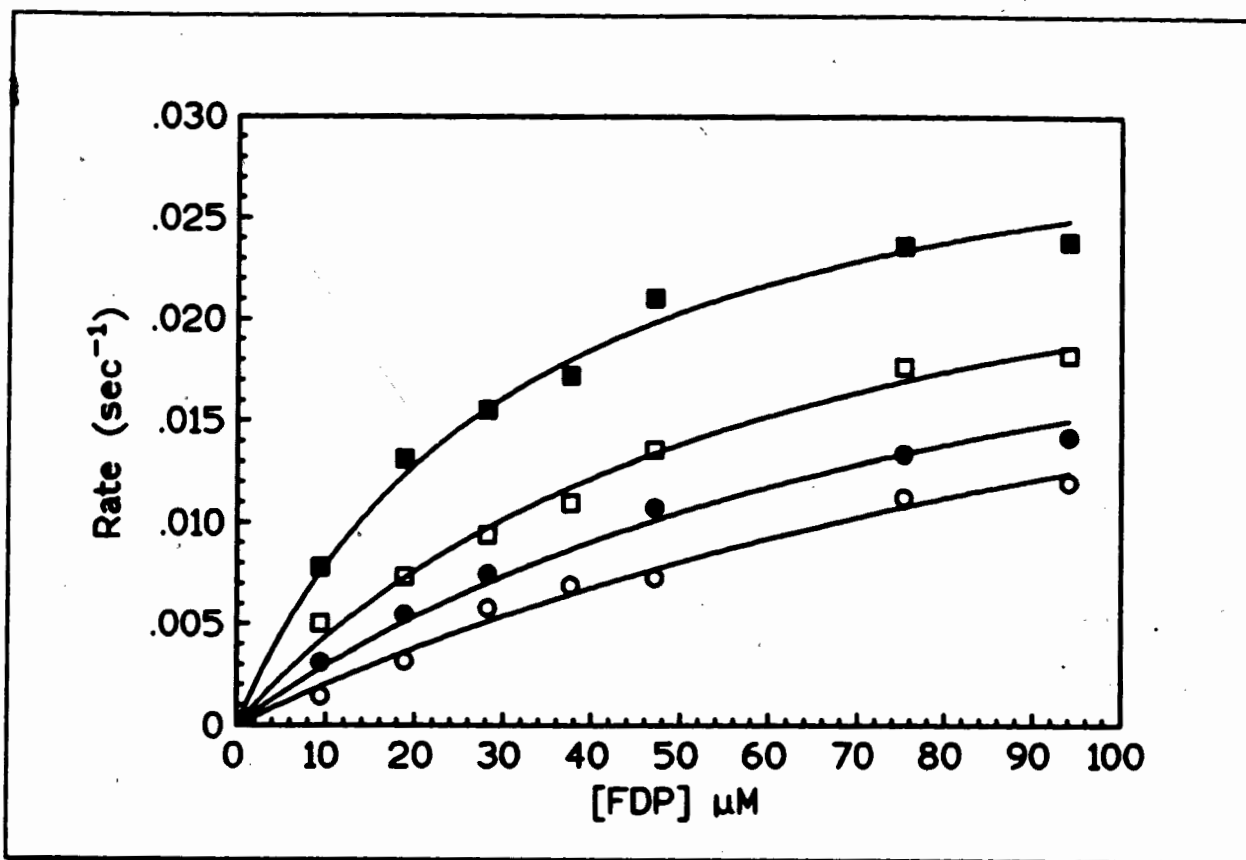
FIGURE 25A.

Plot of reaction rate as a function of substrate concentration for GST-LAR-D1.
Closed squares and open squares represent the analyses at 0.5 μM and 2.5 μM total
inhibitor concentration (all the complexes in solution) respectively. Closed circles and
open circles represent the analyses at 5 μM and 10 μM total inhibitor concentration
respectively. A constant V_{max} of 0.031 sec^{-1} was obtained from a fit of each curve to
equation [23].
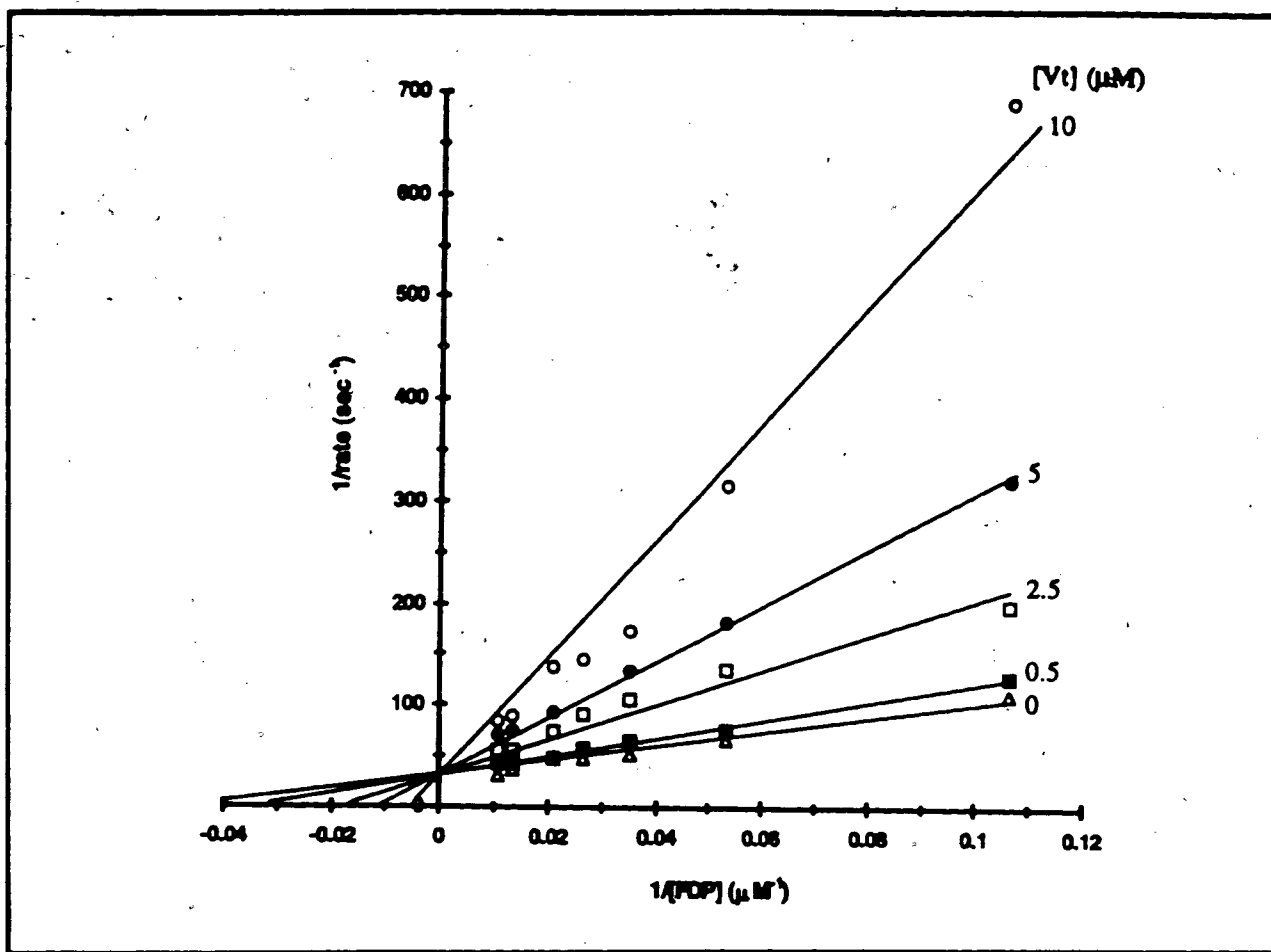
FIGURE 25B.

Lineweaver Burke plot for GST-LAR-D1.

Closed squares and open squares represent the analyses at 0.5 μM and 2.5 μM total inhibitor concentration (all the complexes in solution) respectively. Closed circles and open circles represent the analyses at 5 μM and 10 μM total inhibitor concentration respectively. The results in the absence of inhibitor are represented by open triangles. A constant V_{max} of 0.031 sec^{-1} was obtained from each plot.
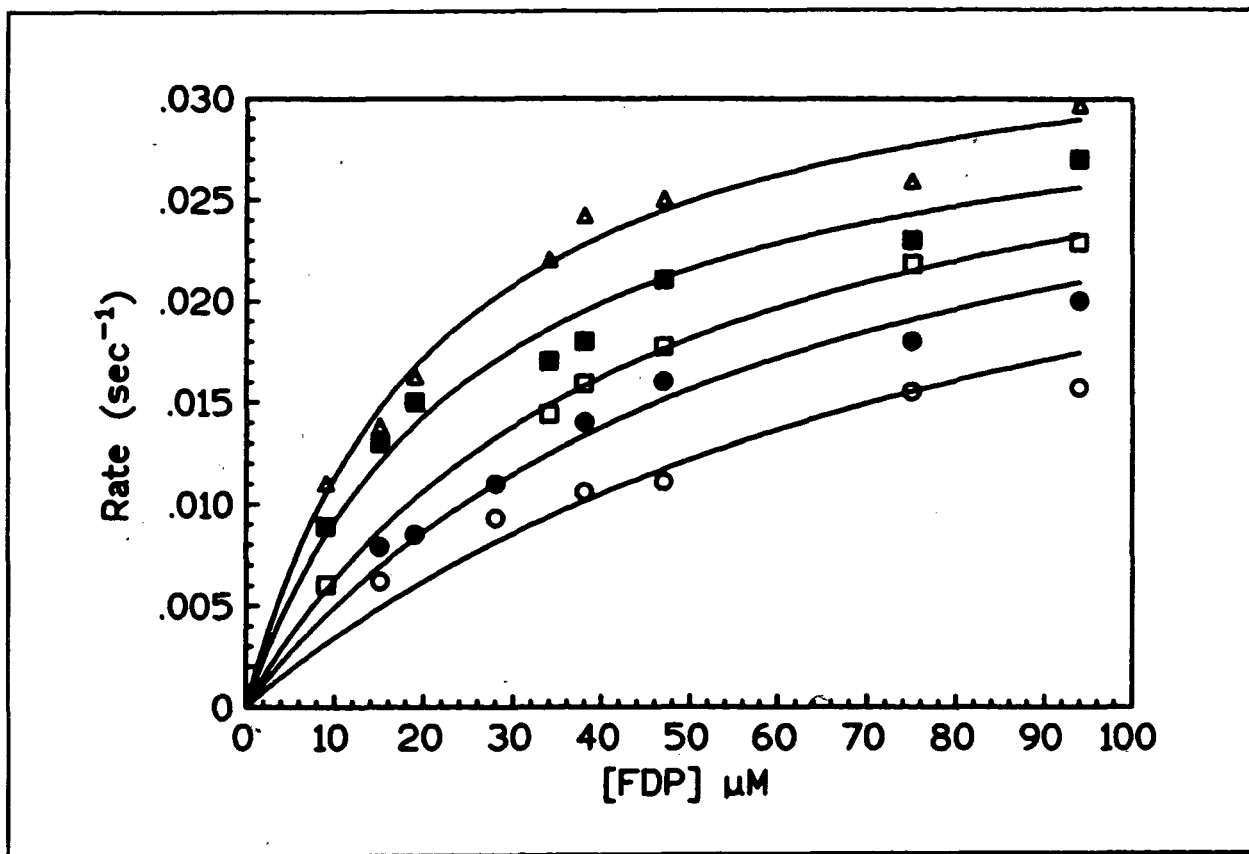
FIGURE 26A.

Plot of reaction rate as a function of substrate concentration for FLAG-PTP1B.

Closed squares and open squares represent the analyses at 0.5 μM and 2.5 μM total inhibitor concentration (all the complexes in solution) respectively. Closed circles and open circles represent the analyses at 5 μM and 10 μM total inhibitor concentration respectively. The control rates in the absence of inhibitor are given by the open triangles. A constant V_{max} of 0.035 sec^{-1} was obtained from a fit of each curve to equation [23].
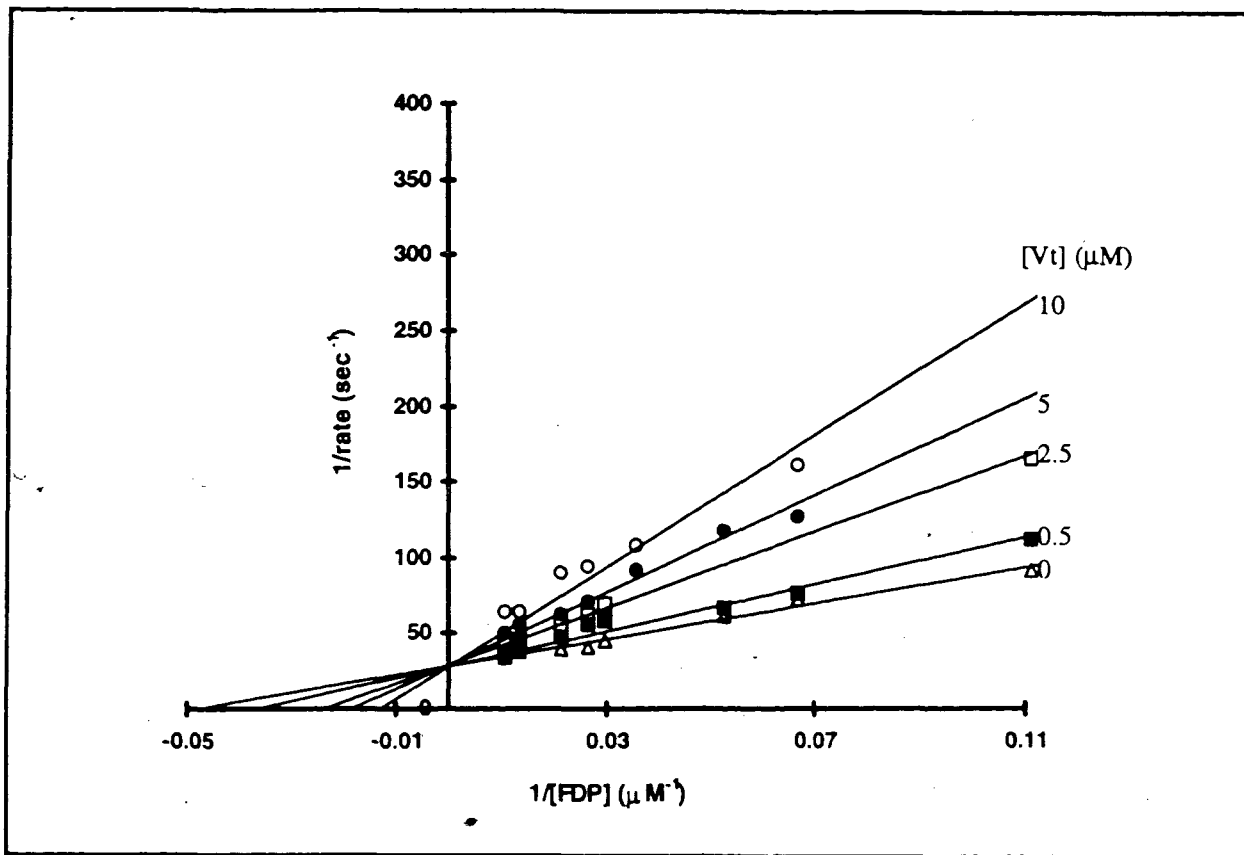
FIGURE 26B.

Lineweaver Burke plot for FLAG-PTP1B.

Closed squares and open squares represent the analyses at 0.5 μM and 2.5 μM total inhibitor concentration (all the complexes in solution) respectively. Closed circles and open circles represent the analyses at 5 μM and 10 μM total inhibitor concentration respectively. The control rates in the absence of inhibitor are given by the open triangles. A constant V_{max} of 0.035 sec^{-1} was obtained from each plot.

68B
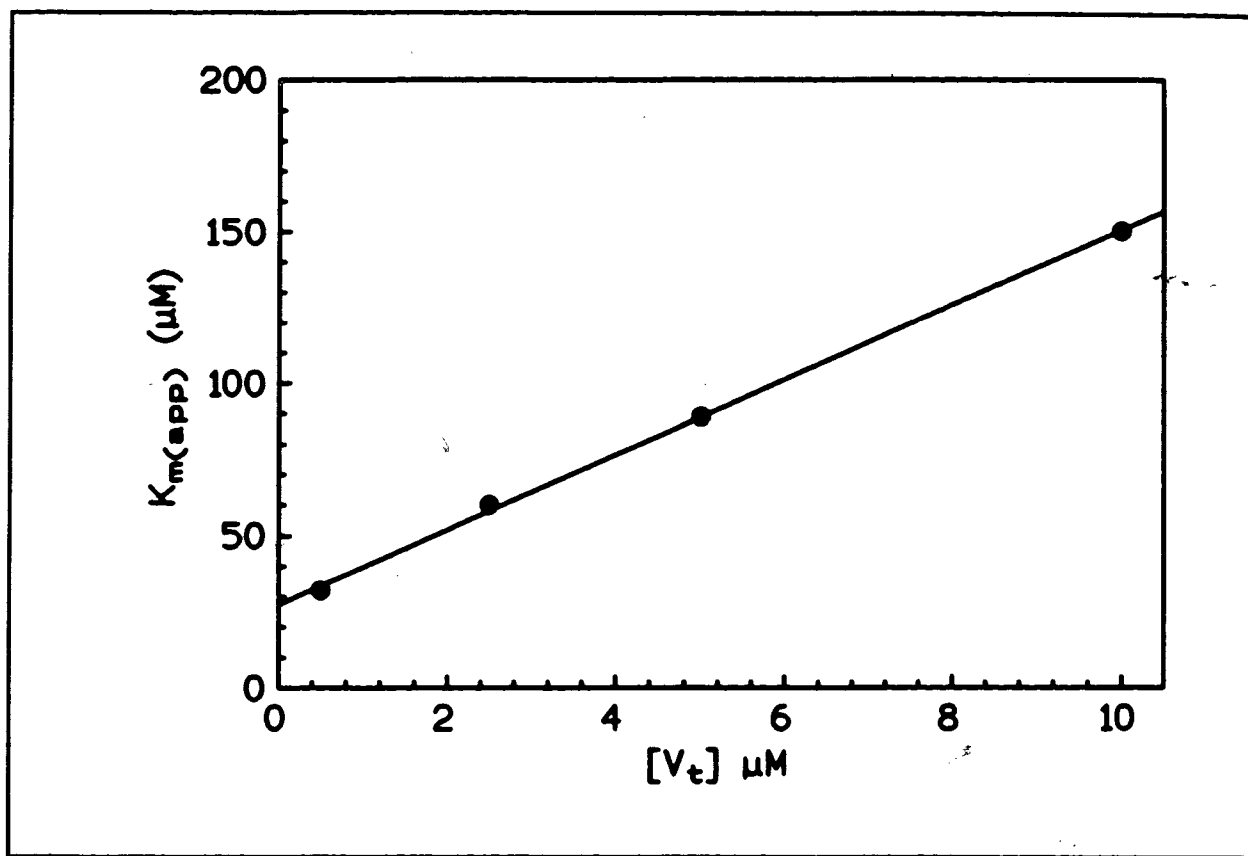
FIGURE 27.

Plot of $K_{m(app)}$ against total inhibitor concentration ([I]) for GST-LAR-D1.

The K_m, which is given by the y intercept of the plot, is 27 ± 6.0 μM. The K_i was

calculated from the slope of the graph to be 2.2 ± 0.3 μM.
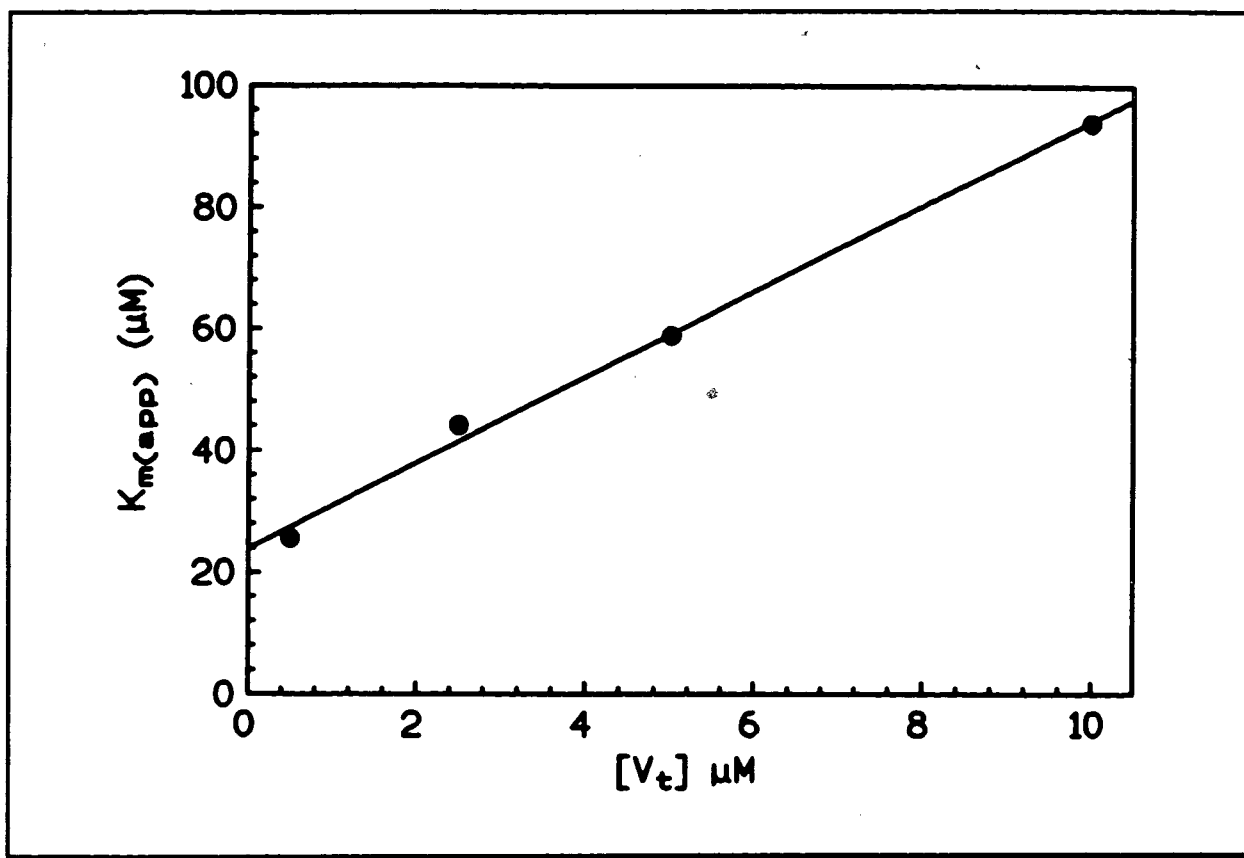
FIGURE 28.

Plot of $K_{m(app)}$ against total inhibitor concentration ([I]) for FLAG-PTP1B.

The K_m, which is given by the y intercept of the plot, is 24 ± 7.9 μM. The K_i was

calculated from the slope of the graph to be 3.4 ± 0.6 μM.

8.2.2. Analysis of the reversibility of inhibition of GST-LAR-D1 by N,N-dimethylhydroxylamine/vanadate and N,N-dimethylhydroxylamine/vanadate-DTT complexes:

In order to further establish that the inhibition, as indicated by the preceding inhibitor concentration study, was reversible and competitive, dilution experiments were carried out, such that the concentrations of DMHA, FDP substrate and buffer remained unchanged, but such that the enzyme and inhibitor were diluted five-fold. The results obtained for GST-LAR-D1 are shown in Figure 29. Contrary to the results obtained with the glycylglycineperoxovanadate inhibitor, the inhibition in this case was fully reversible by dilution, for both enzymes. This result confirmed that the inhibition observed was not due to oxidative inactivation of the enzyme, but rather to a classical reversible mechanism, whereby the inhibitor(s) compete with the FDP substrate for the enzyme active site.
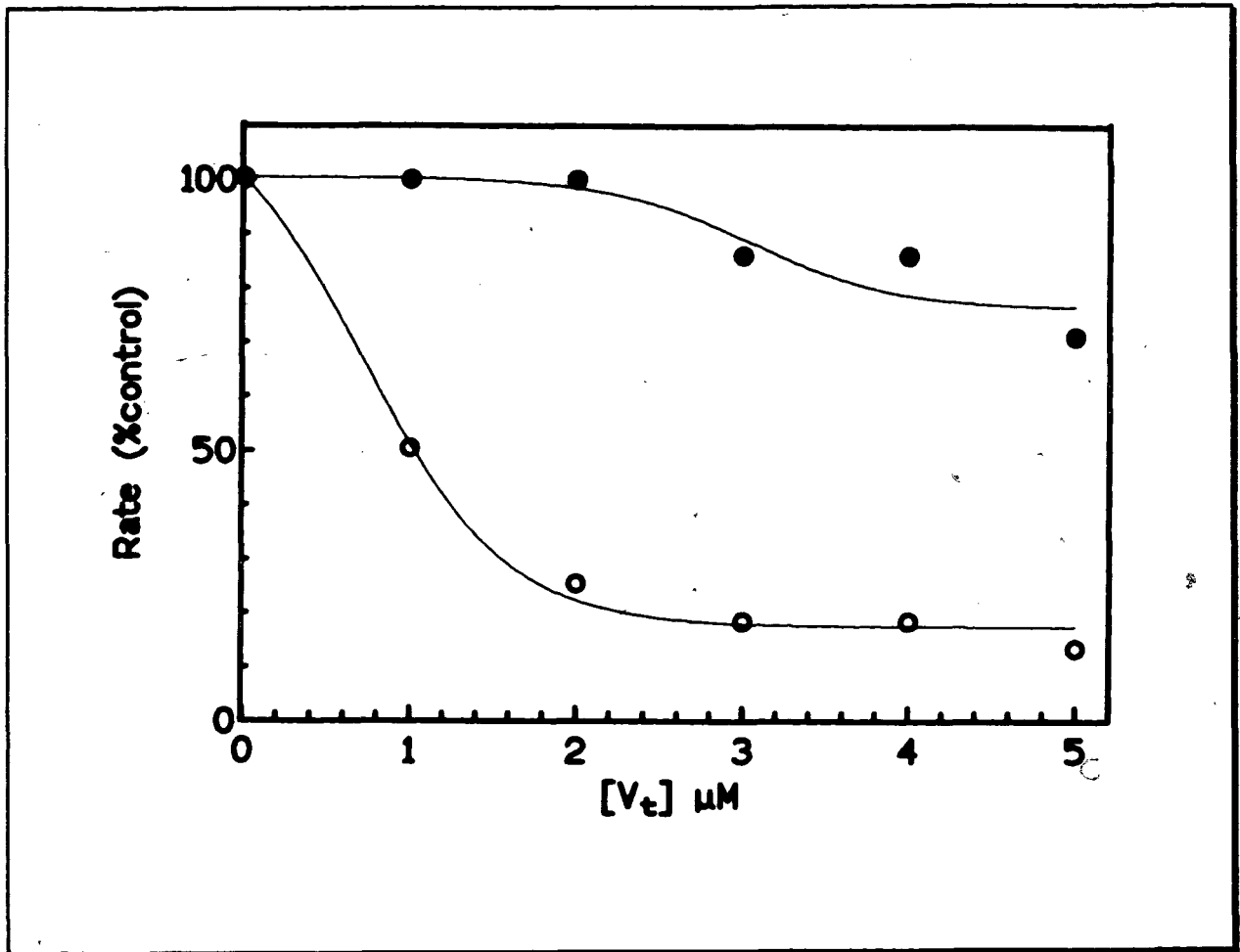
FIGURE 29.

Inhibition of GST-LAR-D1 is completely reversible by dilution.

Open circles represent the data obtained before dilution and closed circles represent the inhibition data obtained after dilution into buffer, DMHA and FDP. The results are expressed as the percentage of the rate of the control before and after dilution, respectively. The control was prepared in the absence of inhibitor and diluted in the same manner as the solutions containing inhibitor solution. This data shown are for a single experiment. The solid line represents the theoretical fit of the data. This analysis was confirmed by two separate replicate experiments which were performed for both PTPases.

72

8.2.3. Investigation of the individual inhibitory potencies of the Vl_1, Vl_2 and VlT complexes:

8.2.3.1. Calculation of the concentrations of each vanadium species present under the conditions of the inhibition studies:

As stated previously, the kinetic experiments discussed in the preceding section gave the combined inhibition constants for the inhibitory complexes present in solution. Therefore, in order to facilitate an evaluation of the individual inhibitory potencies of each of the complexes, the concentrations of each species present under the conditions of the inhibition studies were calculated. This could be done since the formation constants and accompanying equilibrium expressions for Vl_1, VlT and Vl_2 were known from the equilibrium studies discussed in chapters 5 and 6. It was appropriate to fit these formation constants to the vanadium and ligand conditions in the inhibition studies since, as shown by the NMR studies, equilibrium is obtained almost immediately after the addition of DTT, indicating that the kinetic studies were done under equilibrium conditions. The derivation of the expression to calculate these concentrations follows, where, l is the DMHA ligand, V_1 is vanadate, Vl_1 and Vl_2 are the monoligand and bisligand products respectively, and VlT is the V-DMHA-DTT complex.

$$V_1 + l \quad \overset{K_1}{\rightleftharpoons} \quad Vl_1 \qquad\qquad [V_1]\,[l]\,K_1 = [Vl_1] \qquad [3]$$

$$Vl_1 + l \quad \overset{K_2}{\rightleftharpoons} \quad Vl_2 \qquad\qquad [Vl_1][l]K_2 = [Vl_2] \qquad [8]$$

$$Vl_1 + T \quad \overset{K_4}{\rightleftharpoons} \quad VlT \qquad\qquad [Vl_1][T]K_4 = [VlT] \qquad [15]$$
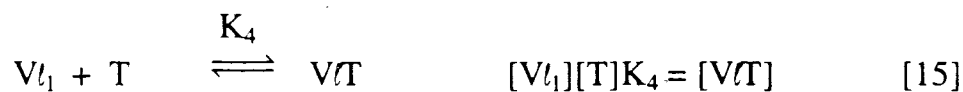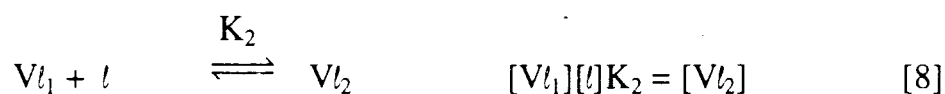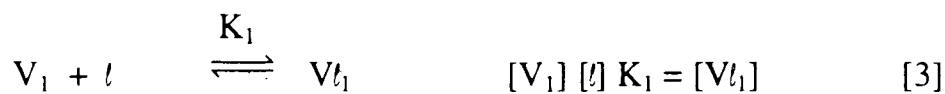
From these expressions, the total vanadium concentration (V_t) can be written as:

$$V_t = [V_1] + [Vl_1] + [VlT] + [Vl_2] \qquad\qquad [25]$$

Substituting into equation [25], for $[Vl_1]$ from equation [3] and for $[VlT]$ from equation [15] gives the following expression:

$$V_t = [V_1] + [V_1] [l] K_1 + [Vl_1][T]K_4 + [Vl_2] \qquad [26]$$

Substituting into equation [26] for $[Vl_2]$ from equation [8], followed by substitution for $[Vl_1]$ (from equation [3]) and subsequent re-arrangement yields the final expression for the concentration of vanadate ($[V_1]$):

$$[V_1] = \frac{V_t}{1 + [l]K_1 + [l][T]K_4K_1 + [l]^2K_2K_1} \qquad [27]$$

Since the total vanadium (V_t, 0.5-10 μM), DTT (2.5 mM) and DMHA ligand (3.0 mM) concentrations were known and, the formation constants K_1, K_2 and K_4 had been calculated under the conditions of the inhibition studies, the concentration of vanadate ($[V_1]$) was readily calculated from equation [27]. Once this value was determined, the concentrations of the other species were then calculated by substituting the known values into equations [3], [8] and [15] as required.

The results obtained are shown in Table III. It is evident from this analysis that it is highly unlikely that vanadate (V_1) contributed in any significant way to the inhibition observed. This is because vanadate was present at effectively negligible concentrations; up to 150 times less than the given K_i for vanadate of 0.4 μM (59).

V_t (μM)	$[V_1]$ (μM)	$[Vt_1]$ (μM)	$[Vt_2]$ (μM)	$[VtT]$ (μM)	$[VtT]$ $+[Vt_2]$ (μM)	FDP $K_{m(app)}$ (μM) LAR-D1	FDP $K_{m(app)}$ (μM) FLAG-PTP1B
0	0	0	0	0	0	27	24
0.5	1.3×10^{-3}	0.08	0.23	0.19	0.42	32	26
2.5	6.5×10^{-3}	0.40	1.2	1.0	2.1	60	44
5.0	13×10^{-3}	0.79	2.3	1.9	4.2	89	59
10.0	26×10^{-3}	1.6	4.6	3.8	8.4	150	94

TABLE III.

Concentrations of each vanadium species present under the conditions of the kinetic inhibition studies.

This table shows the calculated concentrations of the vanadium species present in the inhibition study. Also given are the $K_{m(app)}$ values obtained from the inhibition studies. From these calculations, it appears that the complexes which are present at significant concentrations are Vt_1, Vt_2 and VtT. The conditions are total vanadium (V_t) 0.5 to 10 μM, 3.0 mM DMHA 2.5 mM DTT, and 2.5 mM HEPES at pH 7.3. The values of K_1, K_2 and K_4, as calculated under the conditions of the inhibition study, were 2.0×10^4 M^{-1}, 9.7×10^2 M^{-1} and 9.7×10^2 M^{-1} respectively, as calculated from equations [3], [8] and [15].

8.2.3.2. DMHA titration study:.

DMHA titration experiments were carried out in order to determine if the monoligand was an inhibitor at the concentrations present in these studies. Table IV gives the calculated concentrations of the vanadium species present in these analyses, which are plotted in Figure 30A. At lower concentrations of DMHA, there were substantial amounts of vanadate present, which was consistent with the high degree of inhibition. As the DMHA ligand concentration was increased, the observed inhibition decreased until the ligand concentration was about 2 mM DMHA, after which the observed inhibition began to increase. The results obtained, which are shown in Figure 30B, were confirmed in duplicate experiments.

These observations suggested that the monoligand complex (Vl_1) was not an effective inhibitor at these concentrations. The results can be explained as follows. With progressive, but small amounts of added ligand, significant amounts of vanadate are converted into Vl_1 and V/T. Compared to vanadate, these complexes are poor inhibitors, thus the degree of inhibition decreases. Continued addition of dimethylhydroxylamine results in the formation of Vl_2 which is an effective inhibitor in these conditions. If the monoligand complex was a comparatively good inhibitor at these concentrations, the amount of inhibition would not be expected to significantly decrease as the DMHA ligand concentration increased between 0.1 and 1.5 mM DMHA. It is important to note, however, that although possible to determine in principle, in practice the precise inhibition parameters for the monoligand complex cannot be determined as the measurements are not accurate enough to allow all inhibitors to be accounted for simultaneously, at such low concentrations of Vl_1.

TABLE IV.

Concentrations of each vanadium species present under the conditions of the DMHA titration experiments.

This table shows the calculated concentrations of the vanadium species present in the inhibition studies at increasing DMHA concentrations, which are plotted in Figure 30A. Also given are the % inhibition data which are plotted in Figure 30B. The conditions are as follows: total vanadium concentration (V_t) 2 μM, 2.5 mM DTT and, DMHA concentrations varied from 0.1 to 5 mM.

[DMHA] (mM)	[V_1] (μM)	[Vl_1] (μM)	[Vl_2] (μM)	[VlT] (μM)	[VlT] +[Vl_2] (μM)	% inhibition observed LAR-D1
0.1	2.5×10^{-1}	4.9×10^{-1}	4.8×10^{-2}	1.2	1.3	71%
0.2	1.3×10^{-1}	5.2×10^{-1}	1.0×10^{-1}	1.3	1.4	67%
0.5	5.0×10^{-2}	5.0×10^{-1}	2.4×10^{-1}	1.2	1.4	62%
1.0	2.3×10^{-2}	4.5×10^{-1}	4.4×10^{-1}	1.1	1.5	54%
1.5	1.4×10^{-3}	4.1×10^{-1}	5.9×10^{-1}	9.9×10^{-1}	1.6	37%
2.0	9.0×10^{-4}	3.7×10^{-1}	7.2×10^{-1}	9.0×10^{-1}	1.6	37%
2.5	7.0×10^{-4}	3.4×10^{-1}	8.3×10^{-1}	8.3×10^{-1}	1.7	44%
3.0	5.0×10^{-4}	3.2×10^{-1}	9.2×10^{-1}	7.6×10^{-1}	1.7	42%
5.0	2.0×10^{-4}	2.4×10^{-1}	1.2	5.9×10^{-1}	1.8	47%

FIGURE 30A.

Concentrations of each vanadium species present under the conditions of the DMHA titration experiments.

This figure shows a plot of the calculated concentrations of the vanadium species present in the inhibition studies at increasing DMHA concentrations, as given in TABLE IV. The conditions are total vanadium concentration (V_t) 2 μM, DMHA varied as shown above from 0.1 to 5 mM, 2.5 mM DTT, and 2.5 mM HEPES; pH 7.3.
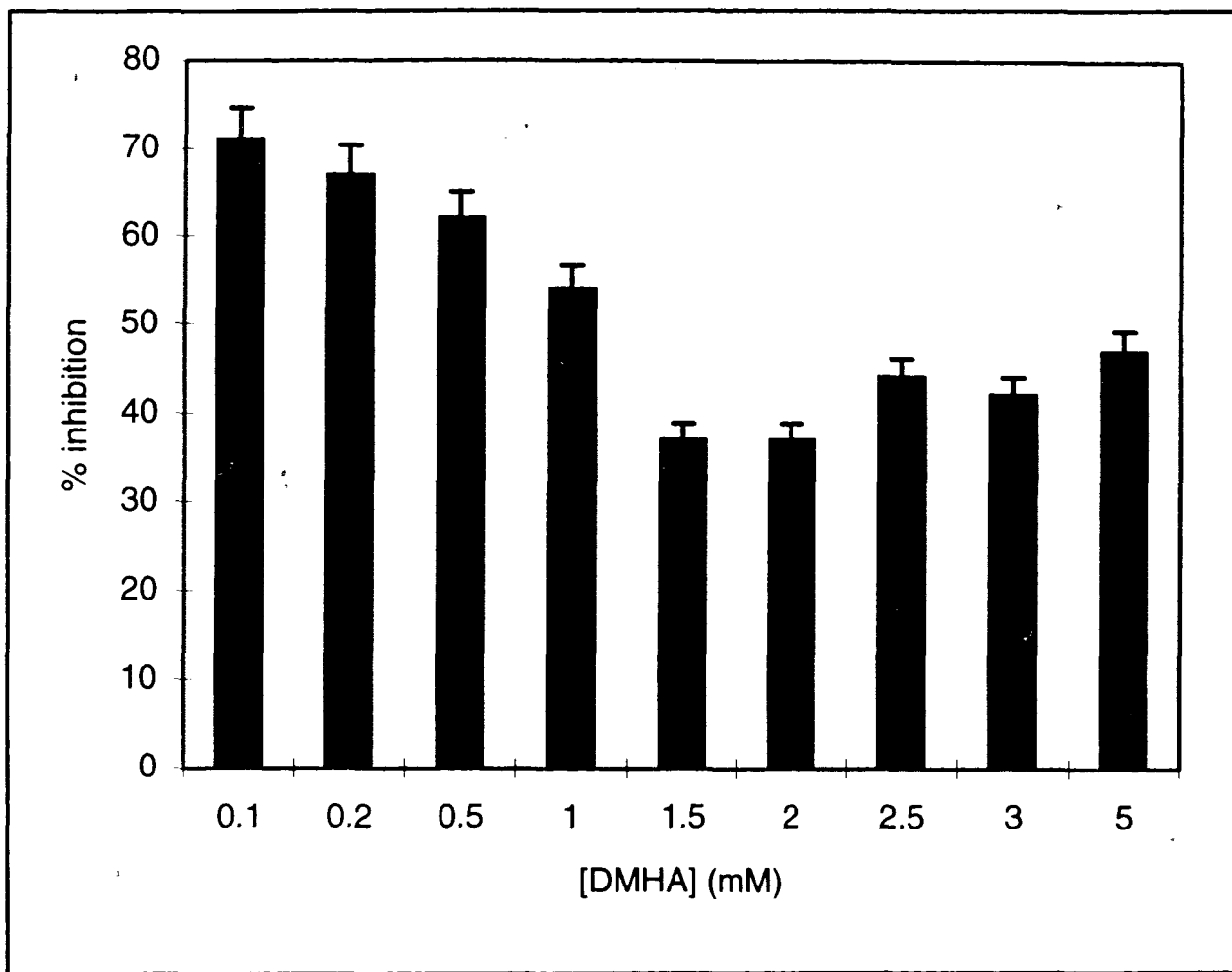
FIGURE 30B.

Inhibition of GST-LAR-D1 at 2 µM V_t as a function of increasing DMHA concentration.

The observed % inhibition data is shown as a function of the DMHA concentration in each assay. Table IV gives the corresponding inhibitor concentrations. The error bars represent the average standard deviation in the observed rates which is expressed as a percentage of these rates. The conditions are total vanadium 2 µM, DMHA varied as shown above, 2.5 mM DTT, and 2.5 mM HEPES at pH 7.3. The results shown here were confirmed in two replicate experiments.

8.2.3.3. Comparison of the inhibitory potencies of VlT and Vl₂ complexes:

In order to gain more information regarding the influence of these two complexes, the individual inhibitory potencies of the V*l*T and V*l*₂ complexes were determined. To evaluate these potencies, experiments were performed with the GST-LAR-D1 enzyme, at variable amounts of total vanadium and at elevated DTT or DMHA concentrations, such that either the V*l*T or the V*l*₂ complex was present as the major species, respectively. Table V shows the concentrations of each species present for the study at 3.0 mM DMHA and 50 mM DTT, and Table VI shows the concentrations present in the study at 10 mM DMHA and 1.25 mM DTT. The concentrations of the various complexes were calculated as described in section *8.2.3.1*. According to the calculated values given in Tables V and VI, V*l*T is the primary inhibitory complex in the study at 50 mM DTT and V*l*₂ is the primary inhibitor in the study at 10 mM DMHA.

It is important to note that there was no evidence from the ^{51}V NMR studies to suggest that any vanadate-DTT complexes were formed, even at the highest ratios of vanadate to DTT. This is consistent with calculations using the equilibrium expressions and formation constants for the vanadate-DTT (68), V*l*₂ and the V*l*T products. These calculations indicated that the vanadate-DTT complexes were present at amounts several fold less than those of vanadate. Studies of vanadate in the presence of DTT (59) did not suggest that the vanadate-DTT complex is an inhibitor, therefore its presence in such small amounts can be neglected.

Using the results of these experiments and the known inhibitor concentrations, the individual inhibition constants for V*l*₂ and V*l*T were calculated. The calculations were based on the expressions given below. Firstly, the expression for competitive inhibition due to the presence of two inhibitors is given by equation [28] (67), where K_{i1} and K_{i2} are the inhibition constants for V*l*₂ and V*l*T, respectively:

$$v = \frac{V_{max}[S]}{K_m\left(1 + \frac{[Vl2]}{Ki1} + \frac{[VfT]}{Ki2}\right) + [S]} \qquad [28]$$

These studies were carried out at the substrate concentration ([S]) equal to the K_m. Since the rate in the absence of inhibitor (v_o) is then given by $V_{max}/2$, equation [28] can be re-written as follows:

$$v = \frac{2v_o[S]}{K_m\left(1 + \frac{[Vl2]}{Ki1} + \frac{[VfT]}{Ki2}\right) + [S]} \qquad [29]$$

Given that [S] is equal to K_m, the equation can be further simplified to give:

$$v/v_o = \frac{2}{2 + \left(\frac{[Vl2]}{Ki1} + \frac{[VfT]}{Ki2}\right)} \qquad [30]$$

It is evident from Tables V and VI that within each study the ratio of each complex to the sum of the complexes was constant. The term for the sum of the inhibitor concentrations and inhibition constants, can therefore be re-written as equation [31], where $I_t = [Vl2]+[VfT]$.

$$v/v_o = \frac{1}{1 + \frac{I_t}{2K_{it}}} \qquad [31]$$

This equation is of the form $y = 1/(1 + x/A)$, therefore, a plot of v/v_o against I_t was made in order to calculate the two values of K_{it} obtained from the study at 50 mM DTT and from the study at 10 mM DMHA. Figure 31 shows the experimental data and the calculated curves obtained from this analysis. The values of K_{it} obtained from

the two analyses were then each inserted into equation [32], together with the appropriate values of x, such that two simultaneous equations were obtained which were then solved for the values of K_{i1} and K_{i2}. The parameter x is simply the mole fraction of $[Vt_2]$ in $[Vt_2] + [VfT] = I_t$.

$$\frac{x}{K_{i1}} + \frac{1-x}{K_{i2}} = \frac{1}{K_{it}} \tag{32}$$

From this analysis, a value of $1.0 \pm 0.3 \, \mu M$ was obtained for K_{i1} and a value of $2.3 \pm 0.8 \, \mu M$ was obtained for K_{i2}. These values were reproduced, as they should be, when they were determined by a series of iterative calculations whereby independent values of each inhibition constant were calculated and then corrected by a series of resubstitutions into equation [31] until the values remained constant.

The results obtained from these experiments indicate that both the Vt_2 and the VfT complexes are good inhibitors of PTPases. The experimental curves and the calculated K_i values both suggest that the Vt_2 complex is a more effective inhibitor than the VfT complex. Furthermore, these calculated individual inhibition constants are in good agreement with the combined inhibition constant value of $2.2 \pm 0.3 \, \mu M$ (determined in section 8.2.1.) and with the magnitude of inhibition observed in the enzyme dilution (8.2.2.) and DMHA titration studies (8.2.3.2.).

V_t (μM)	$[V_1]$ (μM)	$[Vl_1]$ (μM)	$[Vl_2]$ (μM)	$[VfT]$ (μM)	$[VfT]$ +$[Vl_2]$ (μM)	% inhibition observed LAR-D1
1.0	3.1×10^{-4}	1.9×10^{-2}	5.5×10^{-2}	0.93	0.98	22%
2.0	6.4×10^{-4}	3.8×10^{-2}	0.11	1.9	2.0	39%
3.0	9.5×10^{-4}	5.7×10^{-2}	0.17	2.8	3.0	45%
4.0	1.3×10^{-3}	7.6×10^{-2}	0.22	3.7	3.9	46%
5.0	1.6×10^{-3}	9.6×10^{-2}	0.28	4.6	4.9	52%
10.0	3.1×10^{-3}	0.19	0.55	9.3	9.8	59%

TABLE V.

Concentrations of each vanadium species present under the conditions of the kinetic inhibition studies at 50 mM DTT.

This table shows the calculated concentrations of the vanadium species present in the inhibition study at high DTT concentration. From these calculations, it can be seen that VfT is the predominant species present. Also given are the experimental % inhibition data. The conditions are total vanadium (V_t) 1 to 10 μM, 3.0 mM DMHA, 50 mM DTT and 27.5 mM HEPES at pH 7.3.

V_t (μM)	$[V_1]$ (μM)	$[Vl_1]$ (μM)	$[Vl_2]$ (μM)	$[VfT]$ (μM)	$[VfT]+[Vl_2]$ (μM)	% inhibition observed LAR-D1
1.0	4.2×10^{-4}	8.4×10^{-2}	0.82	0.10	0.92	29%
2.0	8.4×10^{-4}	0.17	1.6	0.20	1.8	48%
3.0	1.3×10^{-3}	0.25	2.4	0.31	2.7	58%
4.0	1.7×10^{-3}	0.34	3.3	0.41	3.7	64%
5.0	2.1×10^{-3}	0.42	4.1	0.51	4.6	73%
10.0	4.2×10^{-3}	0.84	8.2	1.0	9.2	76%

TABLE VI.

Concentrations of each vanadium species present under the conditions of the kinetic inhibition studies at 10 mM DMHA.

This table shows the calculated concentrations of the vanadium species present in the inhibition study at high DMHA. In this experiment, Vl_2 is the predominant species. Also given are the experimental % inhibition data. The conditions are total vanadium (V_t) 1 to 10 μM, 10 mM DMHA and 1.25 mM DTT, 2.5 mM HEPES at pH 7.3.
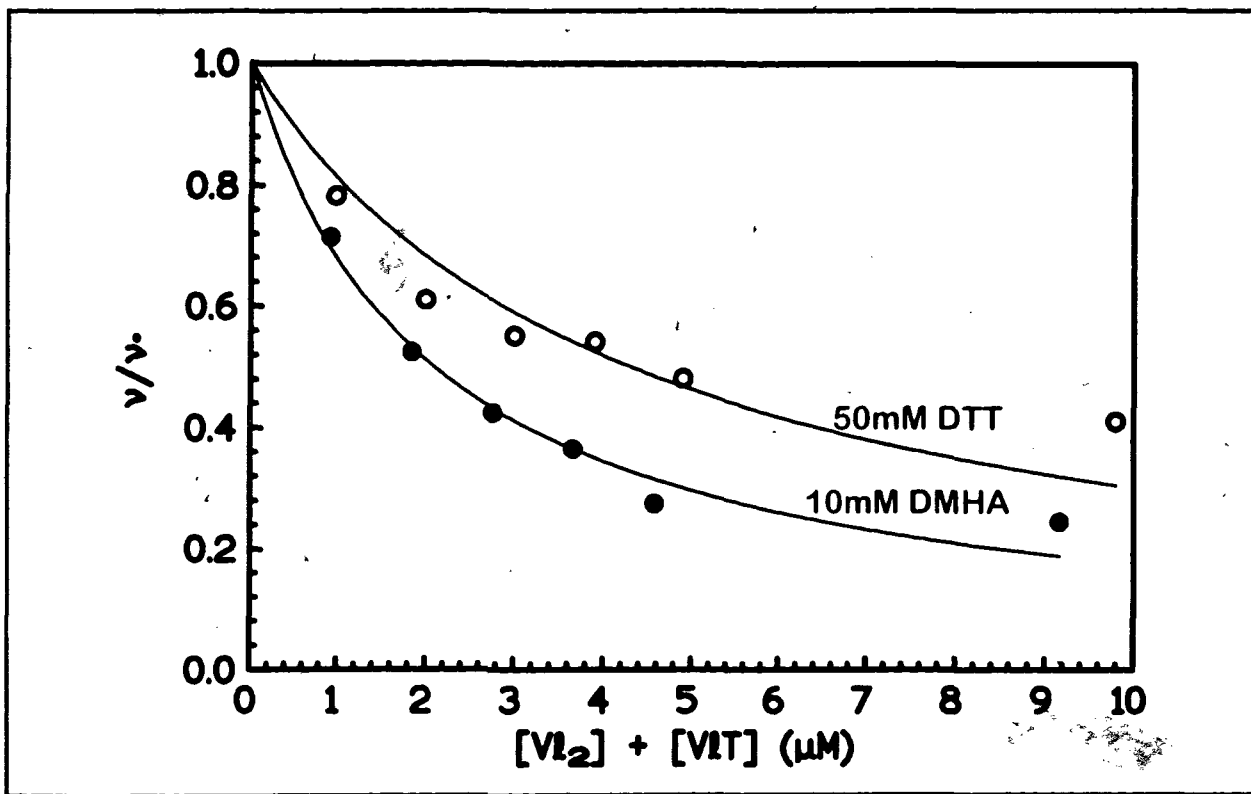
FIGURE 31.

Inhibition of GST-LAR-D1 in the presence of VI$_2$ and VfT complexes at 50 mM DTT and 10 mM DMHA.

This figure shows the calculated curves and the experimental data points for the inhibition studies at 50 mM DTT and 10 mM DMHA. The observed inhibition is plotted on the y axis as v/v_o, where v and v_u represent the rates in the presence and absence of inhibitor, respectively. The total inhibitor concentration (I_t) is plotted on the x-axis and represents the sum of the concentrations of VI$_2$ and VfT. Open circles and closed circles represent the results obtained at 50 mM DTT (Table V) and at 10 mM DMHA (Table VI), respectively. Independent replicate experiments were performed, which gave similar results.

8.2.4. Preliminary results from structural modelling studies of Vl_2 and PTP1B:

In an effort to obtain a preliminary picture of how the Vl_2 complex inhibits, simulated docking experiments for PTP1B were carried out by a laboratory colleague, Nick Glover. For these calculations, a Van der Waals surface was generated from the X-ray coordinates of PTP1B (22). Taking into account the electrostatic potential surface, the computer program Dock (69) was used to obtain the most energetically favourable docked orientation.

The calculations showed that the bisligand complex is easily accommodated within the active site of PTP1B. Figure 32 shows the orientation, as suggested by the computer simulation, adopted by the inhibitor. The complex is inserted end-on into the active site pocket. The orientation within the pocket is such that interactions with active site residues, including the essential cysteine and conserved arginine, are possible. Although the nature of these interactions is yet to be studied in detail, these calculations provide strong support for the results obtained in this study by showing that the bisligand complex has a highly favourable affinity for the PTPase active site.

It seems likely that the end-on insertion also represents the situation with the V/T complex. In this case, the open end of the pocket could readily accommodate the DTT moiety. Unfortunately, since the molecular structure is not known at this time, it is not possible to carry out docking simulations with V/T in order to provide support for these speculations.
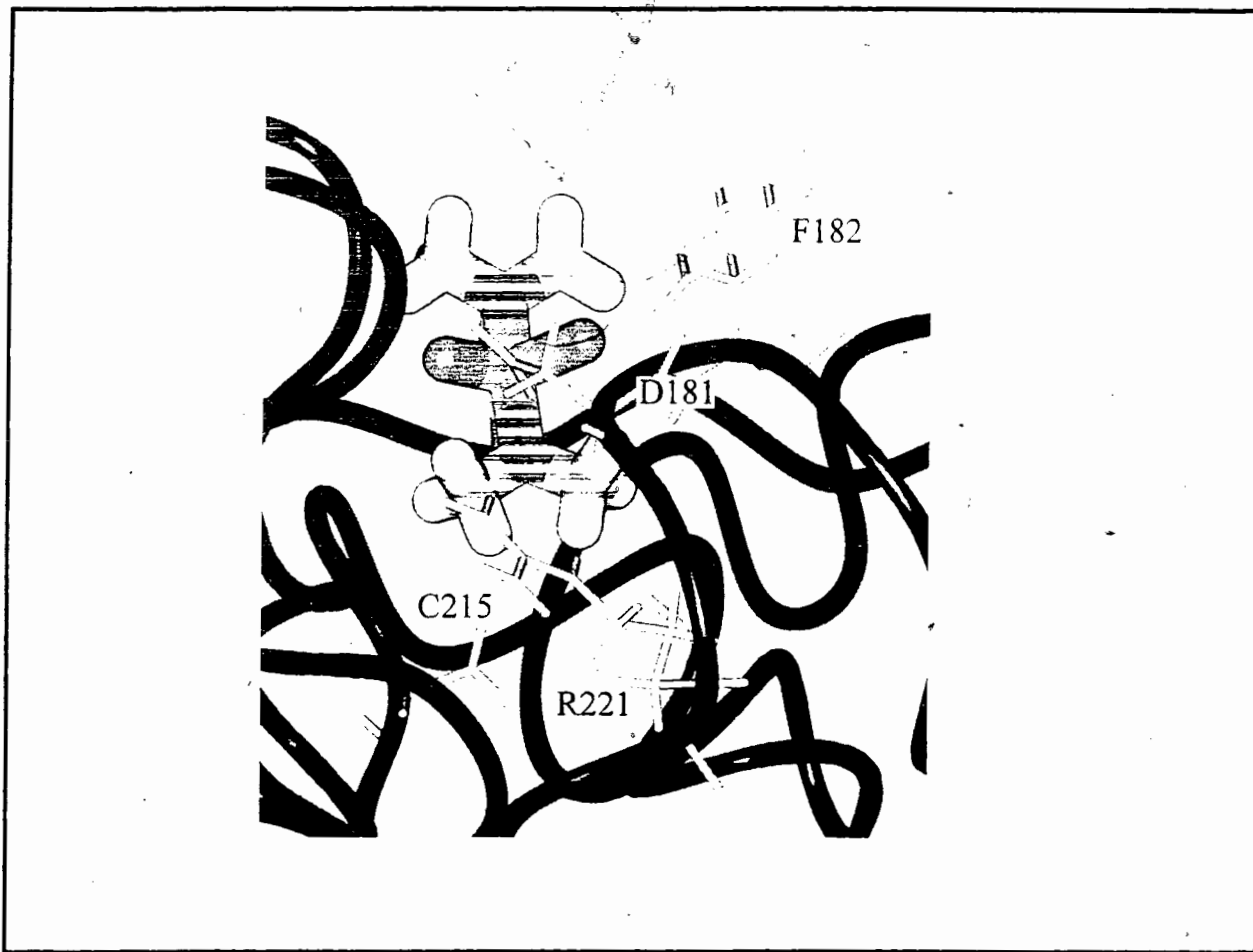
FIGURE 32.

Representation of the bound inhibitor orientation within the active site pocket.

The end-on orientation of Vl_2 in the active site of PTP1B is shown. The backbone coordinates of PTP1B are represented as a ribbon. The side chains of selected conserved residues are shown. These residues are the catalytic cysteine and arginine and conserved surface loop residues; aspartate and phenylalanine. This figure was produced using Insight II (Biosym Technologies), the x-ray coordinates for PTP1B (22), and x-ray coordinates for Vl_2 adapted from those for l_2V-O-Vl_2 (61).

CHAPTER 9

9. Conclusions and Future Perspectives:

The aim of this study was to investigate the mechanisms by which peroxovanadate and vanadate complexes can influence the activity of protein tyrosine phosphatases. The results obtained in this work indicate that the glycylglycine monoperoxovanadate (glyglypV) complex inhibits LAR-D1 PTPase by an irreversible inactivation mechanism. Based on these observations, it is proposed that the inhibition of LAR-D1 PTPase by glyglypV can be explained by oxidation of the catalytic cysteine residue. This is consistent with the known oxidative inactivation of PTP1B by peroxovanadate (59) and glyglyperoxovanadate (65).

The influence of N,N-dimethylhydroxylamine/vanadate and N,N-dimethylhydroxylamine/vanadate-DTT complexes on PTPase activity has also been investigated. The results obtained are consistent with a reversible, competitive mechanism of inhibition. Using the formation constants obtained from ^{51}V NMR experiments, and the results from enzyme inhibition studies, the active inhibitory species under the conditions of the kinetics experiments were identified as the bisligand product (Vl_2), and the N,N-dimethylhydroxylamineDTT/vanadate complex (VlT). These complexes are novel vanadium inhibitors of protein tyrosine phosphatases and this is the first time that it has been shown that protein tyrosine phosphatases are inhibited by vanadium complexes other than vanadate itself.

Preliminary structural modelling studies indicate that the bisligand Vl_2 product can be readily accommodated within the PTPase active site. Further structural modelling work will examine the nature of the binding interactions which occur between this complex and the PTPase active site residues, and is ongoing in our laboratory. In these studies, the Vl_2 complex should prove useful as a molecular template from which to determine more potent PTPase inhibitors by a rational design approach. For example, replacement of the dimethylhydroxylamine ligand methyl side

chains with longer alkyl chains that have functional groups incorporated into them may result in vanadate complexes that target specific PTPase active site residues, thus resulting in improved inhibitory properties. For example, the hydrophobic residues (such as the conserved phenylalanine and alanine residues in PTP1B) lining the active site pocket are potential sites for developing enhanced inhibitor-enzyme interactions. Modelling studies could be used to screen potential candidates determined in this manner. Furthermore, detailed structural information could also be acquired from two-dimensional NMR spectroscopy studies of the enzyme-inhibitor complexes, provided that stable, non-labile vanadium complexes can be obtained. In conjunction with enzyme inhibition experiments, these structural analyses should provide useful insight on the associations which occur between these complexes and PTPases, particularly regarding the influence of the ancillary ligands on the binding conformation and inhibition of the PTPase.

The VtT and VtC complexes which have been studied by ^{51}V NMR spectroscopy in this work, are novel vanadium complexes which have not been previously described. The formation constants and stoichiometry of these complexes have been determined. Using results obtained from the study of other thiol-containing compounds, the mode of coordination to vanadium in these complexes is proposed to involve the thiolate group and one other group which may be either the carboxylate or the amino group in cysteine, or the hydroxyl group in DTT. These complexes, which form within five minutes of mixing, were also obtained when the starting material was the dimeric crystalline bisligand dimethylhydroxylamine complex, whose constituent monomers were otherwise stable to hydrolysis. This finding indicates that the complexes form by an associative displacement mechanism; whereby the DTT or cysteine ligand attacks the bisligand complex to form the VtT or VtC complex, respectively. Determination of the X-ray crystal structures of these complexes would be of value in providing detailed information regarding their coordination geometry and, in confirming the stoichiometry of the solution products.

The formation of VlC complexes provides strong support for the enzyme inhibition results in that it demonstrates that a vanadate/dimethylhydroxylamine complex which is inhibitory, is able to form complexes with cysteine; a critical residue in PTPases. Although the coordination of cysteine to vanadium in these complexes is not monodentate, there are side chains in the active site of the enzyme, which could provide the second required functional group. The ability of glutathione to form these types of complexes suggests that this is not an unlikely possibility.

The results obtained in this work suggest that the monoligand complex is not a potent PTPase inhibitor. This observation, the finding that the inhibition is readily reversible, and the associative mechanism of complexation by the ancillary ligands, suggests that the actual inhibiting species might be represented by a structure similar to what might be encountered as an intermediate in the reaction of Vl_2 + DTT $\rightleftharpoons$ VlDTT + l . It is also possible that there are charge and structural properties which increase the favourability of binding of the bisligand complexes to the active site, that are not present in the monoligand. For example, preliminary modelling studies suggest that one of the dimethylhydroxylamine ligands in the Vl_2 complex makes contacts with residues at the open end of the active site pocket. Molecular dynamics studies which define the possible hydrophobic and ionic interactions between the Vl_2 complex and the enzyme active site, should assist in further examining these influences.

Cell culture assays indicate that the bisligand Vl_2 complex exhibits insulin-mimetic influences. Additionally, in human T-lymphoma cell lines (Jurkat cells) the Vl_2 complex causes a large increase phosphotyrosine levels, whereas vanadate has no effect (Ramachandran, unpublished results). From these results, the findings from the enzyme inhibition studies, and the structural modelling results, it appears possible that in the future, vanadium complexes which are based on the further development of the structural properties of N,N-dimethylhydroxamido vanadates, may be found to have therapeutic applications.

CHAPTER 10

10. References:

1. Barford, D., Jia, Z., and Tonks, N. K. (1995) *Nature Structural Biology* **2**, 1043-1053.

2. Kole, H.K., Smyth, M.S., Russ, P.L., and Burke, T.R. (1995) *Biochem. J.* **311**, 1025-1031.

3. Zhang, Z-Y. (1995) *J. Biol. Chem.* **270**, 6052-16055.

4. Streuli, M. (1996) *Curr. Opin. Cell Biol.* **8**, 182-188.

5. Kulas, D.T., Freund, G.G., and Mooney, R.A. (1996) *J. Biol. Chem.* **271**, 755-760.

6. Hunter, T. (1995) *Cell* **80**, 225-236.

7. Stone, R.L., and Dixon, J.E. (1994) *J. Biol. Chem.* **269**, 31323-31326.

8. Fauman, E.B., and Saper, M.A. (1996) *Trends Biochem. Sci.* **21**, 413-417.

9. Mauro, L.J., and Dixon, J.E. (1994) *Trends Biochem. Sci.* **19**, 151-155.

10. Feng, G-S., and Pawson, T. (1994) *Trends Genet.* **10**, 54-58.

11. Pawson, T., and Gish, G.D. (1992) *Cell* **71**, 359-362.

12. Pei, D., Lorenz, U., Klingmuller, U., Neel, B.G., and Walsh, C.T. (1994) *Biochemistry* **33**, 15483-15493.

13. Fischer, E.H., Charbonneau, H., and Tonks, N.K. (1991) *Science* **253**, 401-406.

14. Ng, D.H.W., Maiti, A., and Johnson, P. (1995) *Biochem. Biophys. Res. Comm.* **206**, 302-309.

15. Cho, H., Ramer, S.E., Itoh, M., Kits, E., Bannwarth, M., Burn, P., Saito, H., and Walsh, C.T. (1992) *Biochemistry* **31**, 133-138.

16. Itoh, M., Streuli, M., Kreuger, N.X., and Saito, H. (1992) *J. Biol. Chem.* **267**, 12356-12363.

17. Peles, E. Nativ, M., Campbell, P.L., Sakurai, T., Martinez, R., Lev, S., Clary, D.O., Schilling, J., Barnea, G., Plowman, G.D., et al. (1995) *Cell* **82,** 251-260.

18. Koretzky, G.A. (1993) *FASEB J.* **7,** 420-426.

19. Furukawa, T., Itoh, M., Kreuger, N.X., and Streuli, M. (1994) *Proc. Natl. Acad. Sci. USA.* **91,** 10928-10932.

20. Walton, K.M., and Dixon, J.E. (1993) *A. Rev. Biochem.* **62,** 101-120.

21. Guan, K.L., and Dixon, J.E. (1991) *J. Biol. Chem.* **266,** 17026-17030.

22. Barford, D., Flint, A.J., and Tonks, N.K. (1994) *Science* **263,** 1397-1404.

23. Hengge, A.C., Sowa, G.A., Wu, L., and Zhang, Z-Y. (1995) *Biochemistry* **34,** 13982-13987.

24. Zhang, Z-Y., Wang, Y., Wu, Y., Fauman, E.B.,Stuckey, J.A., Schubert, H.L., Saper, M.A., and Dixon, J.E. (1994) *Biochemistry* **33,** 15266-15270.

25. Zhang, Z-Y., and Dixon, J.E. (1994) *Adv. Enzymol. Relat. Areas Mol. Biol.* **68,** 1-36.

26. Zhao, Y., and Zhang, Z-Y. (1996) *Biochemistry* **35,** 11797-11804.

27. Zhang, Z-Y., Palfey, B.A., Wu, L., and Zhao, Y. (1995) *Biochemistry* **34,** 16389-16396.

28. Denu, J.M., Lohse, D.L., Vijayalakshmi, J., Saper, M.A., and Dixon, J.E. (1996) *Proc. Natl. Acad. Sci. USA.* **93,** 2493-2498.

29. Ramachandran, C., Aebersold, R., Tonks, N.K., and Pot, D.A. (1992) *Biochemistry* **31,** 4232-4238.

30. Seely, B.L., Staubs, P.A., Reichart, D.R., Berhanu, P., Milarski, K.L., Saltiel, A.R., Kusari, J., and Olefsky, J.M. (1996) *Diabetes* **45,** 1379-1385.

31. Bandyopadhyay, D., Kusari, A., Kenner, K.A., Liu, F., Chernoff, J., Gustafson, T.A., and Kusari, J. (1997) *J. Biol. Chem.* **272,** 1639-1645.

32. Kenner, K.A., Anyanwu, E., Olefsky, J.M., and Kusari, J. (1996) *J. Biol. Chem.* **271**, 19810-19816.

33. Goldstein, B.J. (1992) *J. Cell. Biochem.* **3**, 1-15.

34. Hashimoto, N., Feener, E.P., Zhang, W.R., and Goldstein, B.J. (1992) *J. Biol. Chem.* **267**, 13811-13814.

35. Kulas, D.T., Zhang, W., Golstein, B.J., Furlanetto, R.W., and Mooney, R.A. (1995) *J. Biol. Chem.* **270**, 2435-2438.

36. Kulas, D.T., Goldstein, B.J., and Mooney, R.A. (1996) *J. Biol. Chem.* **271**, 748-754.

37. Li P-M., Zhang, W-R., and Goldstein, B.J. (1996) *Cell. Signal.* **8**, 467-473.

38. Serra-Pages, C., Kedersha, N.L., Fazikas, L., Medley, Q., Debant, A., and Streuli, M. (1995) *EMBO J.* **14**, 2827-2838.

39. Debant, A., Serra-Pages, C., Seipel, K., O'Brien, S., Tang, M., Parl, S-H., and Streuli, M. (1996) *Proc. Natl. Acad. Sci. USA.* **93**, 5466-5471.

40. Burke, T.R., Kole, H.K., and Roller, P.P. (1994) *Biochem. Biophys. Res. Comm.* **204**, 129-134.

41. De Boer, E., van Kooyk, Y., Tromp, M.G.M., Plat, H., and Wever, R. (1986) *Biochim. Biophys. Acta* **869**, 48-53.

42. Robson, R.L. Eady, R.R., Richardson, T.H., Miller, R.W., Hawkins, M., and Postgate, J.R. (1986) *Nature* **322**, 388.

43. Orvig, C., Thompson, K.H., Battell, M., and McNeill, J.H. (1995) in *Vanadium and its role in Life* (Sigel, H., Sigel, A., eds); Metal Ions in Biological Systems; pp. 575-594, Marcel Dekker Inc., New York

44. Gresser, M.J. Tracey, A.S., and Stankiewicz, P.J. (1987) *Adv. Prot. Phosphatases* **4**, 35-37.

45. Etcheverry, S.B., Crans, D.C., Keramidas, A.D., and Cortizo, A.M. (1997) *Arch. Biochem. Biophys.* **338**, 7-14.

46. Sekar, N., Li, J., and Schechter, Y. (1996) *Crit. Rev. Biochem. Molec. Biol.* **31,** 339-359.

47. Stern, A., Yin, X., Tsang, S-S., Davison, A., and Moon, J. (1993) *Biochem. Cell Biol.* **71,** 103-112.

48. Crans, D.C., Mahroof-Tahir, M., and Keramidas, A.D. (1995) *Mol. Cell. Biochem.* **153,** 17-24.

49. Stankiewicz, P.J., Tracey, A.S., and Crans, D.C. (1995) in *Vanadium and its role in Life* (Sigel, H., Sigel, A., eds); Metal Ions in Biological Systems; pp. 287-324, Marcel Dekker Inc., New York

50. Chasteen, N.D. (1983) *Structure and Bonding* **53,** 105-138.

51. Gresser, M.J., and Tracey, A.S. (1990) in *Vanadium in Biological Systems* (Chasteen, N.D., ed.) pp. 63-79, Kluwer Academic Publishers, Netherlands

52. Butler, A., Clague, M.J., and Meister, G.E. (1994) *Chem. Rev.* **94,** 625-638.

53. Posner, B.I., Faure, R., Burgess, J.W., Bevan, P., Lachance D., Zhang-Sun G., Fantus, G., Ng, J.B., Hall, D.A., Soo Lum, B., and Shaver, A. (1994) *J. Biol. Chem.* **269,** 4596-4604.

54. Shaver, A., Ng, J.B., Hall, D.A., and Posner, B.I. (1995) *Mol. Cell. Biochem.* **153,** 5-15.

55. Tracey, A.S., and Jaswal, J.S. (1993) *Inorg. Chem.* **32,** 4235-4243.

56. Tracey, A.S., and Jaswal, J.S. (1992) *J. Am. Chem. Soc.* **114,** 3835-3840.

57. Kadota, S., Fantus, I.G., Deragon, G., Guyda, H.J., Hersh, B., and Posner, B.I. (1987) *Biochem. Biophys. Res. Comm.* **147,** 259-266.

58. Leighton, B., Cooper, G.J.S., DaCosta, C., and Foot, E.A. (1991) *Biochem J.* **276,** 289-292.

59. Huyer, G., Liu, S., Kelly, J., Moffat, J., Payette, P., Kennedy, B., Tsaprailis, G., Gresser, M.J., and Ramachandran C. (1997) *J. Biol. Chem.* **272,** 843-851.

60. Einstein F.W.B., Batchelor, R.J., Angus-Dunne, S.J., and Tracey, A.S. (1996) *Inorg. Chem.* **35,** 1680-1684.

61. Paul, P.C., Angus-Dunne, S.J., Batchelor, R.J., Einstein, F.W.B., and Tracey, A.S. (1997) *Can. J. Chem.* **75,** 429-440.

62. Dechert, U., Adam, M., Harder, K.W., Clark-Lewis, I., and Jirik, F. (1994) *J. Biol. Chem.* **269,** 5602-5611.

63. Bradford, M.M. (1976) *Anal. Biochem.* **72,** 248-254.

64. Desmarais, S. *Merck Frosst, unpublished report.*

65. Huyer, G. *Merck Frosst, unpublished results.*

66. Paul, P.C., Angus-Dunne, S.J., Batchelor, R.J., Einstein, F.W.B., and Tracey, A.S. (1997) *Can. J. Chem.* **75,** 183-191.

67. Cornish-Bowden, A. (1995) *Fundamentals of Enzyme Kinetics*, 2nd Ed., pp. 93-119, Ashgate Publishers, London

68. Tracey, A.S., and Paul, P.C. *Manuscript in preparation.*

69. Meng, E.C., Gschwend, D.A., Blaney, J.M., and Kuntz, I.D. (1993) *Proteins: Structure, Function & Genetics* **17,** 266.

70. Ramachandran, C. *Merck Frosst, unpublished results.*